A Study of the Promolecule Radius of Nitrides, Oxides and Sulfides and of the Bond Critical Point Properties of the Electron Density Distribution in Nitrides

by

Shari Feth

Dissertation submitted to the Faculty of the
Virginia Polytechnic Institute and State University
in partial fulfillment of the requirements for the degree of

DOCTOR OF PHILOSOPHY

in

MATERIALS ENGINEERING AND SCIENCE

APPROVED:

G.V. Gibbs, Chairman

M.B. Boisen, Jr.

R.O. Claus

R.S. Gordon

D.A. Hirschfield

M.F. Hochella, Jr.

December, 1996
Blacksburg, Virginia

Key Words: Electron Density Distributions, Promolecule Radii, Electronegativity, Laplacian, Bond Critical Point Properties

A STUDY OF THE PROMOLECULE RADIUS OF NITRIDES, OXIDES AND SULFIDES AND OF THE BOND CRITICAL POINT PROPERTIES OF THE ELECTRON DENSITY DISTRIBUTION IN NITRIDES

by

Shari Feth

Materials Science and Engineering

G.V. Gibbs, Chairman

(ABSTRACT)

"We cannot afford the luxury any longer of ignoring the nature of the bonding in these interesting compounds...." P.E.D. Morgan, (1974).

An understanding of bonding is paramount to furthering our understanding of materials (Morgan, 1974). The properties of materials are governed by the interactions between atoms. These interactions are governed by the nature of the bonds. In this study, two methods are explored which provide insight into chemical interactions.

First, promolecule radii, calculated for nitride, oxide, and sulfide coordinated polyhedra with bond lengths fixed at the sums of effective ionic and crystal radii, are analyzed. Radii calculated for transition and non–transition cations for the first four rows of the periodic table are highly correlated with crystal radii derived for oxide and sulfide crystals and with ionic radii derived for nitride crystals. Promolecule radii calculated for the coordination polyhedra match experimentally determined bonded radii to within $\sim$ 0.02 Å, on average. Calculated radii anions tend to match ionic radii when bonded to highly electropositive cations and atomic radii when bonded to

highly electronegative cations.

In the second study, molecular orbital calculations were completed on a series of small molecules containing the nitride anion. Bond type can be characterized by studying the systematics of parameters derived from the bond critical point properties of the electron density distributions. A set of criteria is established to suggest how covalent or ionic a bond is. This criteria is based on bond critical point properties such as the Laplacian of the electron density distribution evaluated at the bond critical point, the electron density distribution at the critical point, the local energy density at the critical point, the relative electronegativity of the cation, the curvatures of the electron density distribution, and the distance from the nucleus of the nitride anion to the bond critical point, (the bonded radius of the nitrogen atom). Parameters computed for promolecule data indicate that these easily obtained results offer a method of calculating bond critical properties which are close in value to the more extensive results derived from molecular orbital calculations.

Dedication

I would like to dedicate this to my grandfather, Oliver Frederick Feth, who passed away last year. Granddad always wanted a Doctor in the family.

Acknowledgments

There are many, people who's contributions have made this degree possible. First and foremost, I would like to thank my advisor, Professor G.V. Gibbs, (Jerry). Not only has Jerry conceived this project, but he has put an enormous amount of time and effort into it. His guidance and criticism have been invaluable to me. I have been fortunate to work with such an well-known and admired scientist.

I would also like to thank the other members of my committee, especially Dr. Boisen. Everyone has been immensely supportive in my endeavors to complete this. My sincere thanks to each member; Monte, Rick, Ron, Deidre and Mike. Their time and effort have made this a reality.

The National Science Foundation and the College of Engineering at Virginia Tech is thanked for their support of the Charles Minor Fellowship Program which has supported me. The National Science Foundation is again thanked for supporting the promolecule study with Grant EAR–8803933. Professor Linus Pauling is thanked for his suggestion that I consider the relation, as done in Fig. 7, between the values of the radii and the values of the electronegativity of atoms participating in the bonds. I am grateful to J.W. Downs of Ohio State University for kindly supplying me with the bonded radii determined in his careful study of the electron density distribution of danburite. Also, R.F. Bader is thanked for kindly supplying his AIMPAC programs, and R.T. Downs for use of the SPEEDEN program. I would also like to thank Fran Hill. Although not officially a committee member, she has served as an advisor and friend.

A special thanks goes to Paul Tidwell, my fiancé, who has unfailingly been there through the trials and triumphs. Thanks for your steadfast support and understanding. Having you there has made all the difference.

There are many other people who deserve recognition. In particular, I'd like to thank my family, especially my parents, who have played such a big role both financially and emotionally. Also my Aunts, who have always taken the time to listen. I would be remise without mentioning a number of friends who have been there through it all; Cindy Walker, (especially lately), who has taken care of so many details when I just can't seem to get to them, Liz Walker, who has listened for hours to my tales and Melanie Ott, who has been there through the years serving as emotional support and sounding board.

A sincere thanks to everyone, mentioned and non–mentioned. Without your support, this would not be possible.

Contents

List of Tables

List of Figures

Notation

R(*M*N)	Length of the *M*N Bond
r_b(N)	Bonded Radius of the Nitride Anion
$\rho(\mathbf{r}_c)$	Electron Density Distribution Evaluated at the Bond Critical Point
λ_1 or λ_2	Curvature of the Electron Density Distribution Perpendicular to the Bond at the Bond Critical Point
$\lambda_{1,2}$	Average Curvature of the Electron Density Distribution Perpendicular to the bond at the Bond Critical Point, $\lambda_{1,2} = (\lambda_1 + \lambda_2)/2$
λ_3	Curvature of the Electron Density Distribution Parallel to the Bond at the Bond Critical Point
$\nabla^2\rho(\mathbf{r}_c)$	Laplacian of the Electron Density Distribution Evaluated at the Bond Critical Point, $\nabla^2\rho(\mathbf{r}_c) = \lambda_1 + \lambda_2 + \lambda_3$
χ_M	Relative Electronegativity of the *M*-Cation in an *M*N Bond
r_p	Promolecule Radius
$\chi_{(M)p}$	Relative Electronegativity of the *M*-Cation in an *M*N bond for a Promolecule

1 Introduction

The way atoms interact with each other determines the macroscopic properties of a given material such as its strength, refractive index, ductility and elasticity. These properties, in turn, can be used to design materials that are better suited for specific applications and needs. For example, high performance aircraft are being constructed of lighter and stronger materials that have been specifically designed for the aerospace industry. Engineers and scientists take advantage of the carefully studied and documented properties of new materials. In addition, much research has gone into attempts to develop materials that have the desired characteristics without some of the disadvantages commonly associated with such materials. As an example, strong materials able to withstand high temperature are sometimes desirable. Since each specific material trait is directly related to its structure, an understanding of structure is imperative. The structure in turn is dependent on the interactions between its constituent atoms. In crystals or molecules, these interactions are governed by the bonds between atoms. Therefore, a better understanding of bonding and a systematic way of characterizing it can provide important clues to materials characteristics and properties.

Previous research has shown that gas phase molecules can be used to undertand the structure of crystals. In 1939, J.C. Slater theorized that the forces that bind the cations of diamond are similar to those that bind the cations in cyclohexane. Thus, diamond can be viewed as a giant molecule held together by the same forces found in smaller molecules. This suggests that the forces that govern the structure of diamond behave as if they are short ranged, similar to the behavior in molecules. Almenningen (1963) stated that a structural analysis of the gas-phase molecule disiloxane showed

that the geometry of the SiOSi unit is the same in both the disiloxane molecule and in some silicates. A later structural analysis of solid disiloxane (disilyl ether) by Barrow, (1979) revealed that the geometry of the SiOSi unit is the same in both the solid and gas phases. In 1982 Gibbs also found that the forces that govern the bond lengths and angles of the SiOSi unit in quartz are similar to those found in the disiloxane molecule. As these studies suggest, there is a similarity between the structure of molecules and that of the crystalline materials. This indicates that the forces governing bonding in molecules are similar to the bonding forces in crystalline structures and that small gas phase molecules can be used to study crystalline structures of a similar nature as indicated for diamond and some silicates.

Looking at molecules containing silicon and nitrogen, Julian and Gibbs (1985) found that the trisilylamine Si_3N unit had the same geometry as the Si_3N unit in an α–Si_3N_4 crystal as shown in Fig. 1. The average experimentally observed bond length for the α–Si_3N_4 crystal, is 1.749 Å. I determined the average calculated bond length for the trisilylamine molecule to be 1.748 Å. Angles are also shown in Fig. 1 for the experimentally observed crystal and for the calculated molecule. This close agreement suggests that the arguments presented previously hold for nitrides as well. That is, the arrangements and bonding found in nitride gas phase molecules is similar to that found in nitride crystals.

According to Cremer and Kraka (1984), "The behavior and distribution of electrons around the nucleus constitute the fundamental character of an atom... [and] a detailed analysis of the molecular electron density distribution should yield a valid description of the chemical bond." Recently, theoretical electron density distributions have been successfully used to study interactions between bonded atoms. In partic-

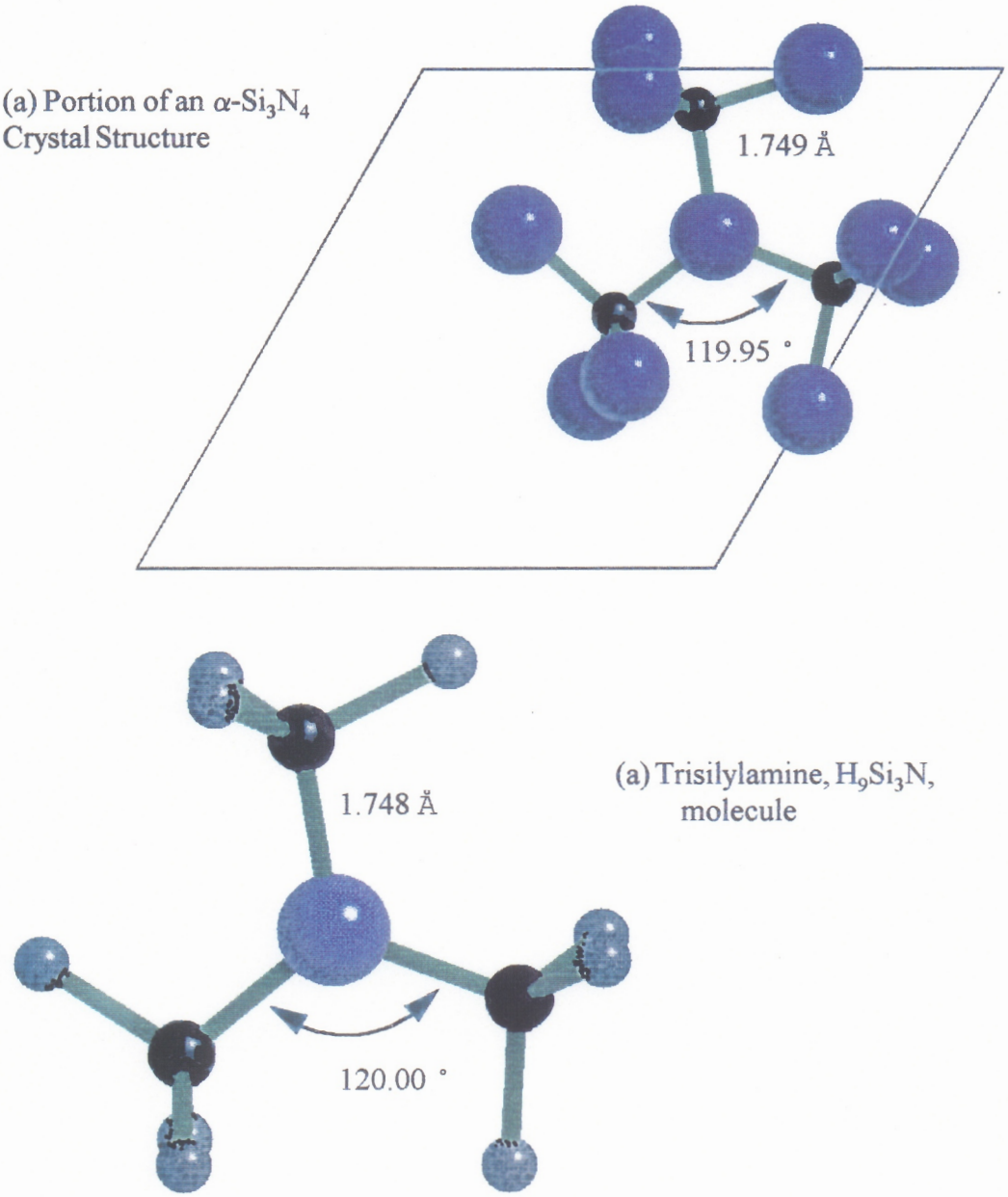

Figure 1: Comparison of the Si_3N Unit from an α-Si_3N_4 Crystal with the Trisilylamine Molecule, H_9Si_3N. The experimentally observed bond length and angle for the α-Si_3N_4 crystal and the calculated, (determined in this study), bond length and angle for trisilylamine are shown.

ular, Bader and Essén (1984) have been successful in defining bonded interactions of each bond in a molecule. In this study, I use both molecular orbital and promolecule calculations to explore the nature of the bonding in nitrides.

A *promolecule* is a molecular model of a small cluster of atoms wherein the electron density of each of the atoms is spherically averaged and centered at its position in the molecule. The calculation of the electron density distribution of a promolecule is a straight-forward and fast computation. Because the promolecule model uses a simple superposition of spherical functions, interactions obtained using this model are reasonable well understood (Spackman and Maslen, 1986). A good approximation of the electron density distribution of a structure can be obtained and studied with this model. Today, these calculations can easily be completed the PC within a few minutes, affording the researcher with a readily available tool for quick insight into atomic interactions.

The molecular orbital model offers a more in-depth understanding of bonding but requires more extensive research and is computationally much more expensive. Both promolecule and molecular orbital calculations have been performed in this study. A comparison of the results provided by both methods is made giving some indication of the limitations of promolecule model.

Nitrides are important because of their unusual properties. Silicon and carbon nitrides are particularly important because of their high strength, wear resistance, excellent thermal-shock properties, low coefficient of friction, and resistance to corrosion, (Wendel and Goddard, 1992; Xu and Ching, 1988). A considerable amount of research has been carried out on these materials, but information on other nitrides is less extensive. In addition, little is known about the nature of the bonds in these ma-

terials and how they vary as one cation is replaced by another. As theoretical models have progressed in accuracy, it is now possible to quantify the nature of bonding in nitrides to a much better degree.

Previous research has shown for a number of insulating materials that the effects of bonding appears to be largely short–ranged. With this in mind, I studied the observed nitride molecules tabulated in Landolt-Börnstein (Callomon et al., 1976 and 1987) and carried out calculations on more than 60 existing and related molecules. I found that the results agree closely with observed results. I determined the geometries associated with the minimum energy and calculated an electron density distribution, $\rho(\mathbf{r})$, for each molecule.

The properties of the electron density at its minimum along a ridge of $\rho(\mathbf{r})$ connecting two atoms can be used to define bond characteristics. This minimum in the ridge is known as the bond critical point, bcp. In this study, I will calculate the properties of the bcp for each of the molecules. How the bcp properties vary with the relative electronegativities of the M–cation in the MN bonds and the character of the bonds will be explored. The trends obtained in this study provide a basis for accessing the character of the bonds.

2 Promolecule Calculations of Bonded Radii

2.1 Introduction

The observed electron density, $\rho(\mathbf{r})$, adopts an arrangement in a crystal wherein the total energy of the resulting configuration is minimized (Bader, 1981). Within this context, a well–defined set of radii known as bonded radii can be derived by measuring along the bond path the distances between the bonded atoms and the (3,–1) critical point, (Bader, 1990). See appendix A for a definition of a (3,–1) critical point. These radii provide a measure of the sizes of ions, particularly as size relates to the electron density distribution along the path connecting a pair of bonded atoms. In addition, it has been asserted that bonded radii may provide an improved and more realistic basis for correlating and understanding physical and chemical properties that depend on the electron density distribution. For example, Cahen (1988) found that the ease with which Cu can be leached from enargite, Cu_3AsS_4, is much more easily understood in terms of a crystal structure constructed of atoms with bonded radii rather than from one constructed with either ionic or crystal radii.

In recent years, bonded radii, $r_b(X)$, calculated for the X–cations in a variety of nitride, oxide, fluoride and sulfide molecules were found to increase with increasing minimum energy bond lengths (Spackman and Maslen, 1986; Gibbs et al., 1987; Bartelmehs et al., 1989; Buterakos et al., 1992; and Nicoll, 1993). Similarly, the bonded radii of the anions in these molecules were also found to increase in size with increasing bond length. This is in sharp contrast with ionic and crystal radii where each cation and anion is assumed to have a given radius for a given coordination number, all other properties such as spin state, oxidation number, etc., being equal. In a discussion of the significance of the radii of the ions in the alkali halides, Slater

(1965) observed that the bonded radius of the chloride ion, $r_b(Cl)$, obtained for the longer KCl bond in sylvite is $\sim$ 0.15 Å larger than that derived for the shorter NaCl bond in rock salt. More recently, a similar result was reported (Gibbs et al., 1992) for the oxide ion in coesite where $r_b(O)$ is observed to increase from 0.92 to 0.97 Å as the SiO bond lengths in the mineral increase from 1.595 to 1.621 Å. It is noteworthy that these radii are smaller than either Wasastjerne's ionic radius (Wasastjerne, 1923) of the oxide ion (1.32 Å) or Shannon and Prewitt's crystal radius (1969) (1.26 Å) and larger than its atomic radius (0.65 Å).

Promolecule radii, r_p, similar to bonded radii can be found using a promolecule model. A calculation of the promolecule radii for the ions comprising the coordinated polyhedra (assuming observed geometries) for a number of alkali halides shows that the resulting radii match those derived by Tosi and Fumi (1964) to within 0.04 Å, on average. Gibbs et al. (1992) also showed that the promolecule radius of the oxide ion calculated for the silicate tetrahedra in the high pressure silica polymorph, coesite, shows a similar increase with bond length. Further, promolecule radii match observed bonded radii to within $\sim$ 0.02 Å as shown in Fig. 2. The bonded radii were calculated for the atoms comprising the SiO_4, SiO_6, BeO_4, BO_4 and CaO_7 coordinated polyhedra in the minerals stishovite, SiO_2, bromellite, BeO, and danburite, $CaB_2Si_2O_8$, (Spackman et al., 1987; Downs, 1991; Downs and Swope, 1992). This close agreement suggests that promolecule radii, calculated for the atoms that comprise the coordinated polyhedra within a crystal can provide reasonable estimates of their bonded radii, despite the rearrangement in $\rho(\mathbf{r})$ that may occur upon bond formation.

Promolecule radii calculated for the bonded atoms that comprise the coordinated

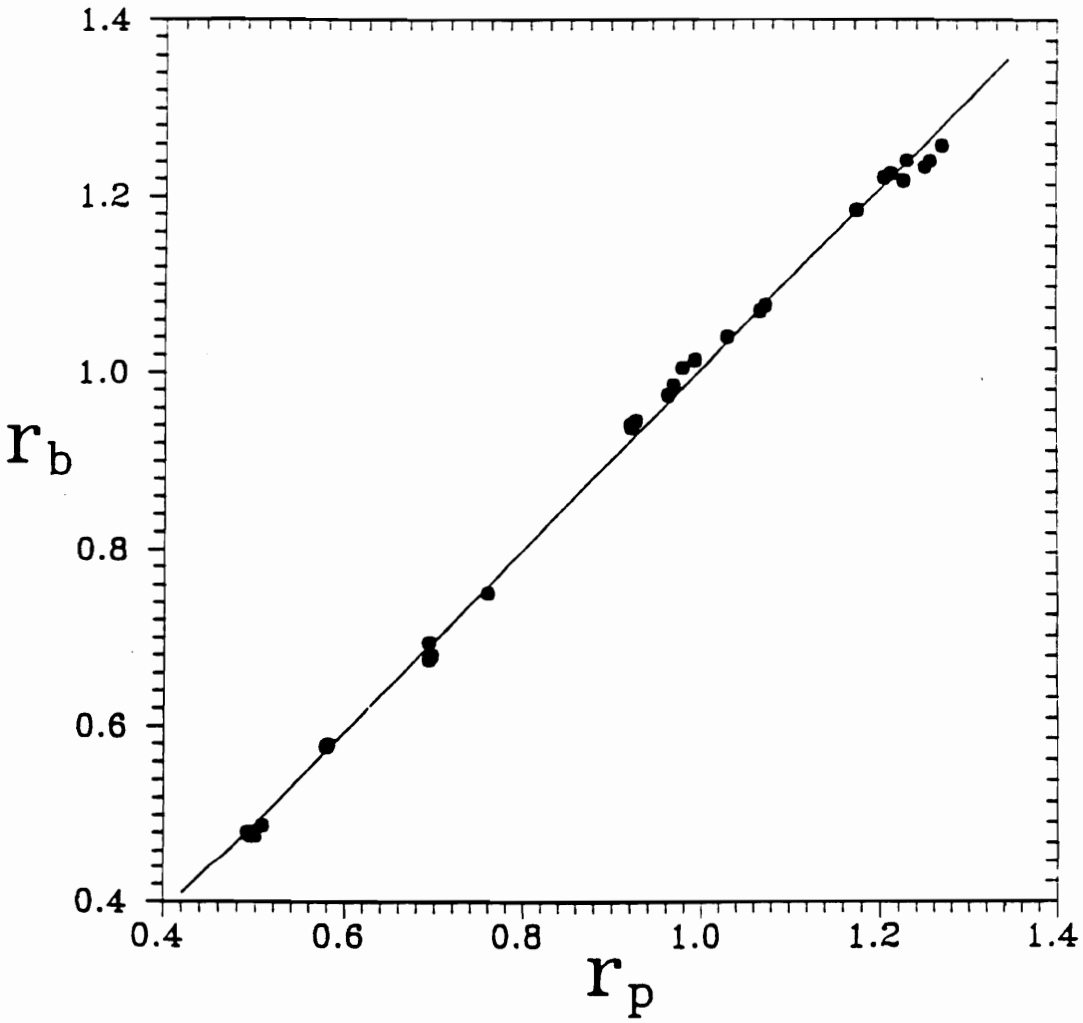

Figure 2: Promolecule radii, $r_p(N)$, calculated for the atoms comprising the SiO_4, SiO_6, BO_4, and CaO_7 coordinated polyhedra in stishovite (SiO_2), bromellite (BeO), and danburite ($CaB_2Si_2O_8$), versus bonded radii (r_b) obtained from experimental electron density maps.

polyhedra of a crystal also show a close correspondence with procrystal radii calculated for the crystal, (Nicoll, 1993). A *procrystal* is a model of the electron density distribution within a crystal where, like a promolecule, $\rho(\mathbf{r})$ is generated by the superposition of spherical free–atoms, each located at its observed positions in the crystal, (Coppens, 1982). Such a model has been used by crystallographers for more than 50 years in the calculation of structure factors and in a determination of least–squares estimates of the positional and thermal parameters of the atoms of a crystal. Like a promolecule radius, the procrystal radius of an atom is defined to be the distance between the position of an atom and a (3,–1) critical point in the electron density measured in the direction of a bonded atom. Procrystal radii have also been calculated for the atoms in structure analyses of danburite, $CaB_2Si_2O_8$, (Downs, 1991) and bromellite, BeO, (Downs and Swope, 1992). Nicoll (1993) has found that the promolecule radii calculated for the coordinated polyhedra of these minerals agree in each case to within 0.002 Å with the procrystal radii. Since the radial functions used to mimic the electron density in a procrystal or promolecule drop off rapidly, the effects of next nearest neighbor atoms should be minimal. Thus, promolecule radii for coordinated polyhedra are expected to match the procrystal radii.

During the last twenty five years, several precise sets of ionic and crystal radii have been derived for oxides (Shannon, 1976), sulfides (Shannon, 1981), and nitrides (Baur, 1987). Since promolecule radii can provide reasonable estimates of bonded radii, sets of promolecule radii were calculated in this study for a variety of regular coordinated polyhedra to examine how well they match and correlate with the ionic and crystal radii. The calculations were completed on nitride, oxide and sulfide coordinated polyhedra containing non–transition and transition metal cations from

the first four rows of the periodic table (Feth et al., 1993). This study shows that high correlations are obtained between promolecule radii and both ionic and crystal radii. It also shows that the promolecule radii for the cations tend to be larger than such radii whereas those for anions tend to be smaller except for highly ionic bonds where promolecule radii tend to match ionic and crystal radii.

2.2 Correlations of Ionic and Crystal Radii with Promolecule Radii

2.2.1 Nitride Radii:

Using more than 500 XN bond lengths observed for a variety of crystals, Baur (1987) derived a set of empirical ionic radii for the nitrides. These radii serve to reproduce bond length data with a precision of $\sim$ 0.02 Å if such local factors as coordination number, oxidation number, etc., are taken into account. Promolecule radii were calculated for the electron density distributions of promolecule representations of triangular XN_3 – tetrahedral XN_4 – and octahedral XN_6 – coordinated polyhedra (Table 1). Using the software PROMIN, (Gibbs et al., 1992), the total electron density distribution for each promolecule was generated, and the (3,–1) critical point of the electron density was found along the line between the atoms. In the calculations, R(XN) was fixed at the sum of the radii of the X cation (Baur, 1987) and the nitride anion assuming a constant radius of 1.46 Å. As observed above, the promolecule radius for each atom was taken to be the distance between the atom and the point of minimum electron density in the direction of a bonded atom. In these calculations and the others completed for oxide and sulfide coordinated polyhedra, the gradient for each point of minimum electron density revealed that the point qualifies as a (3,–1) critical point, see Appendix A (Bader, 1990).

The promolecule radii calculated for the non–transition and transition cation containing nitride coordinated polyhedra are compared in Fig. 3 with the ionic radii derived for them by Baur (1987). As evinced by Fig. 3a, the promolecule radii are highly correlated with the ionic radii of the non–transition metal cations for the first four rows of the periodic table (coefficient of determination, $r^2 = 0.99$). In addition,

Table 1: Promolecule Radii, $r_p(X)_N$, $r_p(X)_O$ and $r_p(X)_S$, for X-cations in Nitrides, Oxides and Sulfides

X	$r_p(X)_N$	$r_p(X)_O$	$r_p(X)_S$	X	$r_p(X)_N$	$r_p(X)_O$	$r_p(X)_S$
$^{IV}Ag^{+1}$			1.31	$^{IV}Cu^{+2}$		1.00	
$^{VI}Ag^{+1}$			1.34	$^{VI}Cu^{+2}$	1.09	1.07	
$^{VI}Ag^{+3}$		1.25		$^{VI}Fe^{+2}LS$	1.01		1.07
$^{IV}Al^{+3}$	0.81	0.78	0.89	$^{IV}Fe^{+2}HS$		1.02	1.11
$^{VI}Al^{+3}$		0.83	0.95	$^{VI}Fe^{+2}HS$		1.09	1.17
$^{IV}As^{+5}$		0.84	1.04	$^{VI}Fe^{+3}LS$	1.01		1.08
$^{III}B^{+3}$	0.49	0.47	0.63	$^{IV}Fe^{+3}HS$		0.96	1.07
$^{IV}B^{+3}$	0.53	0.50	0.76	$^{VI}Fe^{+3}HS$		1.03	1.13
$^{III}Be^{+2}$	0.57	0.55		$^{VI}Fe^{+4}$			1.08
$^{IV}Be^{+2}$	0.61	0.58	0.64	$^{IV}Ga^{+3}$	0.97	0.92	1.05
$^{IV}Br^{+7}$		0.82		$^{VI}Ga^{+3}$		0.99	1.13
$^{III}C^{+4}$		0.49	0.80	$^{IV}Ge^{+4}$	0.93	0.87	1.03
$^{IV}Ca^{+2}$	1.23			$^{VI}Ge^{+4}$		0.94	
$^{VI}Ca^{+2}$	1.26	1.22	1.31	$^{VI}I^{+5}$		1.29	
$^{IV}Cd^{+2}$	1.19	1.16	1.26	$^{IV}I^{+7}$		0.94	
$^{VI}Cd^{+2}$		1.24	1.34	$^{VI}I^{+7}$		1.01	
$^{IV}Cl^{+7}$		0.69		$^{IV}In^{+3}$	1.14	1.07	1.21
$^{VI}Co^{+2}$			1.11	$^{VI}In^{+3}$		1.15	1.28
$^{VI}Co^{+2}LS$	1.00			$^{IV}K^{+1}$		1.43	1.51
$^{IV}Co^{+2}HS$		1.00	1.08	$^{VI}K^{+1}$	1.49	1.44	1.52
$^{VI}Co^{+2}HS$	1.08	1.07		$^{III}Li^{+1}$	0.77		
$^{VI}Co^{+3}$			1.07	$^{IV}Li^{+1}$	0.79	0.76	0.83
$^{VI}Co^{+3}LS$	1.00	0.98		$^{VI}Li^{+1}$	0.83	0.82	0.88
$^{VI}Co^{+3}HS$		1.01		$^{IV}Mg^{+2}$	0.93	0.88	0.97
$^{IV}Co^{+4}$		0.92		$^{VI}Mg^{+2}$	0.95	0.94	1.04
$^{VI}Cr^{+3}$	1.06	1.02	1.13	$^{VI}Mn^{+2}$			1.21
$^{IV}Cr^{+4}$		0.93		$^{IV}Mn^{+2}HS$	1.07	1.04	1.13
$^{VI}Cr^{+4}$			1.11	$^{VI}Mn^{+2}HS$	1.13	1.12	
$^{IV}Cr^{+6}$		0.87		$^{VI}Mn^{+3}$			1.15
$^{IV}Cu^{+1}$			1.10	$^{VI}Mn^{+3}HS$		1.03	

Table 1: Promolecule Radii, continued

X	$r_p(X)_N$	$r_p(X)_O$	$r_p(X)_S$	X	$r_p(X)_N$	$r_p(X)_O$	$r_p(X)_S$
$^{VI}Mn^{+4}$		0.98	1.10	$^{IV}Ru^{+7}$		0.98	
$^{IV}Mn^{+6}$		0.86		$^{IV}S^{+6}$		0.64	
$^{IV}Mn^{+7}$		0.86		$^{IV}Sb^{+5}$			1.16
$^{VI}Mo^{+3}$			1.26	$^{VI}Sb^{+5}$		1.04	
$^{IV}Mo^{+4}$	1.08			$^{VI}Sc^{+3}$		1.09	1.20
$^{VI}Mo^{+4}$	1.15		1.23	$^{IV}Se^{+6}$		0.82	
$^{IV}Mo^{+6}$		1.00	1.15	$^{IV}Si^{+4}$	0.74	0.70	0.85
$^{VI}Mo^{+6}$		1.08	1.22	$^{VI}Si^{+4}$		0.76	
$^{III}N^{+5}$		0.60		$^{IV}Sn^{+4}$			1.17
$^{IV}Na^{+1}$	1.10	1.09	1.16	$^{VI}Sn^{+4}$	1.15	1.09	1.25
$^{VI}Na^{+1}$	1.15	1.10	1.19	$^{VI}Sr^{+2}$		1.37	1.46
$^{VI}Nb^{+3}$	1.17		1.28	$^{IV}Tc^{+7}$		0.97	
$^{VI}Nb^{+4}$			1.26	$^{IV}Te^{+4}$		1.07	1.27
$^{VI}Nb^{+5}$		1.11	1.25	$^{VI}Te^{+4}$		1.28	
$^{IV}Ni^{+2}$		0.98	1.05	$^{VI}Te^{+6}$		1.02	
$^{VI}Ni^{+2}$	1.07	1.04		$^{VI}Ti^{+2}$			1.17
$^{VI}Ni^{+3}LS$		0.98	1.10	$^{VI}Ti^{+3}$		1.06	1.16
$^{VI}Ni^{+3}HS$			1.12	$^{IV}Ti^{+4}$	1.01		
$^{VI}Ni^{+4}$			1.07	$^{VI}Ti^{+4}$			1.15
$^{IV}P^{+5}$	0.68	0.65	0.94	$^{VI}V^{+2}$		1.10	
$^{VI}Pd^{+2}$		1.22		$^{VI}V^{+3}$		1.04	1.14
$^{VI}Pd^{+3}$		1.17		$^{VI}V^{+4}$			1.12
$^{IV}Rb^{+1}$			1.65	$^{IV}V^{+5}$		0.91	1.06
$^{VI}Rb^{+1}$	1.63	1.57		$^{VI}Y^{+3}$	1.28	1.22	1.33
$^{VI}Rh^{+3}$	1.14		1.22	$^{IV}Zn^{+2}$	1.02	1.00	1.09
$^{VI}Rh^{+5}$		1.07		$^{VI}Zn^{+2}$		1.06	1.15
$^{VI}Ru^{+2}$	1.16			$^{IV}Zr^{+4}$	1.14		
$^{VI}Ru^{+3}$	1.16	1.13	1.23	$^{VI}Zr^{+4}$	1.21	1.15	1.29
$^{VI}Ru^{+4}$			1.22				

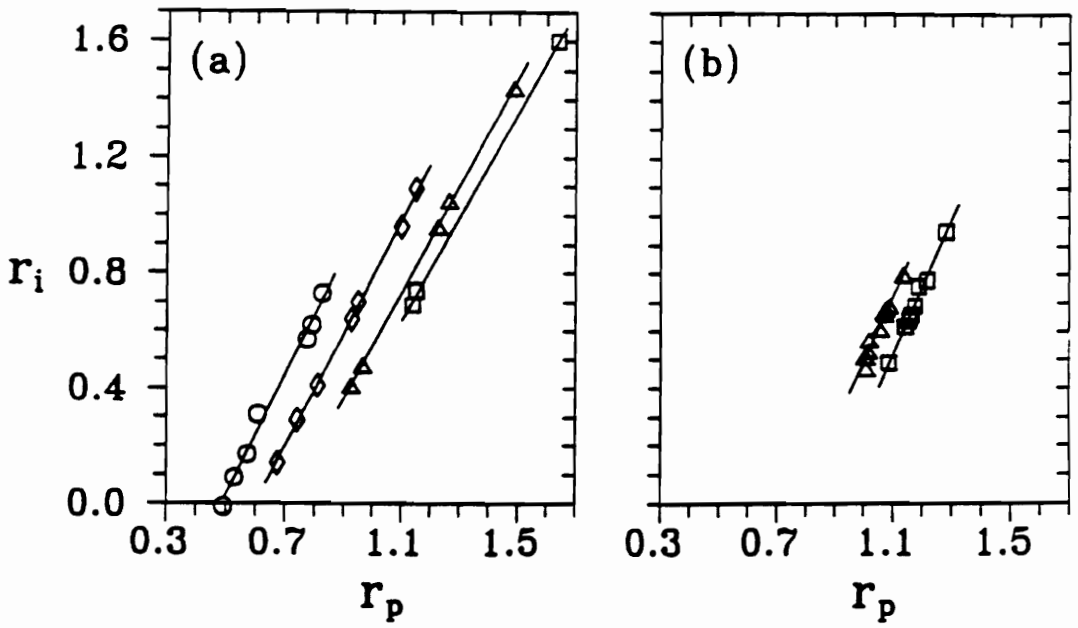

Figure 3: Promolecule radii, r_p for cations plotted versus ionic radii, r_i, derived by Baur for (a) non–transition and (b) transition metal cations bonded to the nitride ion. Radii for first–row cations are plotted as circles, those for second–row cations are plotted as diamonds, those for third–row cations are plotted as triangle and those for fourth–row cations are plotted as squares.

the promolecule radii calculated for transition metal atoms for the third and fourth rows of the periodic table are also highly correlated, $r^2 = 0.98$, with the ionic radii (Fig. 3b). The slopes of the regression lines calculated for the non-transition cations range from 2.08 for row 1 to 1.97 for row 2 to 1.85 for row 3 to 1.79 for row 4, whereas those for the transition metals for rows 3 and 4 are both 2.38. A test for parallelism of the regression lines for non–transition metal cation data indicates that their slopes are significantly different with their slopes decreasing in a regular way with row number (see Appendix B). On the other hand, the slopes for the lines determined for the transition metal atoms are identical, but they are not as large as those for the non–transition metal atoms. When the two data sets are separated on the basis of coordination number, regression analyses did not result in improved fits. This result suggests that the trends in Fig. 3 are largely independent of coordination numbers assumed in the calculations.

As observed for the bonded and promolecule radii of the nitride ion in nitride molecules, $r_p(N)$, increases with R(XN) (Buterakos et al., 1992; Gibbs et al., 1992). It ranges between 0.87 Å when bonded to $^{IV}Mo^{4+}$ and 1.43 Å when bonded to a more electropositive cation like $^{VI}Rb^{+}$. The promolecule radius of the nitride anion calculated for RbN_6 matches the 6–coordinate ionic radius of the anion (1.46 Å) assumed by Baur, (1987), to within 0.03 Å. On the other hand, when it is bonded to a more electronegative cation, $r_p(N)$ matches more closely the atomic radius of N, (0.75 Å). In other words, when the nitride anion is bonded to a highly electropositive cation, its radius tends to match its ionic radius, but when it is bonded to a more electronegative cation, it tends to be much smaller and to match its atomic radius. Also the promolecule radius of the Rb cation (1.63 Å) matches the ionic radius (1.60 Å) of Rb^{+}

equally well. On the other hand, the promolecule radius of the more electronegative Mo^{4+} cation is much larger (1.08 Å) than its ionic radius (0.49 Å).

The radii derived by Baur (1987), Shannon and Prewitt (1969), and Shannon (1976 and 1981), are relative rather than absolute in magnitude, being based on assumed values for the nitride (1.46 Å), oxide (1.26 Å) and sulfide (1.70 Å) ions. Moreover, for a given coordination number, these radii are assumed to show little or no variation with bond length. On the other hand, radii obtained from electron density distributions show a relatively large variation depending on the bond length and the character of the bond. Despite this variability, the well–developed correlations between crystal (and ionic) and promolecule radii (Figs. 3–5) indicate that Baur, Shannon and Prewitt did a very good job ranking the relative magnitudes of their radii. It is also clear that the accuracy with which a set of radii generate bond lengths is independent of the radius assumed for an anion.

2.2.2 Oxide Radii:

Shannon and Prewitt (1969) and more recently Shannon (1976) have derived a set of crystal radii for the oxides using bond length data from more than a 1000 crystalline materials. These radii have been successfully applied over the years as a tool for generating bond lengths, for providing a basis for proposing whether one cation can stably replace another in a given structure type and for generating structural field maps. These radii reproduce averaged bond lengths for coordinated polyhedra with a precision of $\sim$ 0.01 Å when the conditions of the atom and the local chemical environment are taken into account. Promolecule radii, calculated for 3–, 4– and 6–coordinated non–transition and transition atoms (Table 1), are plotted against Shannon's radii (1976) in Fig. 4. As observed for nitride radii, the slopes of the

lines for the non–transition cations are indicated by a test for parallelism, (Appendix B), to be significantly different, decreasing from 2.08 for row 1 to 2.00 for row 2 to 1.78 for row 3 to 1.72 for row 4. The slopes of these lines, although significantly different, are similar to those observed for the nitrides. A test for parallelism of the lines with slopes 2.27 and 2.13 for the third and fourth row the transition metal cations, respectively, indicates that they are slightly but significantly different. The regression line for the first row cations was calculated excluding the radii for highly electronegative $^{III}C^{4+}$ and $^{III}N^{5+}$, data that show a significant departure from the trend established by the other cations of the first row. That for the second row was calculated excluding the radius of the highly electronegative Cl^{+7} cation which departs from the trend established by the other second row cations. No explanation is offered to clarify why the promolecule radii for these cations are larger than might be expected from the trends established by the other first and second row cations. It is noteworthy, however, that the radii that depart from the trends are for cations with high oxidation states. None of the radii for third and fourth row cation departs from the trends.

As observed for the nitride ion, the promolecule radius of the O atom correlates with R(XO) with its radius ranging between 0.68 Å in $N^{5+}O_3$ to 1.32 Å in KO_6. It is noteworthy that $r_p(O)$ in KO_6 is 0.06 Å larger than that derived for the oxide ion by Shannon and Prewitt (1969), but that it agrees exactly with that measured by Wasastjerne (1923) in his studies of dielectric constants and refractive indices of ionic crystals. For oxides, as observed for the nitrides, promolecule radii obtained for ionic bonds tend to match ionic radii. For the more covalent bonds, the promolecule radii obtained for cations tend to be larger than those obtained for cations whereas those

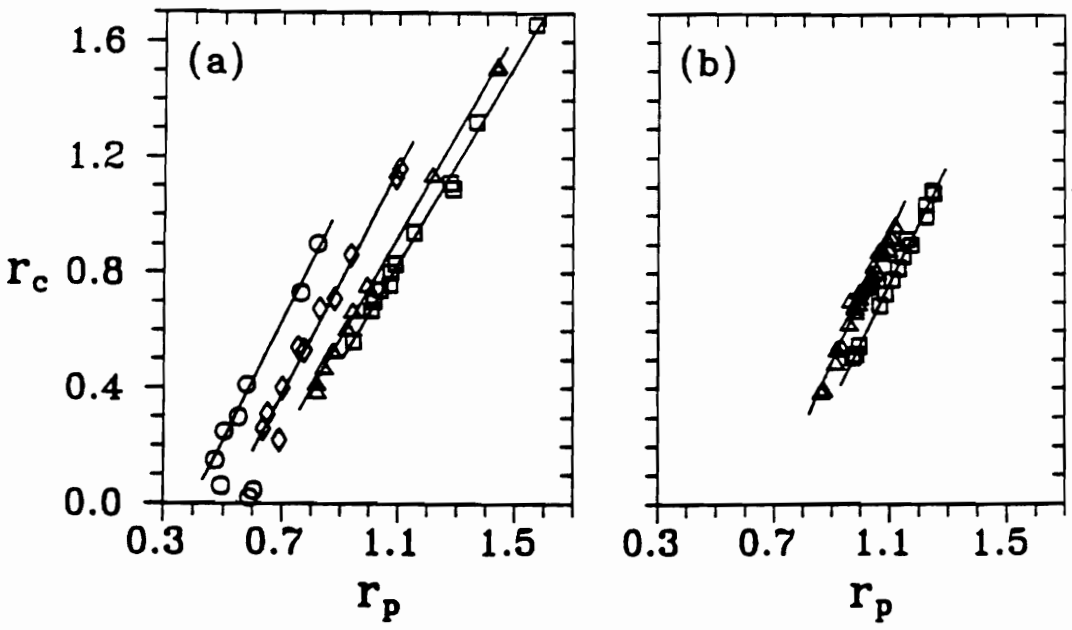

Figure 4: Promolecule radii, r_p(N), for cations plotted versus crystal radii, r_c, derived by Shannon for (a) non–transition and (b) transition metal cations bonded to the sulfide ion. See legend for Figure 2 for description of symbols.

for the oxide ion tend to be smaller and to approach the atomic radius of the O atom (0.65 Å).

2.2.3 Sulfide Radii:

Crystal radii have also been derived from bond length data recorded for more than 750 sulfide structures and molecular complexes. Promolecule radii were calculated for 3–, 4– and 6–coordinate polyhedra (Table 1) with bond lengths fixed at the sum of radius of the sulfide ion (1.70 Å) and the radii of the cations derived by Shannon, (1981). As observed for the other two data sets, the slopes of the regression lines fit to the promolecule and the crystal radii data, plotted in Fig. 5, are statistically different, (Appendix B). The slopes decrease for the non–transition metal radii from 2.86 for row 1 to 2.22 for row 2 to 2.13 for row 3 to 2.08 for row 4. The correlations for the four data sets are well–developed with r^2– values ranging between 0.87 and 0.99. The slopes of the regression lines fit to the transition metal radii for rows 3 and 4, 2.50 and 2.94 respectively, are also significantly different. The regression line for the first row cations was calculated omitting the radii for $^{III}C^{+4}$ and $^{IV}B^{+3}$ while that for the second row was calculated omitting $^{III}P^{+5}$. As observed for the oxide data in Fig. 4a, the radii for these cations depart from the trend established by the remaining first row cations. Again, the promolecule radii for $^{III}C^{+4}$, $^{IV}B^{+3}$ and $^{IV}P^{+5}$ are larger than might be expected from the trend established by the other first row cations. Again, as observed for the oxide data, the cation radii that depart from the trends in Fig. 4a are for first and second row cations that have relatively large oxidation numbers.

The promolecule radius obtained for the sulfide ion shows a wide range of values as observed in studies of its bonded radius in molecules. It ranges between 0.91 Å when bonded to $^{IV}C^{4+}$ and 1.72 Å when bonded to $^{VI}Li^{+}$. The radius of the S atom

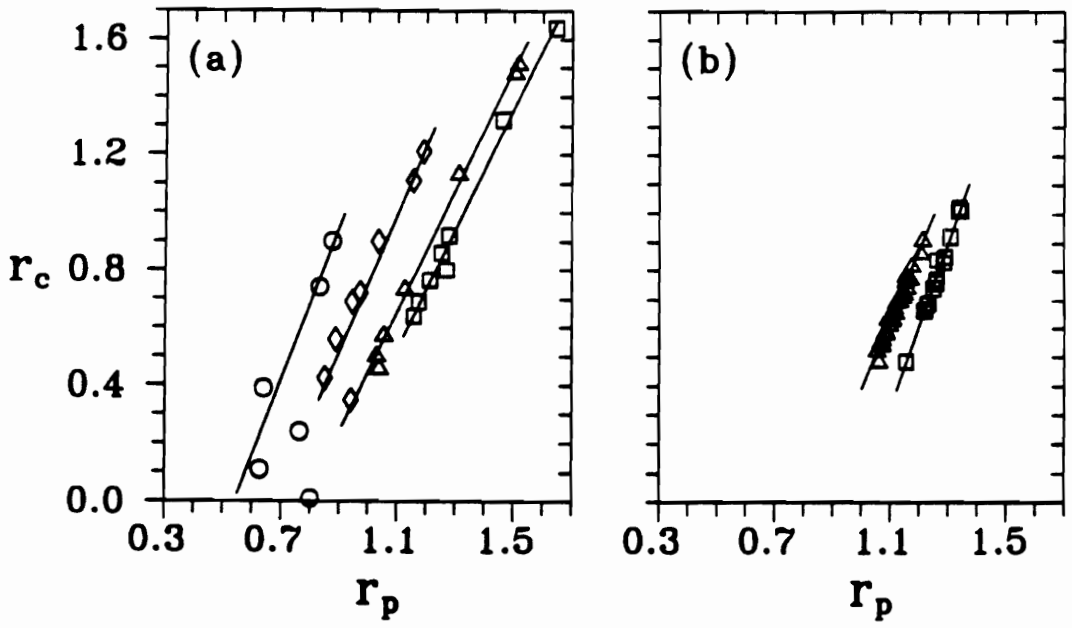

Figure 5: Promolecule radii, r_p(N), for cations plotted versus crystal radii, r_c, derived by Shannon for (a) transition and (b) non-transition metal cations bonded to the sulfide ion. See legend for Figure 2 for description of symbols.

in LiS_6 is 0.02 Å larger than the crystal radius (1.70Å) of the ion derived by Shannon, (1981), and 0.03 Å larger than the ionic radius (1.69 Å) measured by Wasastjerne, (1923). As observed for oxide and nitride ions, the promolecule radius of the S atom closely approximates its ionic radius when it is bonded to an electropositive cation but decreases in size in a regular way as the electronegativity of the cation to which it is bonded increases.

The radii derived by Baur (1987), Shannon and Prewitt (1969), and Shannon (1976 and 1981) are relative rather than absolute in magnitude, being based on assumed values for the nitride (1.46 Å), oxide (1.26 Å) and sulfide (1.70Å) ions. Moreover, for a given coordination number, these radii are assumed to show little or no variation with bond length. On the other hand, radii obtained from electron density distributions show a relatively large variation depending on the bond length and the character of the bond. Despite this variability, the well–developed correlations between crystal (and ionic) and promolecule radii (Figs. 3–5) indicate that Baur, Shannon and Prewitt did a very good job ranking the relative magnitudes of their radii. It is also clear that the accuracy with which a set of radii generate bond lengths is independent of the radius assumed for an anion.

As observed above, radii obtained from electron density maps appear to be independent of coordination number. For example, radii calculated for the atoms comprising a NaCl dimer are strikingly similar to those calculated for a $NaCl_6$ coordinated polyhedron when the bond lengths within both molecules are set at the observed NaCl distance in rock salt. In addition, the resulting promolecule radii agree to within 0.01Å of the bonded radii of Na and Cl ions obtained from the experimental density maps, (Gibbs et al., 1992). The question that arises is how well do promolecule radii, cal-

culated for diatomic molecules, match those calculated for a coordinated polyhedra when the bond lengths in the two are assumed to be the same? In responding to this question, radii were calculated for a series of XO dimers with R(XO) set at the radius sum of the cation and anion used to calculated the promolecule radii. The resulting radii match those used to prepare Fig. 4 almost exactly (Fig. 6). In addition, radii calculated for a number of XN and XS molecules match those used to prepare Figs. 3 and 5 equally as well. These results suggest that promolecule radii are governed in large part by the separation between the atoms that comprise the bond and the electron density distribution of the bonded atoms. However, such radii are not independent of coordination number inasmuch as both the strength and the length of a bond is determined by coordination number.

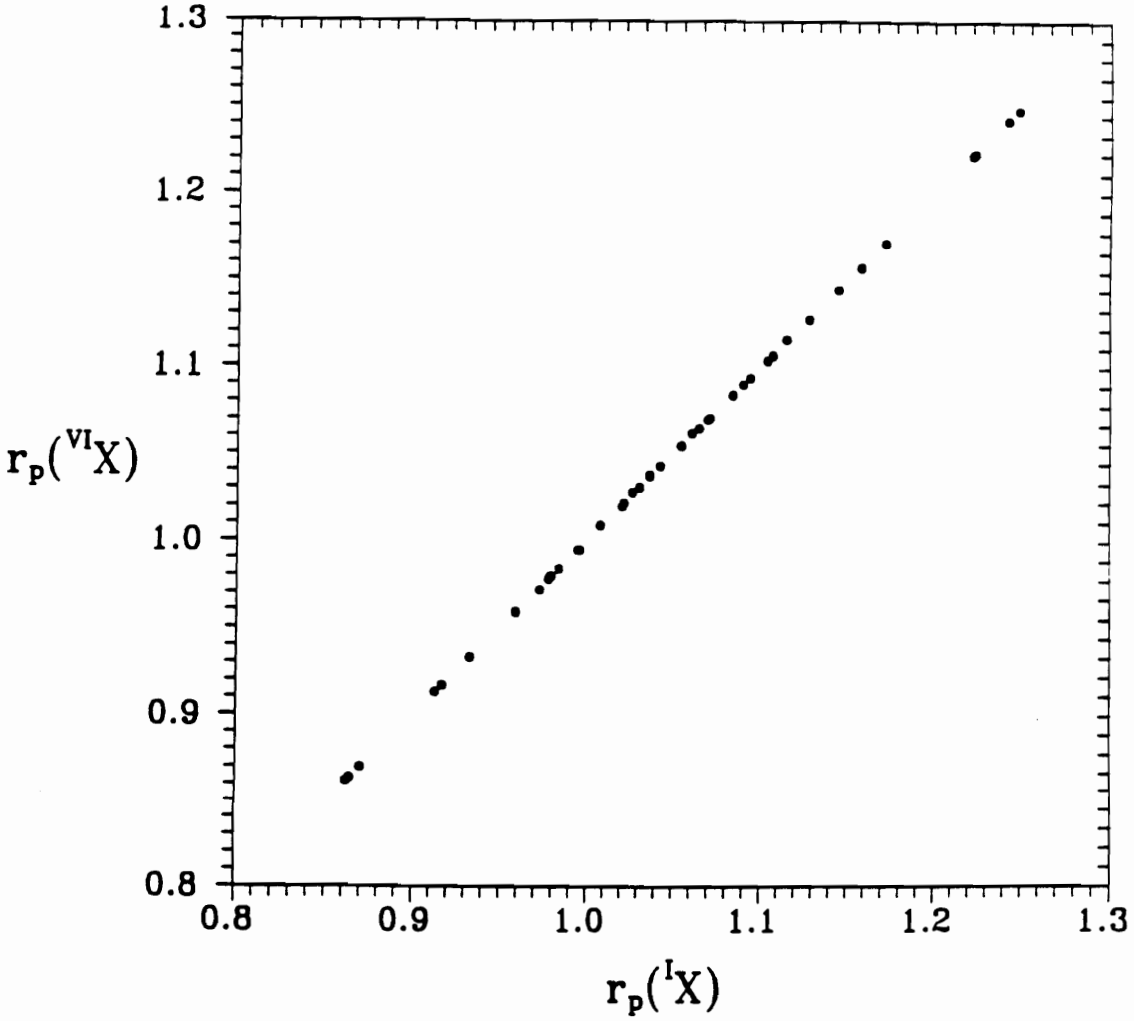

Figure 6: Promolecule radii, $r_p(N)(X)$, used to construct Figure 3 vs. promolecule radii, $r_p(N)(X_{dimer})$, calculated for X-cations for XO dimers.

2.3 Discussion

In the derivations of the various sets of ionic and crystal radii, it was assumed that the radius of a given anion is constant for a given coordination number. With this assumption and with a consideration of various other factors, these radii have been very successful in generating bond lengths that match average bond lengths observed for coordinated polyhedra in crystalline materials. On the other hand, evidence has been available for more than 50 years that indicates that the radius of an oxide ion, for example, may not be constant but may decrease in size as the polarizing power of the cations to which it is bonded increases, (Fajans, 1941). More recently, Johnson, (1973), reported a direct correlation between the polarizing power of a series of cations with the radius of the oxide ion. In this correlation, the radius of the ion was reported to decrease linearly from 1.40 Å when bonded to Rb to $\sim$ 0.8 Å when bonded to Be. He reported a similar correlation for the sulfide ion with its radius decreasing linearly from $\sim$ 1.8 Å when bonded to Rb to $\sim$ 1.4 Å when bonded to Be. In other words, the radii of both the oxide and sulfide ions are indicated to decrease in a regular way as the partial ionic character of the bonds involving these anions decrease, (Pauling, 1960). In an examination of the extent to which the promolecule radius of the oxide ion correlates with the amount of partial ionic character of an XO bond, a scatter diagram (Fig. 7) was prepared of $r_p(O)$ vs. $\chi(X)$, the electronegativity of the cations bonded to the oxide ion for the data used to construct Fig. 4a. An examination of the plot shows that $r_p(O)$ decreases in a regular way from 1.32 Å when $\chi(X)$ is 0.8 (a bond with $\sim$ 85% partial ionic character) to 0.68 Å when $\chi(X)$ is 3.0 (a bond with $\sim$ 5% partial ionic character). In other words, the promolecule radius of the oxide ion varies monotonically from its atomic radius (0.65 Å) when bonded to a

highly electronegative cation to its ionic radius (1.32 Å) when bonded to a highly electropositive cation. Similar correlations obtain for sulfide and the nitride ions.

Finally, as observed by Downs and Swope, (1992), the oxide ions in danburite are highly polarized exhibiting a bonded radius of $\sim$ 0.94 Å in the directions of the SiO bonds, a radius of $\sim$ 1.00 Å in the directions of the BO bonds and a radius of $\sim$ 1.18 Å in the directions of the CaO bonds. As we have seen in this study, promolecule radii calculated for these oxide ions match those observed to within 0.02 Å, on average. This agreement suggests that the polarization of the electron density distribution of an anion is largely a result of the superposition of atomic densities at a given bond length. It also suggests that insofar as the electron density distribution is concerned, the concept of radius as traditionally employed has little physical meaning. Judging from the correlations that obtain between crystal (ionic) and promolecule radii, the evidence seems to reaffirm the observation made by O'Keeffe, (1981), that tables of crystal and ionic radii have little significance other than as tables for generating average bond lengths for coordinated polyhedra.

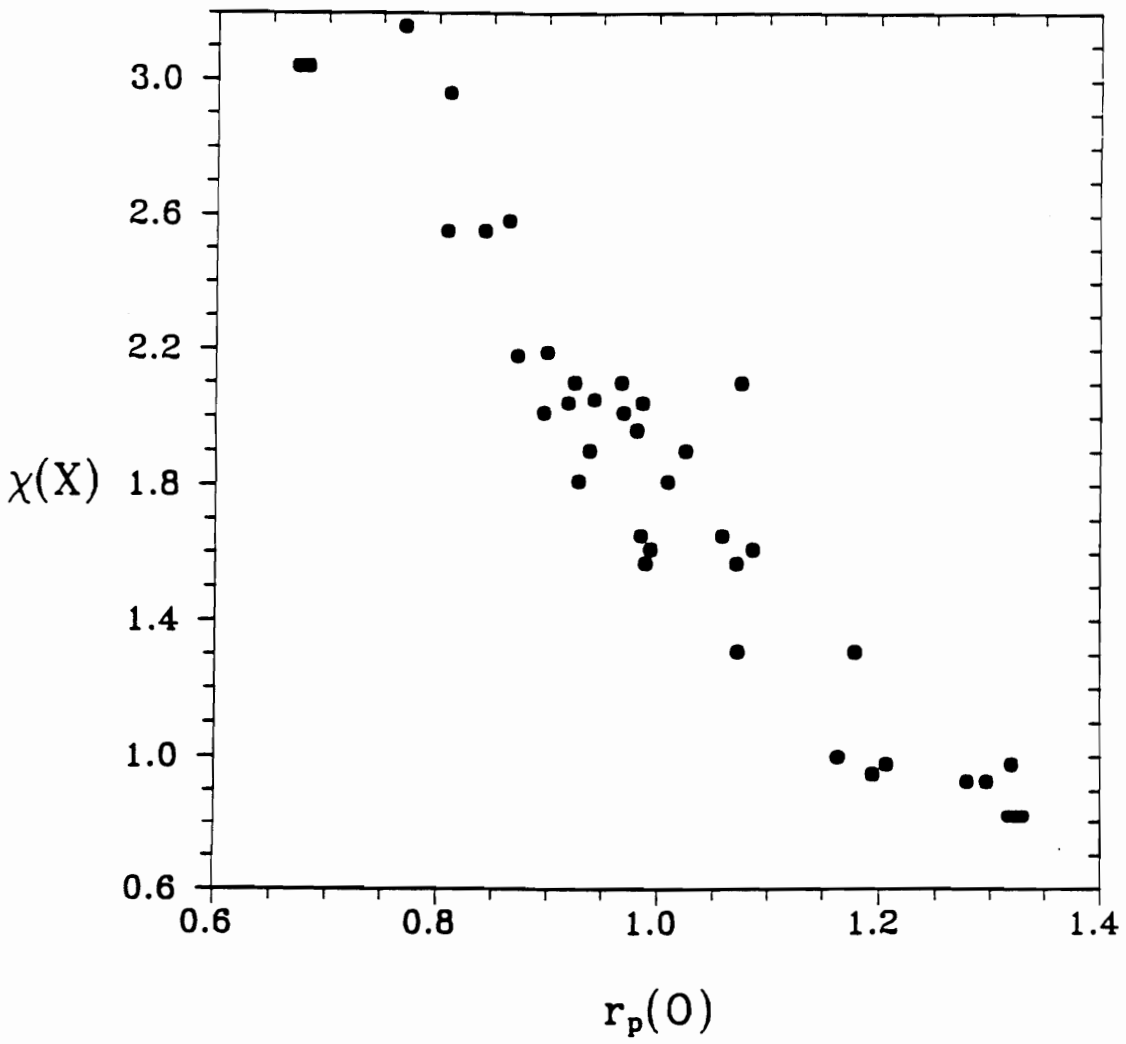

Figure 7: Promolecule radii, $r_p(O)$, calculated for the oxide ion vs. the electronegativity, $\chi(X)$, of the X–cations bonded to the ion for the data used to construct Fig. 3a.

3 Bond Critical Point Properties of the Electron Density Distribution

3.1 Introduction

The properties of electron density distributions, $\rho(\mathbf{r})$, evaluated at bond critical points, bcp or $\mathbf{r_c}$, can be used to classify and describe some aspects of chemical bonding (Bader, 1990). These properties relate well to both experimentally observed parameters as well as those provided by computational quantum mechanics. Bader's bond critical point model combines pertinent information about the value of $\rho(\mathbf{r})$ between two bonded atoms with quantum mechanical based concepts and heuristic ideas on bonding. Consequently, the concepts of atoms, bonds and structure can be defined from a knowledge of the topology of $\rho(\mathbf{r})$.

By studying diatomic molecules, Bader and Essén (1984) proposed a method for evaluating atomic interactions and bond type. In their analysis, they define a bond between two atoms to exist when a ridge of electron density connects the nuclei of the two atoms forming a saddle point which qualifies as a (3,–1) critical point, (see Appendix A). By evaluating the properties of $\rho(\mathbf{r})$ at this point, denoted $\mathbf{r_c}$, they were able to establish a set of criteria for characterizing the nature of the bonding interaction. For purposes of illustration, a level line electron density distribution was calculated in a plane through the Si_3N atoms of the H_9Si_3N molecule (Fig. 8) along with a 3D surface plot of the same distribution (Fig. 9). The central nitride anion can be considered to be bonded to each of the Si cations because ridges of electron density connect the nitride anion with each of the Si cations. On the other hand, the Si cations are not bonded because they are not connected by ridges of $\rho(\mathbf{r})$The distance between the nucleus of the nitride anion and $\mathbf{r_c}$ is defined to be the bonded

radius of the nitride anion, $r_b(N)$.

The eigenvalues of the Hessian (see Appendix A) of $\rho(\mathbf{r_c})$, λ_i (where i = 1,2 or 3) determine the values of the two curvatures of $\rho(\mathbf{r_c})$ perpendicular to the bond, λ_1 and λ_2, and the curvature of $\rho(\mathbf{r_c})$ along the bond, λ_3. The sum of these curvatures is the Laplacian, $\nabla^2\rho(\mathbf{r_c}) = \lambda_1 + \lambda_2 + \lambda_3$. The negative of Laplacian of the electron density distribution for the plane shown in Figs. 8 and 9 is displayed in Fig. 10. This distribution displays those regions where $\rho(\mathbf{r})$ is either enhanced or depleted. Regions of enhancement are delineated by areas where the Laplacian is above the plane whereas regions of depletion are delineated by areas where the Laplacian is lower than the plane.

One of the important features of the Laplacian distribution is the delineation of the shell structure of the atoms. For example, the nitride anion at the center of the map shows a sharp peak ascribed to its K–shell electrons surrounded by a corrugated ridge ascribed to its valence electrons. On the other hand, each Si cation displays two peaks that can be ascribed to its K– and L–shell electrons. As the valence electrons of the M–shell on Si are diffuse, they are poorly delineated in the map (Gibbs, 1994). The bonded interaction between the nitride anion and each of its coordinating Si atoms results in an enhancement of its valence shell along each of the SiN bonds of the molecule. This can be seen in the corrugated appearance of the valence shell for the nitride anion. A single, unbound, ground state nitride atom has a valence shell that appears cylindrical (Kraka and Cremer, 1990 and Fig. 11).

Bader and Essén (1984) use the properties of $\rho(\mathbf{r_c})$ to differentiate between three types of bonds, Fig. 12. A shared (or covalent) interaction is characterized by a value for $\rho(\mathbf{r_c})$ that is relatively large while the value for $\nabla^2\rho(\mathbf{r_c})$ is large in magnitude and

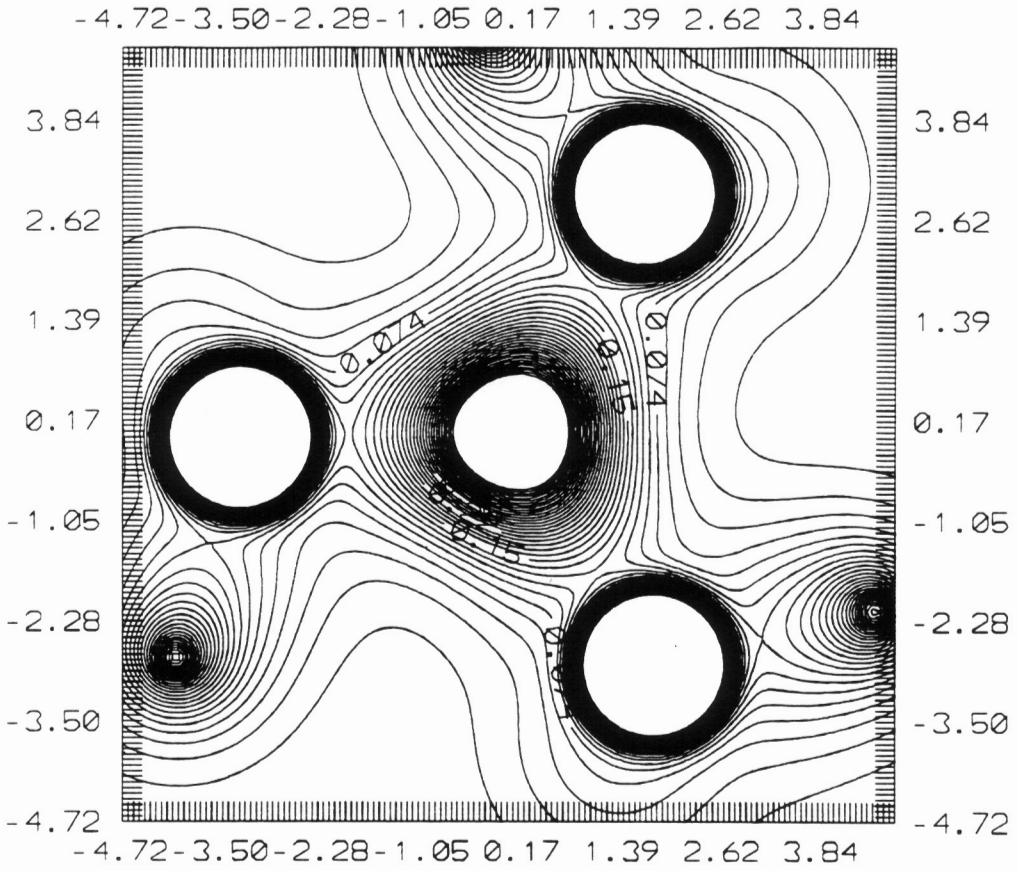

Figure 8: Electron density distribution of H_9Si_3N, a contour plot of the electron density distribution evaluated for the plane containing the silicon and three nitrogen atoms. The contour interval is 0.01 e/Å^3.

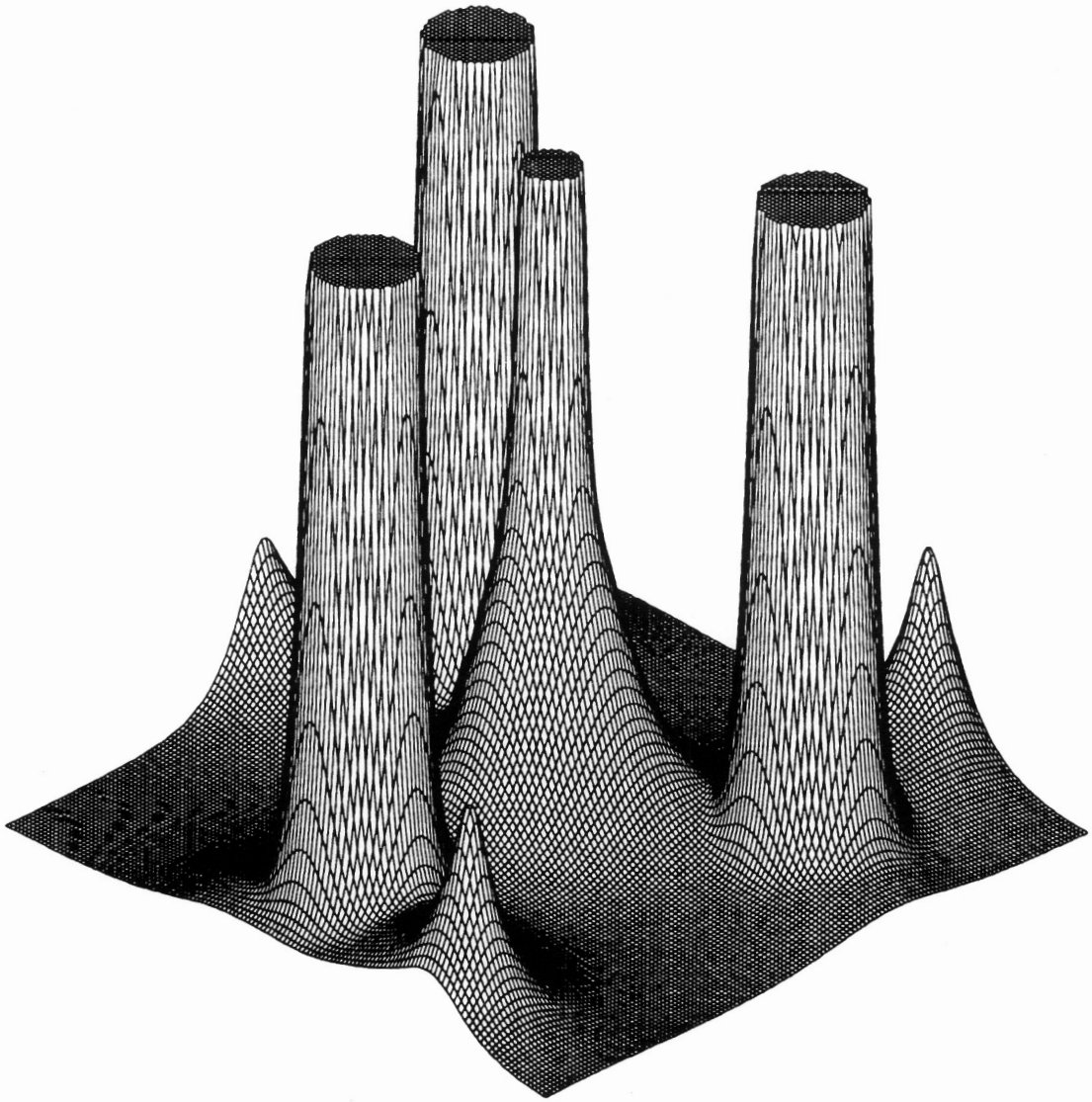

Figure 9: Three–dimensional surface plot of the electron density distribution of the H_9Si_3N molecule evaluated for the same plane as the previous figure. Peaks were truncated for clarity.

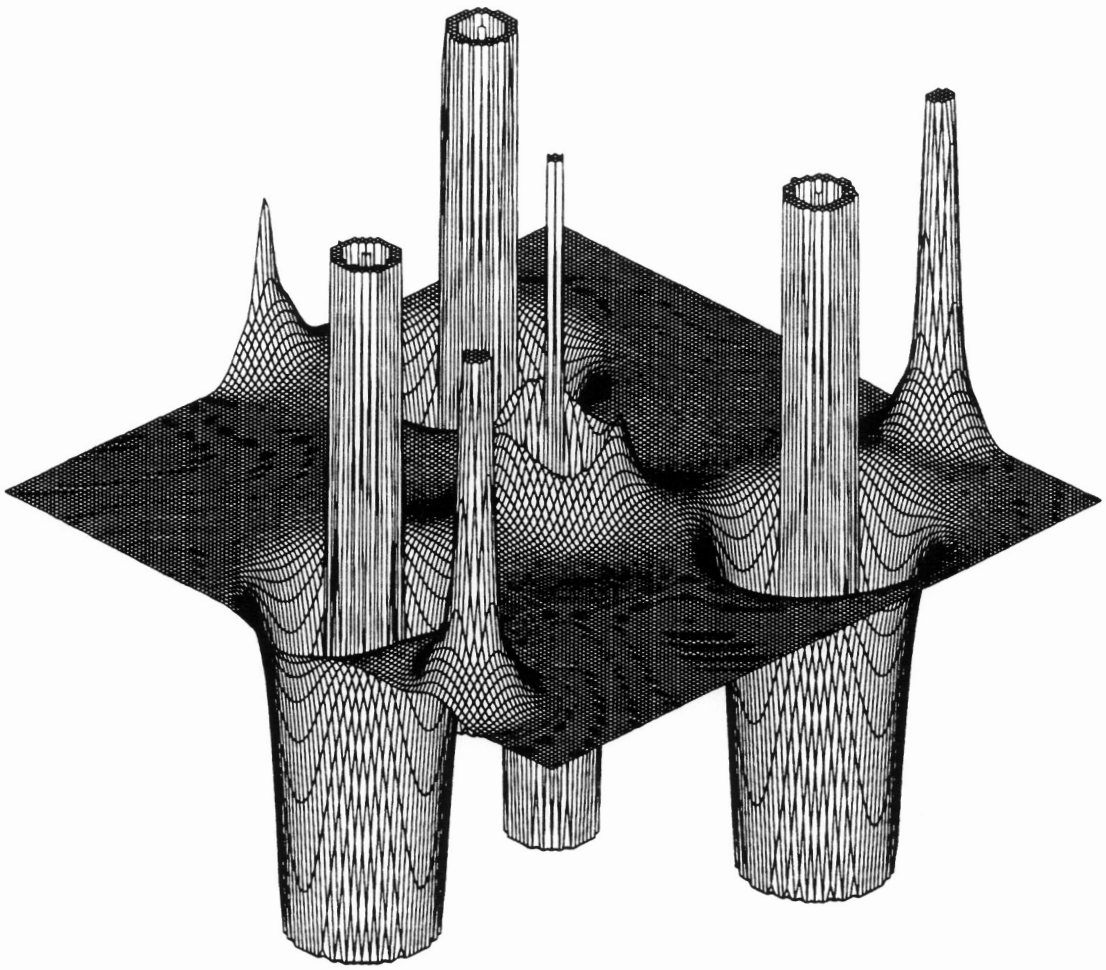

Figure 10: Three–dimensional surface plot of the negative of the laplacian of the electron density distribution for the same plane of the H_9Si_3N molecule as was plotted in Figs. 8 and 9. Notice that the electronic shell structure of the atoms is visible in this type of plot. Again peaks were truncated for clarity.

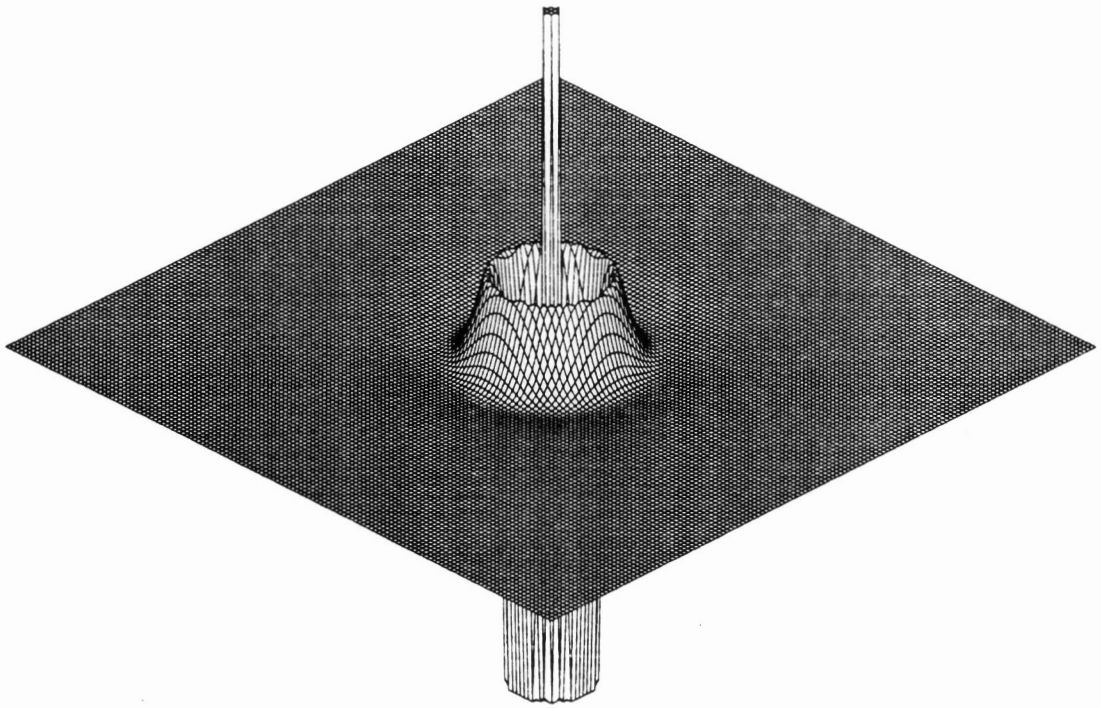

Figure 11: Three–dimensional surface plot of the negative of the laplacian of the electron density distribution for an isolated N atom. Notice that the electronic shell structure of the atom is cylindrical. Again peaks were truncated for clarity.

negative. The ratio, $|\lambda_1|/\lambda_3$, measures the curvature of $\rho(\mathbf{r})$ perpendicular to and along the bond path at the critical point. In a covalent type interaction, $|\lambda_1|/\lambda_3$ is generally greater than 1.0. This indicates that the electron density distribution shows a larger curvature perpendicular to the bond than parallel to it. Since the value of $\rho(\mathbf{r_c})$ is greater for a covalent interaction than for one that is closed–shell (or ionic), this can be thought of as a build up of charge along the path connecting the two nuclei. For the case of a closed–shell (or ionic) interaction, the magnitude of $\rho(\mathbf{r_c})$ is generally smaller than for a covalent interaction and $\nabla^2\rho(\mathbf{r_c}) > 0$. In this case, $|\lambda_1|/\lambda_3$ is less than 1.0, indicating that the curvature along the bond is sharper. This reflects a steeper, sharper well in $\rho(\mathbf{r})$ along the ridge connecting the two nuclei. The third type of bond, an intermediate bond, is associated with values for $\rho(\mathbf{r_c})$, $|\lambda_1|/\lambda_3$, and $\nabla^2\rho(\mathbf{r_c})$ that fall between those of the two limiting bond types described above. For reviews of the theory and its interpretation, see Bader (1993), Edgecombe (1986), as well as Bader's book (1990) and Appendix A of this work.

In an independent study by Cremer and Kraka (1984), interactions were described based on the properties $\rho(\mathbf{r})$ and the local energy density evaluated at the bond critical point, bcp. The local energy density, $\mathrm{H}(\mathbf{r_c})$, is defined as the sum of the local kinetic and potential energies at the bcp, $\mathrm{H}(\mathbf{r_c}) = \mathrm{G}(\mathbf{r_c}) + V(\mathbf{r_c})$, where $\mathrm{G}(\mathbf{r}_c)$ is the local kinetic energy density at the bcp and $V(\mathbf{r_c})$ is the local potential energy density at the bcp which is always negative. They analyzed a series of small molecules and suggest that a covalent interaction is expected when a (3,–1) bond critical point exists, there is an accumulation of charge at the bcp and the local potential energy dominates the local kinetic energy, i.e. when $\mathrm{H}(\mathbf{r_c}) < 0.0$. An interaction can be characterized as predominately ionic in nature when a bond critical point exists between two nuclei,

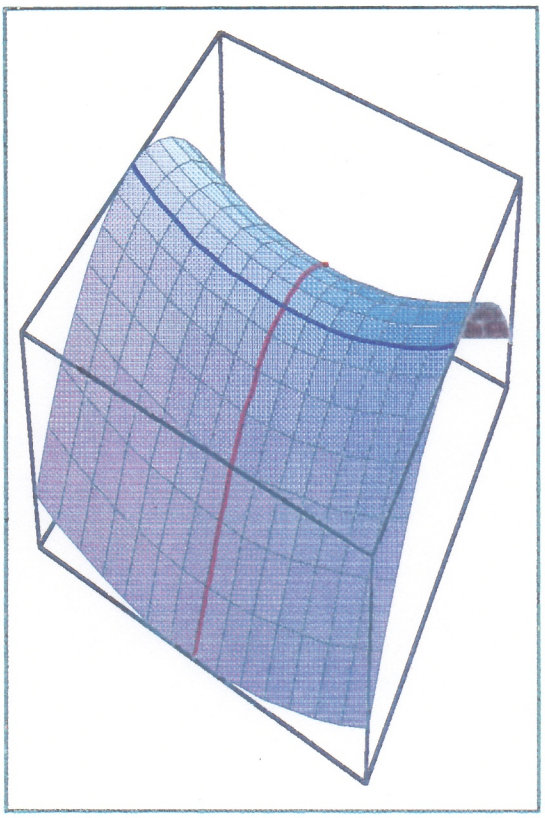

(a) Covalent (shared)

- $\rho(\mathbf{r}_c)$ relatively large
- $|\lambda_1|/\lambda_3 > 0$

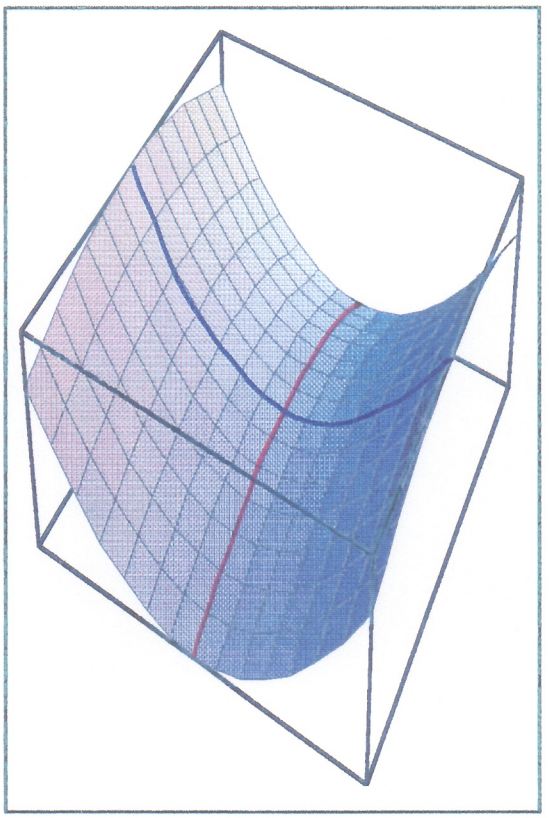

(b) Ionic (closed-shell)

- $\rho(\mathbf{r}_c)$ relatively small
- $|\lambda_1|/\lambda_3 < 0$

Figure 12: Comparison of Shared and Closed-shell interactions. The portion of the electron density distribution depicted in (a) is for a shared interaction, the value of $\rho(\mathbf{r}_c)$ is relatively large and the curvature along the bond, (shown in blue) is less than the curvature perpendicular to the bond, (shown in red). The lower plot, (b), shows a closed-shell interaction where the value of $\rho(\mathbf{r}_c)$ is relatively small and the curvature along the bond, (blue) is greater than the curvature perpendicular to the bond, (red).

shared electron density destabilizes the bond and $H(\mathbf{r_c})$ is positive.

Boyd and Edgecombe (1988) studied the bond critical point model and derived an expression for hydrides that can be used calculate the relative electronegativity of a cation in a bonded interaction from the bcp properties of $\rho(\mathbf{r})$. Using the expression, the relative electronegativity of the M–cation in a MN bond is directly determined from parameters calculated in a bond critical point approach. According to Allen (1989) this approach is "plausible and promising" in that the values derived using the expression follow the trends expected for an electronegativity scale and agree closely with the values published by Pauling in 1960. No attempt was made by Boyd and Edgecombe to relate the electronegativity to the bcp properties.

In a later study of oxides, Hill et al. (in press) used an similar equation for the relative electronegativity of the cation in an MN bond, χ_M. They examined the nature of interactions in terms of the relative electronegativity of the cation, χ_M, and the properties of the electron density distribution evaluated at the bcp. They discovered a number of trends which can be used to help characterize bonding. It was found that as the covalent nature of the bond increases, χ_M, $\rho(\mathbf{r_c})$ and $\nabla^2\rho(\mathbf{r_c})$ increase, while the curvatures of the electron density both perpendicular and parallel to the bond become sharper. By examining χ_M, they also determined that the ionic character of a bond increases with an increase in the bond length. It was suggested that each MO bond is a unique entity which possesses a distinct set of critical point properties, especially apparent for the more electronegative cations. Although the bonds studied by Hill (in press) exhibit a wider range of bond lengths than those from this work, the trends obtained are similar.

The molecular orbital results obtained in this study on a number of nitride

molecules will be examined with respect to results obtained by earlier authors to determine whether the relationships found previously hold. The bcp properties calculated for these nitride molecules generally exhibit trends similar to those found by Bader (1990), Bader and Essén (1984), Cremer and Kraka (1984), Boyd and Edgecombe (1988) and Hill et al. (in press) but with some notable exceptions. Earlier calculations (Buterakos et al., 1992) have shown that bond lengths calculated using molecules match observed bond lengths in crystals to within ~ 0.04 Å. In this section, we will examine how the bond lengths and properties of critical points compare between the molecules calculated here and the values determined both experimentally and theoretically for molecules and for crystals. To date, no similar study has been performed on a nitride system such as this or at a level of calculation as "accurate" as this. With the results presented here, I enhance our understanding of bonding characteristics and offer a quantitative approach to evaluating bonding.

3.2 Calculations

3.2.1 Molecular Orbital Calculations

For this study, molecular orbital calculations at the Becke3lyp 6-311G(2d,p) level were undertaken on a relatively large number of small molecules containing nitrogen, (see Appendix C). The basis set used in the calculations is of a sufficiently high level as to offer reasonably accurate results. The ability exists for performing first principle calculations on periodic arrays, but the additional atoms preclude the use of a basis set as robust as that chosen for this study. Although bulk and dynamic properties of a crystal may be better modeled by calculations on periodic arrangements, the time and computational requirements are great. Additionally, it has been established that calculations on small oxide and nitride clusters or molecules provide information on local properties such as bond lengths and radii that are similar to observed values, (Gibbs, 1994; Feth et al., 1993; Buterakos, 1992; Almennigen et al., 1963). For these reasons, when it comes to understanding the local properties and structure of a crystal, calculations performed on molecules have offered insight where the crystal calculations have not (Gibbs, 1994). Thus, for this work, calculations were undertaken on a series of small molecules containing bonds between nitrogen and the cations of the first two rows of the periodic table.

The basis set chosen for these calculations, Becke3lyp 6-311G(2d,p), includes expressions to account for electron correlation and electron exchange. In addition, this basis set contains one p–type orbital on the hydrogen and two d–type orbitals on all other atoms. Earlier studies indicates that (p–d)π bonding may play an important role in governing the SiN bond (Beach, 1984; Filleux-Blanchard, 1979), but a later study (Cruickshank, 1985) indicates that although there may or may not be some

physical significance to the contribution of the d–type orbitals, they are a necessary inclusion in the calculations to model experimental geometries and electron densities. The d–orbitals may serve simply to correct deficiencies in the s– and p–basis sets, and model the polarization of the bond (Gibbs, 1994). The studies presented here neither support nor disprove the contribution of the d–orbitals in the (p-d)π bonding, but instead simply acknowledge the necessity of their inclusion in the basis set.

In the series of small molecules studied, the majority contain a central nitride anion coordinated by three cations. Others contain cations coordinated by three, four or six nitride anions. In most, hydrogen atoms were used on the periphery of the molecule to charge balance it, while in a few cases, Li, Be or B cations were used. More than 60 different molecules were considered which can be grouped into 16 different classes. Representative geometries of the 16 classes are depicted in Figs. 13–16. Note that the number of hydrogen atoms used to charge balance the molecule varies from molecule to molecule, depending on the cations involved. In Fig. 13, the geometries of molecules which contain a central nitride anion coordinated by three cations are depicted. The central anion is surrounded by either one, two or three $M2$ cations (where $M2$ = Li, Be, B, Na, Mg, Al, P, or S), surrounding it and either two, one, or no $M1$ cations (where $M1$ = C or Si), respectively, (see Fig. 13a-c). The hydrogen atom bonded to the nitride anion in Fig. 13d behaves as a cation. In Fig. 14, two views of the H_9C_3N molecule and of the H_9Si_3N molecule are displayed. The view on the left shows the relationship of the cations to the nitride anion while the view on the right shows the pyramidal nature of the H_9C_3N molecule. In this molecule, the central nitride anion is displaced from the plane containing the carbon atoms while the central nitrogen atom in H_9Si_3N is in the plane with the Si atoms as observed. The fact that

the starting geometry for these two molecules was approximately the same indicates the high degree of reliability of these calculations. The geometries of the molecules where a central cation is coordinated by three, four or six nitride anions are drawn in Figs. 15 and 16. In the Li_6SN_4, $Li_2Be_4(M3)N_4$, $Be_8(M3)N_6$, and $BeBBe_6LiN_6$ molecules (Fig. 15d and Figs. 16a-c where $M3$ = Li or Be), charge balance on the molecule was obtained by surrounding the central coordinated polyhedra with Li, Be or B atoms.

The program GAUSSIAN 94 (Frisch et al., 1993) was used to determine the configuration with the minimum energy. With the exception of the H_9C_3N molecule mentioned above, the molecules were not symmetry constrained, (Fig. 14a), yet the molecules containing the nitride anion coordinated by three cations optimized to a near planar configuration for these four atoms. Note that the hydrogen atoms were generally not in the same plane as the nitrogen atom and cations. From the wave function data of GAUSSIAN 92/94, the properties of the electron density distribution at the critical point were determined using the AIMPAC series of programs (Biegler-Konig et al., 1982) supplied by Bader. Table 2 lists some of the properties determined for the 62 molecules considered. Most molecules optimized to a point group of *1*. Those molecules which optimized to a higher symmetry are indicated with square brackets listing the point group following the molecule's name. Table 2 contains calculated values for the bond length, R(MN), the bonded radius of nitride anion, r_b(N), the electron density distribution at the bcp, $\rho(\mathbf{r_c})$, the Laplacian of the electron density at the bcp, $\nabla^2\rho(\mathbf{r_c})$, and the relative electronegativity of the M–cation in the bond, χ_M. The relative electronegativity of the cation in an MX bond was calculated using the equation modified by Hill et al. (in press), for oxide

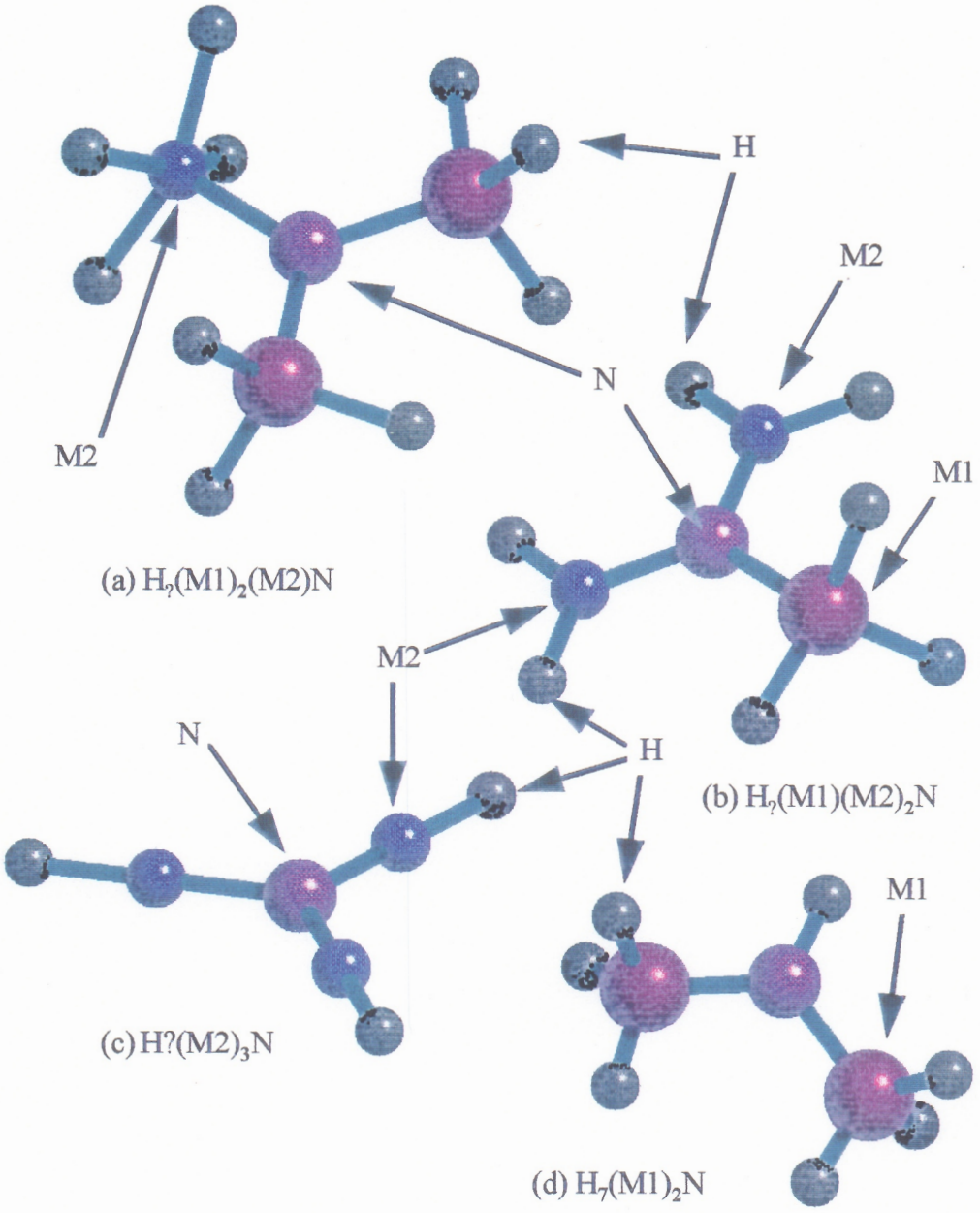

Figure 13: Typical geometries of molecules used in this study, a central nitrogen anion is coordinated by three cations. M1 = C or Si; M2 = Li, Be, B, Na, Mg, Al, P or S. H atoms were used to charge balance the molecules, thus the number of H atoms varies for molecules with different M cations.

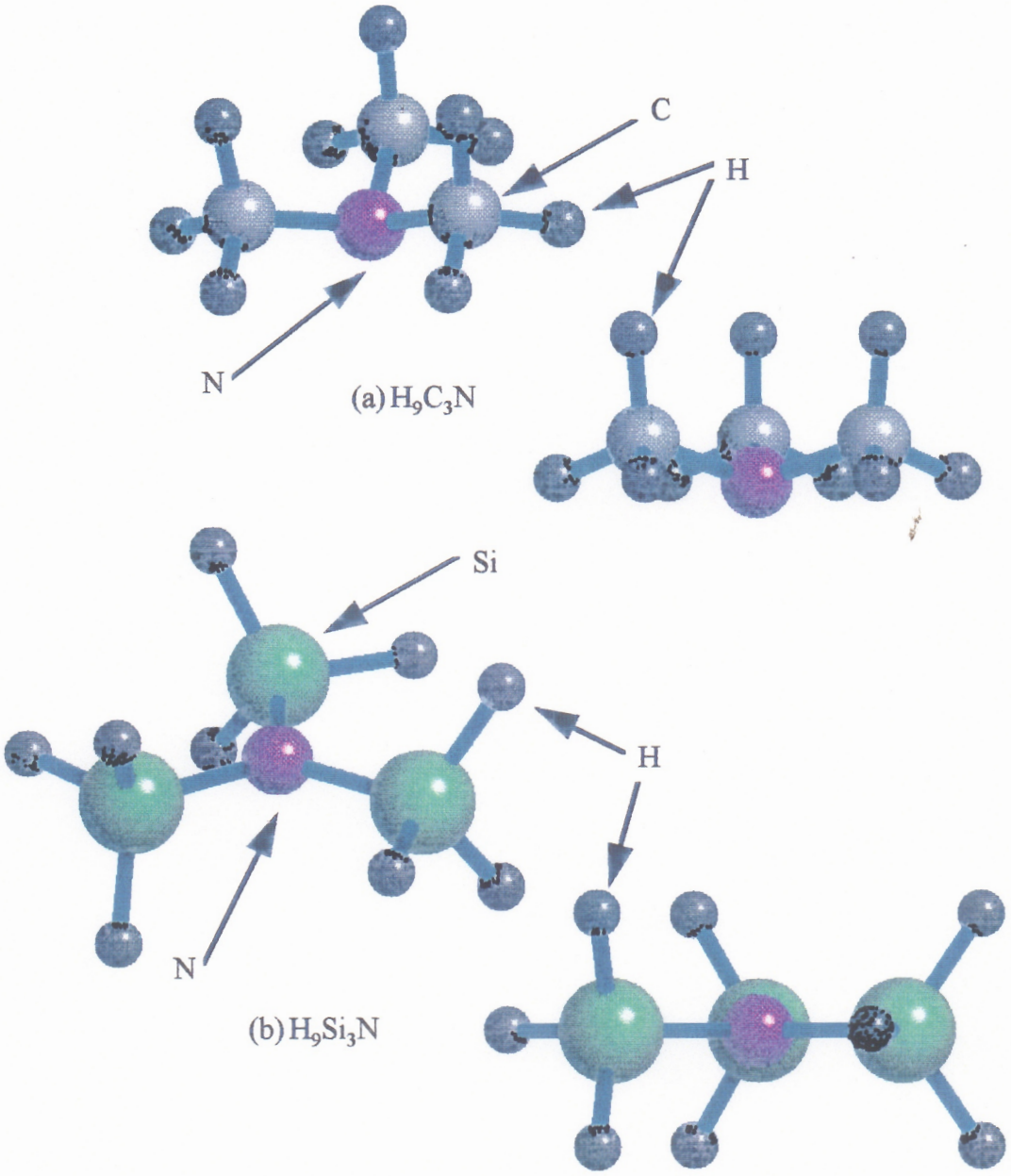

Figure 14: Geometries of the H_9C_3N and H_9Si_3N molecules used in this study. Note that the H_9C_3N molecule is pyramidal, (a), while the H_9Si_3N molecule is planar, (b).

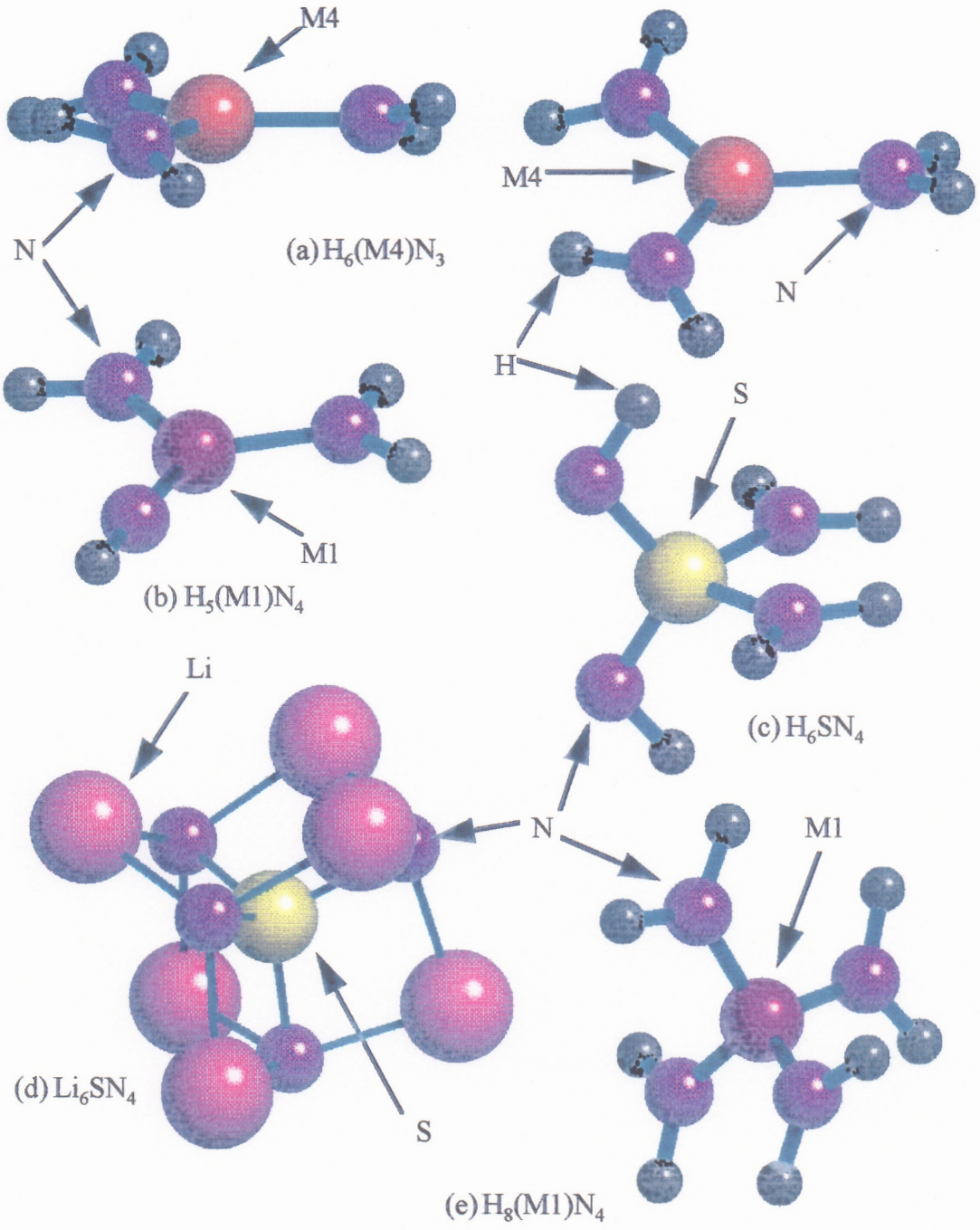

Figure 15: Geometries of molecules containing a central cation coordinated by three or four nitrogen anions. M1 = C or Si; M4 = Be or Al.

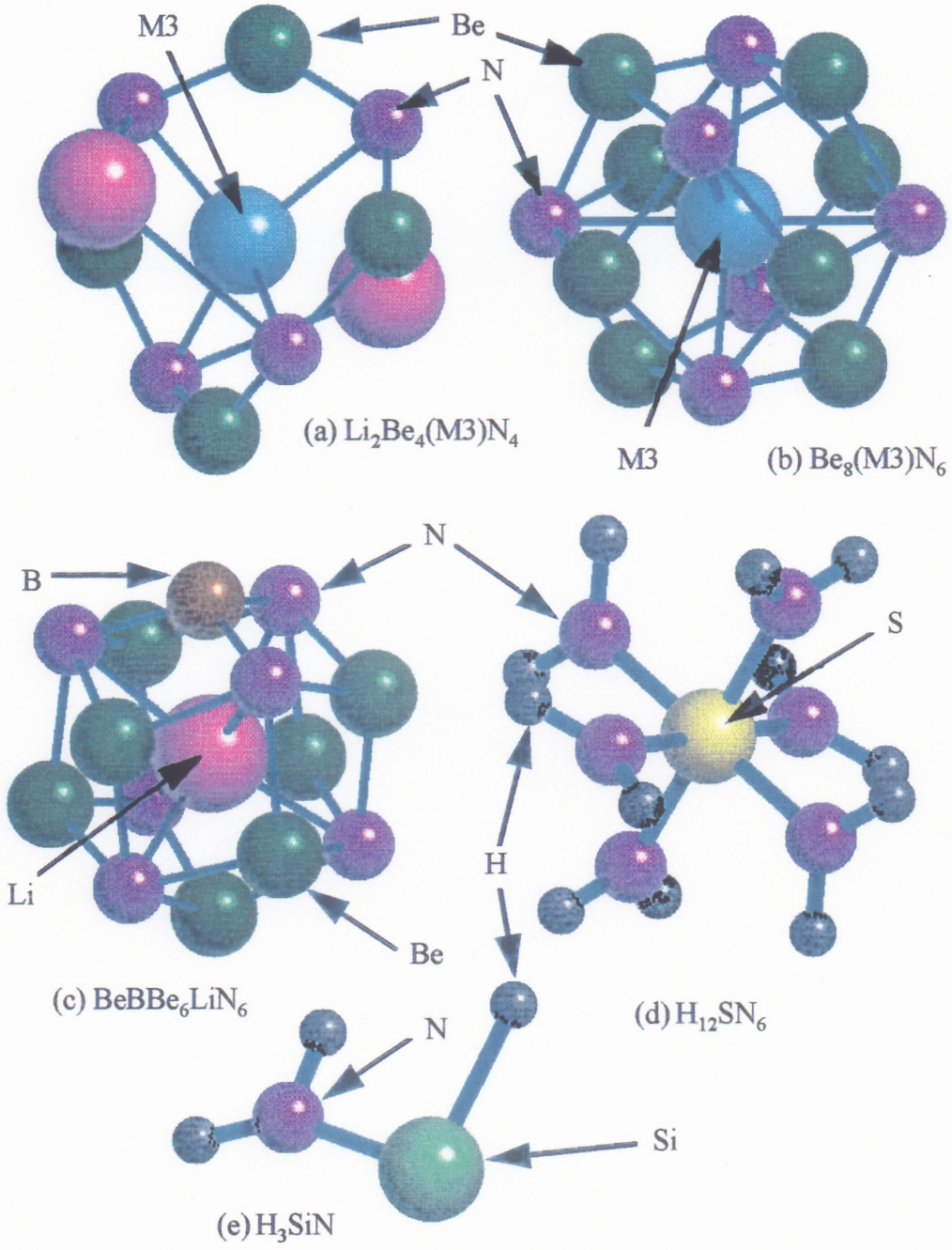

Figure 16: Geometries of molecules containing a central cation coordinated by four or six nitrogen anions with the exception of (e) which contains one Si atom and one nitrogen atom. M3 = Li or Be.

molecules;

$$\chi_M = 2.34 \times F_M^{-0.23} \quad (1)$$

where $F_M = r_b(N)/(N_M \times \rho(\mathbf{r_c}))$ and $r_b(N)$ is the bonded radius of the nitride anion in this study, N_M is the valence of the M–cation, and $\rho(\mathbf{r_c})$ is the value of the electron density at $\mathbf{r_c}$.

3.2.2 Promolecule Calculations

A procrystal representation of the electron density distribution of a crystal is constructed by positioning a set of spherically averaged electron density distributions for non–interacting, ground state, neutral atoms at the experimentally observed location of each atom in the crystal. One advantage of this method is that the model uses a simple superposition of spherical functions, and results obtained are well understood. A number of previous workers have stated that when procrystal electron density distributions are analyzed, the number of critical points and the bond paths are the same as the number of critical points and the bond paths observed experimentally (Hill et al., in press; Downs and Swope, 1992; Downs, 1995; Downs, 1991). A similar approximation to the electron density distribution can be used to study molecules, a promolecule model. In the promolecule model, spherically averaged electron density distributions for non–interacting atoms are placed at the location of the energy–optimized geometry for each molecule as determined from GAUSSIAN. Bond critical point properties are then determined for the promolecules associated with the molecules studied in the molecular orbital calculations. The program SPEEDEN, first written by Gibbs et al. (1992) and later modified by Downs (1996) was used to determine the values of the promolecule radius of the nitride anion, $r_p(N)$, the electron density distribution

Table 2: Bond Critical Point Properties for the Optimized Geometries of Nitride Molecules. All molecules optimized to a point group of *1* unless noted otherwise in "[ ]".

Molecule	MN	R(MN) Å	r_b(N) Å	$\rho(\mathbf{r_c})$ e/Å^3	$\nabla^2\rho(\mathbf{r_c})$ e/Å^5	H($\mathbf{r_c}$) H/Å^3	χ_M
Li_3N	LiN	1.717	1.074	0.400	10.344	0.045	1.86
H_3Li_2SiN	SiN	1.665	0.999	0.971	21.716	–0.384	3.20
	LiN	1.719	1.076	0.399	11.191	0.076	1.86
	LiN	1.793	1.130	0.349	9.150	0.068	1.79
H_6LiSi_2N	SiN	1.703	1.011	0.927	11.955	–0.545	3.16
	LiN	1.785	1.125	0.359	8.366	0.046	1.80
H_3Li_2CN	CN	1.412	0.799	2.077	-22.804	-2.392	4.01
	LiN	1.754	1.102	0.378	10.031	0.064	1.83
	LiN	1.666	1.033	0.420	12.688	0.085	1.90
H_6LiC_2N	CN	1.444	0.803	1.861	-15.466	–1.761	3.90
	LiN	1.738	1.096	0.410	10.029	0.047	1.87
$H_3Be_3N[m]$	BeN	1.503	0.972	0.851	14.603	–0.362	2.66
H_7BeSi_2N	SiN	1.745	1.057	0.796	16.208	–0.253	3.02
	BeN	1.509	0.987	0.820	19.666	–0.120	2.63
$H_5Be_2SiN[m]$	SiN	1.744	1.038	0.843	9.996	–0.474	3.07
	BeN	1.507	0.977	0.855	14.423	–0.366	2.66
$H_5Be_2CN[m]$	CN	1.485	0.904	1.689	–18.250	–1.982	3.72
	BeN	1.506	0.986	0.853	19.775	–0.156	2.65
H_7BeC_2N	CN	1.462	0.830	1.757	–14.823	–1.687	3.82
	BeN	1.497	0.973	0.899	15.701	–0.388	2.69
H_6B_3N	BN	1.444	0.968	1.355	5.632	–1.424	3.25
H_6BN_3	BN	1.430	0.955	1.356	6.828	–1.397	3.27
H_8BSi_2N	SiN	1.767	1.059	0.836	8.924	–0.479	3.05
	BN	1.411	0.940	1.390	8.739	–1.445	3.30
H_7B_2SiN	SiN	1.781	1.071	0.828	8.417	–0.476	3.03
	BN	1.429	0.955	1.375	6.783	–1.442	3.28

Table 2: Bond Critical Point Properties of the Nitrides, Continued

Molecule	MN	R(MN) Å	r_b(N) Å	$\rho(\mathbf{r_c})$ e/Å^3	$\nabla^2\rho(\mathbf{r_c})$ e/Å^5	H($\mathbf{r_c}$) H/Å^3	χ_M
$H_8BC_2N[m]$	CN	1.458	0.843	1.784	−16.175	−1.819	3.82
	BN	1.386	0.925	1.461	12.613	−1.505	3.35
H_7B_2CN	CN	1.478	0.850	1.700	−14.452	−1.641	3.78
	BN	1.421	0.951	1.405	8.063	−1.473	3.30
H_7C_2N	CN	1.443	0.832	1.814	−16.565	−1.866	3.85
H_9C_3N	CN	1.454	0.829	1.826	−16.194	−1.814	3.86
H_5CN_3	CN	1.397	0.813	2.068	−22.170	−2.386	3.97
	CN	1.275	0.764	2.691	−32.325	−3.968	4.27
$H_8CN_4[\overline{4}\,2m]$	CN	1.450	0.822	1.862	-17.304	−1.860	3.88
H_9C_2SiN	SiN	1.724	1.030	0.911	11.511	−0.526	3.13
	CN	1.448	0.832	1.804	−16.054	−1.827	3.85
$H_9CSi_2N[m]$	SiN	1.736	1.036	0.884	10.538	−0.510	3.10
	CN	1.476	0.839	1.665	−13.139	−1.545	3.77
$Na_3N[m]$	NaN	2.116	1.162	0.266	5.784	0.041	1.67
H_3Na_2SiN	SiN	1.671	0.988	1.006	14.247	−0.618	3.23
	NaN	2.120	1.172	0.275	6.019	0.043	1.68
H_6NaSi_2N	SiN	1.691	1.002	0.950	12.784	−0.560	3.18
	NaN	2.162	1.199	0.252	5.333	0.044	1.63
H_3Na_2CN	CN	1.453	0.791	1.807	−13.118	−1.590	3.89
	NaN	2.126	1.176	0.275	5.796	0.040	1.68
H_6NaC_2N	CN	1.440	0.798	1.879	−15.560	−1.781	3.92
	NaN	2.104	1.167	0.291	6.458	0.046	1.70
H_3Mg_3N	MgN	1.908	1.077	0.444	10.662	0.018	2.24
H_5Mg_2SiN	SiN	1.703	1.011	0.936	12.231	−0.557	3.16
	MgN	1.922	1.090	0.438	10.307	0.019	2.23
H_7MgSi_2N	SiN	1.721	1.023	0.898	11.096	−0.523	3.12
	MgN	1.942	1.103	0.420	9.685	0.023	2.20

Table 2: Bond Critical Point Properties of the Nitrides, Continued

Molecule	MN	R(MN) Å	r_b(N) Å	$\rho(\mathbf{r_c})$ e/Å^3	$\nabla^2\rho(\mathbf{r_c})$ e/Å^5	H($\mathbf{r_c}$) H/Å^3	χ_M
$H_5Mg_2CN[m]$	CN	1.479	0.813	1.677	−11.697	−1.425	3.80
	MgN	1.915	1.089	0.461	10.745	0.011	2.25
$H_7MgC_2N[m]$	CN	1.458	0.817	1.788	−14.642	−1.671	3.85
	MgN	1.910	1.086	0.465	11.022	0.016	2.26
H_6Al_3N	AlN	1.806	1.048	0.614	12.116	−0.129	2.66
$H_6AlN_3[m]$	AlN	1.775	1.033	0.681	14.316	−0.142	2.74
H_7Al_2SiN	SiN	1.750	1.044	0.851	9.666	−0.488	3.07
	AlN	1.808	1.055	0.632	12.413	−0.134	2.68
H_8AlSi_2N	SiN	1.732	1.030	0.871	10.490	−0.498	3.10
	AlN	1.823	1.064	0.614	11.603	−0.133	2.65
H_7Al_2CN	CN	1.482	0.836	1.655	−12.582	−1.489	3.77
	AlN	1.799	1.052	0.659	13.083	−0.147	2.71
H_8AlC_2N	CN	1.455	0.831	1.787	−15.498	−1.759	3.84
	AlN	1.780	1.038	0.678	14.196	−0.144	2.73
H_3SiN	SiN	1.664	0.985	0.974	16.105	−0.534	3.21
H_3SiN	SiN	1.664	0.985	0.974	16.105	−0.534	3.21
$H_7Si_2N[mm2]$	SiN	1.734	1.034	0.872	10.649	−0.493	3.10
H_9Si_3N	SiN	1.748	1.042	0.847	9.737	−0.480	3.07
H_5SiN_3	SiN	1.536	0.887	1.218	27.609	−0.689	3.46
	SiN	1.690	1.004	0.961	13.248	−0.562	3.19
$H_8SiN_4[\bar{4}2m]$	SiN	1.718	1.026	0.913	11.730	−0.530	3.13
$H_{12}P_3N[m]$	PN	1.722	1.038	1.074	1.620	−0.977	3.41
$H_{10}PSi_2N[m]$	SiN	1.754	1.047	0.835	9.608	−0.467	3.06
	PN	1.701	1.023	1.127	1.714	−1.058	3.46
$H_{11}P_2SiN[m]$	PN	1.709	1.029	1.105	1.791	−1.022	3.44
	SiN	1.762	1.053	0.819	9.357	−0.452	3.04
$H_{11}P_2CN[m]$	PN	1.697	1.024	1.141	2.556	−1.067	3.47
	CN	1.469	0.855	1.679	−14.307	−1.683	3.76

Table 2: Bond Critical Point Properties of the Nitrides, Continued

Molecule	MN	R(MN) Å	r_b(N) Å	$\rho(\mathbf{r_c})$ e/Å^3	$\nabla^2\rho(\mathbf{r_c})$ e/Å^5	H($\mathbf{r_c}$) H/Å^3	χ_M
$H_{10}PC_2N[m]$	CN	1.453	0.843	1.764	−15.778	−1.810	3.81
	PN	1.675	1.011	1.205	3.660	−1.151	3.53
H_6P_3N	PN	1.746	1.046	1.036	0.592	−0.932	3.38
H_8PSi_2N	SiN	1.752	1.047	0.847	9.544	−0.483	3.07
	PN	1.743	1.042	1.029	0.570	−0.923	3.38
$H_7P_2SiN[m]$	SiN	1.757	1.051	0.843	9.407	−0.480	3.06
	PN	1.739	1.041	1.045	0.685	−0.945	3.39
H_7P_2CN	CN	1.472	0.845	1.695	−14.117	−1.635	3.78
	PN	1.727	1.037	1.077	1.524	−0.984	3.42
H_8PC_2N	CN	1.457	0.838	1.764	−15.454	−1.761	3.82
	PN	1.696	1.022	1.136	3.560	−1.052	3.47
$H_6SN_4[mm2]$	SN	1.689	0.919	1.442	−10.528	−1.345	3.92
	SN	1.525	0.876	1.998	−16.082	−2.799	4.27
$H_{12}SN_6[mmm]$	SN	1.747	0.931	1.338	−8.469	−1.078	3.84
$Li_6SN_4[\bar{4}2m]$	SN	1.632	0.845	1.638	−10.283	−1.526	4.11
$Li_2Be_4BeN_4[\bar{4}2m]$	BeN	1.723	1.144	0.557	9.058	−0.174	2.33
$Li_2Be_4MgN_4[\bar{4}2m]$	MgN	1.945	1.113	0.458	10.702	0.001	2.24
$Be_8MgN_6[m3m]$	MgN	1.935	1.109	0.497	11.283	−0.025	2.28
$BeBBe_6LiN_6[3m]$	LiN	1.835	1.167	0.416	8.796	0.000	1.85
	LiN	1.909	1.290	0.378	7.588	−0.013	1.76
$Be_8BeN_6[m3m]$	BeN	1.850	1.239	0.476	6.741	−0.156	2.20

at the critical point for the promolecule, $\rho(\mathbf{r_c})_{\mathrm{p}}$, and the relative electronegativity of the cation, $\chi_{(M)_{\mathrm{p}}}$, as determined by equation 1 for a promolecule. Results obtained using a promolecule model can be explained in terms of the superposition of spherical $\rho(\mathbf{r})$, with no consideration being given to any rearrangement of $\rho(\mathbf{r})$ that may take place on bonding. Thus, this model is well understood, a significant advantage. The results of the promolecule calculations are displayed in Table 3.

Table 3: Bond critical point properties for the energy–optimized geometries of nitride promolecules.

Molecule	MN	R(MN) Å	r_p(N) Å	$\rho(\mathbf{r_c})_\mathrm{p}$ e/Å^3	$\nabla^2\,\rho(\mathbf{r_c})_\mathrm{p}$ e/Å^5	$\chi_{(M)\mathrm{p}}$
Li_3N	LiN	1.718	1.044	0.317	8.832	1.78
H_3Li_2SiN	SiN	1.662	0.950	0.800	13.549	3.09
	LiN	1.715	1.042	0.317	8.926	1.78
	LiN	1.789	1.097	0.279	7.426	1.71
H_6LiSi_2N	SiN	1.703	0.979	0.744	11.176	3.02
	LiN	1.785	1.091	0.264	7.406	1.69
H_3Li_2CN	CN	1.412	0.788	1.585	0.274	3.78
	LiN	1.755	1.074	0.306	8.342	1.75
	LiN	1.666	1.008	0.363	10.203	1.85
H_6LiC_2N	CN	1.444	0.798	1.496	1.684	3.72
	LiN	1.738	1.058	0.294	8.386	1.74
H_3Be_3N	BeN	1.503	0.962	0.552	18.666	2.42
H_7BeSi_2N	SiN	1.745	1.007	0.699	9.081	2.96
	BeN	1.509	0.966	0.542	18.282	2.40
H_5Be_2SiN	SiN	1.744	1.006	0.702	9.160	2.96
	BeN	1.507	0.965	0.546	18.418	2.41
H_5Be_2CN	CN	1.485	0.811	1.397	2.913	3.65
	BeN	1.506	0.964	0.544	18.438	2.41
H_7BeC_2N	CN	1.462	0.803	1.453	2.284	3.69
	BeN	1.497	0.957	0.550	18.896	2.42
H_6B_3N	BN	1.444	0.956	0.943	13.803	3.00
H_6BN_3	BN	1.430	0.945	0.960	15.002	3.02
H_8BSi_2N	SiN	1.767	1.021	0.675	8.032	2.93
	BN	1.411	0.931	0.991	17.104	3.06
H_7B_2SiN	SiN	1.781	1.030	0.661	7.424	2.91
	BN	1.429	0.945	0.964	15.264	3.03

Table 3: Bond Critical Point Properties of Promolecules, Continued

Molecule	MN	R(MN) Å	r_p(N) Å	$\rho(\mathbf{r_c})_p$ e/Å^3	$\nabla^2 \rho(\mathbf{r_c})_p$ e/Å^5	$\chi_{(M)p}$
H_8BC_2N	CN	1.454	0.801	1.475	2.069	3.70
	BN	1.383	0.911	1.030	19.981	3.10
H_7B_2CN	CN	1.478	0.809	1.414	2.787	3.66
	BN	1.421	0.939	0.974	16.053	3.04
H_7C_2N	CN	1.443	0.797	1.498	1.657	3.72
H_9C_3N	CN	1.450	0.800	1.483	1.962	3.71
H_5CN_3	CN	1.397	0.787	1.623	–0.320	3.78
	CN	1.275	0.774	1.977	–6.744	3.97
H_8CN_4	CN	1.450	0.800	1.477	1.940	3.71
H_9C_2SiN	SiN	1.722	0.991	0.719	10.207	2.99
	CN	1.451	0.800	1.483	1.937	3.71
H_9CSi_2N	SiN	1.737	1.001	0.704	9.442	2.97
	CN	1.476	0.808	1.418	2.702	3.66
Na_3N	NaN	2.116	1.133	0.228	5.181	1.62
H_3Na_2SiN	SiN	1.671	0.956	0.782	12.961	3.07
	NaN	2.120	1.139	0.232	5.220	1.62
H_6NaSi_2N	SiN	1.691	0.970	0.758	11.875	3.04
	NaN	2.162	1.165	0.208	4.670	1.57
H_3Na_2CN	CN	1.453	0.799	1.464	1.935	3.70
	NaN	2.126	1.140	0.222	5.071	1.61
H_6NaC_2N	CN	1.440	0.796	1.507	1.517	3.73
	NaN	2.104	1.127	0.234	5.400	1.63
H_3Mg_3N	MgN	1.908	1.048	0.377	8.666	2.17
H_5Mg_2SiN	SiN	1.703	0.978	0.746	11.206	3.02
	MgN	1.922	1.058	0.366	8.343	2.15
H_7MgSi_2N	SiN	1.719	0.989	0.726	10.335	3.00
	MgN	1.943	1.072	0.351	7.863	2.12

Table 3: Bond Critical Point Properties of Promolecules, Continued

Molecule	MN	R(MN) Å	r_p(N) Å	$\rho(\mathbf{r_c})_p$ e/Å^3	$\nabla^2 \rho(\mathbf{r_c})_p$ e/Å^5	$\chi_{(M)p}$
H_5Mg_2CN	CN	1.479	0.808	1.402	2.754	3.65
	MgN	1.915	1.053	0.368	8.484	2.15
H_7MgC_2N	CN	1.458	0.802	1.459	2.155	3.69
	MgN	1.910	1.049	0.370	8.627	2.16
H_6Al_3N	AlN	1.806	1.019	0.511	10.356	2.57
H_6AlN_3	AlN	1.775	0.997	0.537	11.551	2.61
H_7Al_2SiN	SiN	1.750	1.009	0.694	8.805	2.95
	AlN	1.808	1.021	0.508	10.277	2.57
H_8AlSi_2N	SiN	1.732	0.998	0.713	9.719	2.98
	AlN	1.823	1.031	0.495	9.778	2.54
H_7Al_2CN	CN	1.479	0.808	1.410	2.771	3.66
	AlN	1.795	1.012	0.519	10.748	2.58
H_8AlC_2N	CN	1.452	0.800	1.479	1.978	3.71
	AlN	1.776	0.998	0.536	11.503	2.61
H_3SiN	SiN	1.664	0.953	0.793	13.771	3.09
H_3SiN	SiN	1.664	0.953	0.793	13.770	3.09
H_7Si_2N	SiN	1.734	0.999	0.706	9.577	2.97
H_9Si_3N	SiN	1.748	1.008	0.695	8.915	2.95
H_5SiN_3	SiN	1.536	0.861	1.003	22.945	3.33
	SiN	1.690	0.971	0.762	12.193	3.04
H_8SiN_4	SiN	1.718	0.988	0.722	10.399	2.99
$H_{12}P_3N$	PN	1.722	0.979	0.954	1.684	3.37
$H_{10}PSi_2N$	SN	1.754	1.012	0.687	8.638	2.94
	PN	1.701	0.974	0.983	2.601	3.40
$H_{11}P_2SiN$	PN	1.709	0.976	0.972	2.231	3.39
	SiN	1.762	1.017	0.678	8.229	2.93
$H_{11}P_2CN$	PN	1.697	0.972	0.985	2.788	3.40
	CN	1.469	0.805	1.435	2.534	3.68

Table 3: Bond Critical Point Properties of Promolecules, Continued

Molecule	MN	R(MN) Å	r_p(N) Å	$\rho(\mathbf{r_c})_p$ e/Å^3	$\nabla^2 \rho(\mathbf{r_c})_p$ e/Å^5	$\chi_{(M)p}$
$H_{10}PC_2N$	CN	1.453	0.800	1.475	2.014	3.70
	PN	1.675	0.963	1.011	3.996	3.43
H_6P_3N	PN	1.748	0.985	0.918	0.873	3.33
H_8PSi_2N	SiN	1.753	1.011	0.688	8.672	2.95
	PN	1.743	0.985	0.928	1.005	3.34
H_7P_2SiN	SiN	1.755	1.012	0.684	8.538	2.94
	PN	1.742	0.984	0.928	1.045	3.34
H_7P_2CN	CN	1.472	0.806	1.424	2.617	3.67
	PN	1.727	0.981	0.943	1.509	3.36
H_8PC_2N	CN	1.457	0.801	1.463	2.150	3.70
	PN	1.696	0.972	0.980	2.844	3.39
H_6SN_4	SN	1.689	0.860	1.241	1.685	3.84
	SN	1.525	0.853	1.588	–0.799	4.08
$H_{12}SN_6$	SN	1.747	0.872	1.129	3.100	3.75
Li_6SN_4	SN	1.632	0.851	1.385	–0.093	3.95

3.3 Results

3.3.1 Bond Length

The minimum energy bond lengths obtained in this study agree with the available experimental bond lengths of molecules to within $\sim$ 0.02 Å. This indicates the accuracy from the results of these calculations is such that the bond lengths in molecules are accurately reproduced. Earlier workers (Gibbs, 1994; Feth et al., 1993; Almennigen et al., 1963) have established that calculations performed using molecules are readily applicable to crystals. Thus, the work presented in this paper is expected to provide results that may apply to chemically similar crystals.

In general, for a given MN bond, the bond length decreases monotonically with increasing $\rho(\mathbf{r_c})$, (Fig. 17). The upper plot depicts bonds involving first row cations bonded to the nitride anion while the lower one involves those bonds with second row cations. The results are similar to trends established using the values given by Bader and Essén (1984) and Boyd and Edgecombe (1988). The data from this study suggests that there are four distinct roughly parallel trends in both the upper and lower plots. Similar trends have been observed for oxide molecules (Hill et al., in press) where it was found that the relationship between bond length and electron density could be modeled with a simple power equation. They found the exponent of the power equation to be $\sim$ –0.20 for LiO, BeO and BO bonds and to be $\sim$ –0.35 for CO and NO bonds for the first row interactions. An exponent of $\sim$ –0.15 was found for NaO, MgO and AlO bonds and an exponent of $\sim$ –0.30 determined for SiO, PO and SO bonds. Hill et al. (in press) suggest that the more ionic bonds exhibit a wider range of bond lengths for a given change in $\rho(\mathbf{r_c})$, while the more covalent bonds exhibit smaller change in the bond length for a given change in the value of $\rho(\mathbf{r_c})$. A similar analysis

was conducted using the values calculated for nitride molecules. Relating $\rho(\mathbf{r_c})$and R(MN) by a power equation yields exponents for BeN bond data of –0.35, for BN bond data of –0.50 and of –0.30 for CN bond data. Attempts to fit the LiN data set using a power, a linear and an exponential curve resulted in approximately the same low values for the coefficient of determination, r^2, indicating no significant trends exist. Thus no exponent data is available for this data set. The BeO and BO bond data, (Hill et al. in press) exhibit a steeper slope than the BeN and BN bond data. The slope for the data from CO bonds is also steeper than the slope for the data from CN bonds. Therefore, a change in the bond length of a first row cation bonded to oxygen is associated with a larger change in the value of $\rho(\mathbf{r_c})$ than what is seen for a similar change in the bond length of the same cation bonded to nitrogen. In the lower plot of Fig. 17, the data for NaN, MgN and AlN bonds plot as one common trend while the data for SiN, PN and SN bonds tend to separate into individual trends. Fitting a power equation to the combined data sets from NaN, MgN and AlN bonds yields an exponent of –0.20 while the average exponent of power equations fitted to the SiN, PN and SN bond data is $\sim$ –0.30. Hill et al. (in press) found separate trends for the NaO, MgO and AlO bond data. It should be pointed out that the span of bond lengths used in this study is smaller than that used in the Hill et al. study, (in press), and it is possible that if a wider spread of bond lengths were available, this data set would show six separate trends as was observed for the oxides. In any case, the overall trends observed for nitrides are similar to those observed for oxides, although the slopes of the trends from the oxide bond data tends to be steeper than the slopes of the trends from the bond data for the same cations bonded to nitrogen. The value of the exponents determined by fitting a power equation for the data from

this study are similar to the value of the exponents determined for bond data from cations bonded to oxygen. The data for the Hill (in press) study and for this study indicate that the trends from the bond data for more electropositive cations shows a steeper slope for $\rho(\mathbf{r_c})$ versus R(MN) than the trends from the bond data involving the more electronegative cation. Therefore, a change in the bond length of the more ionic bonds is associated with little change in $\rho(\mathbf{r_c})$, while in the more covalent bonds a slight change in the bond length is associated with a more significant change in the value of $\rho(\mathbf{r_c})$.

As established for diatomic hydride molecules (Bader, 1990) and for the oxides (Hill et al. in press) the bonded radius of a number of anions increases linearly with increasing bond length. This trend also is observed for the nitrides, see Fig. 18. The trends between R(MN) and r_b(N)for LiN, BeN, BN bonds tend to fall along separate but roughly parallel lines, (upper plot, Fig. 18). Note that for the CN bond data a linear trend between R(CN) and r_b(N) is poorly developed, $r^2 \sim 0.40$. The lower plot (Fig. 18) shows that R(MN) versus r_b(N) for second row cations fall along six separate but roughly parallel trends. As observed for the oxides, (Hill et al. in press), r_b(N) tends to increase with increasing bond length and decreasing electronegativity of the M–cation. The bonded radius of the nitrogen anion varies from a minimum value of r_b(N) = 0.79 Å for the CN bond data to a maximum value of r_b(N) = 1.29 Å for the LiN bond data. The minimum value of r_b(N) is close to the atomic radius of nitrogen of 0.75 Å while the upper value is similar to the radius of the nitride anion ($\sim$ 1.43 Å). As was observed by Feth et al. (1993), for promolecules and with Gibbs et al. (1994) for oxides, the bonded radius of the anion spans a range of values from its atomic radius to its ionic radius. The bonded radius of the nitride anion is

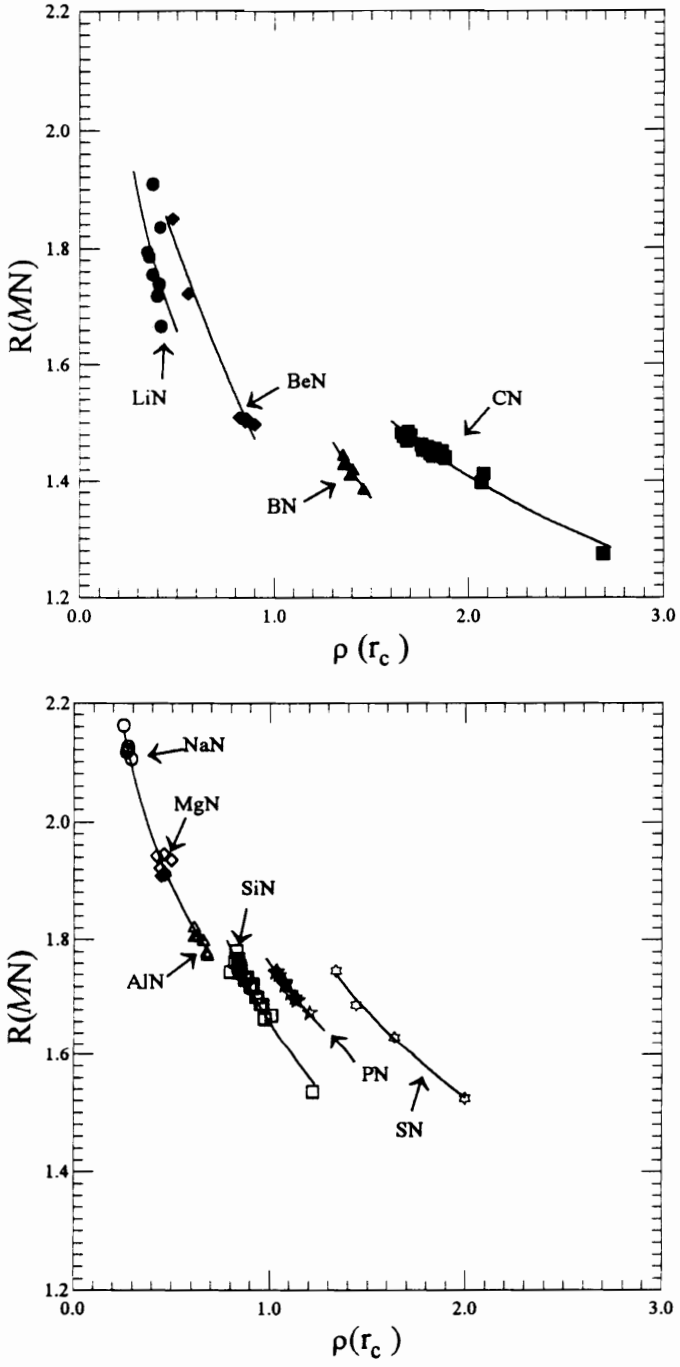

Figure 17: Electron Density Distribution at the Bond Critical Point, $\rho(\mathbf{r_c})$, Versus the MN Bond Lengths, R(MN).

smaller when bonded to the more electronegative cations and larger when bonded to the more electropositive cations indicating the electronegativity of the cation may be useful in determining bond type.

3.3.2 Electronegativity

An analysis of the critical point properties of the diatomic hydrides (Boyd and Edgecombe, 1988) indicates that both $\rho(\mathbf{r_c})$ and r_b(H) correlate with the bond length, R(AH). Hill et al. (in press) obtained similar trends for the data from oxides, and Figs. 17 and 18 of this work show the same types of trends for nitrides. Studying these results also indicates that there is a correlation between $\rho(\mathbf{r_c})$, r_b(N) and the electronegativity of the cation. The bonded radius of the anion tends to decrease while $\rho(\mathbf{r_c})$ tends to increase as the electronegativity of the cation increases. Boyd and Edgecombe (1988) have used the bonded radius of the H atom, the valence of the cation, the value of the electron density at $\mathbf{r_c}$ and the length of the AH bond to come up with a parameter for estimating the relative electronegativity of the cation. The original equation by Boyd and Edgecombe predicts that the electronegativity of the cation should increase with increasing bond length, directly opposite to what was shown in the trends for the data from oxides (Hill et al. in press) and to what was shown in the Figs. 17 and 18. Because of this and since the bond length and the bonded radius of the anion are so highly correlated, Hill et al. (in press) revised the expression for the relative electronegativity of the M–cation, equation 1. This revised equation no longer contains the bond length. The relative electronegativities of M–cations bonded to nitrogen were calculated using Eq. 1. Fig. 19 shows the general trend associated with the values calculated for χ_M with respect to bond length, R(MN), for the molecules of this study. R(MN) is correlated with χ_M indicating

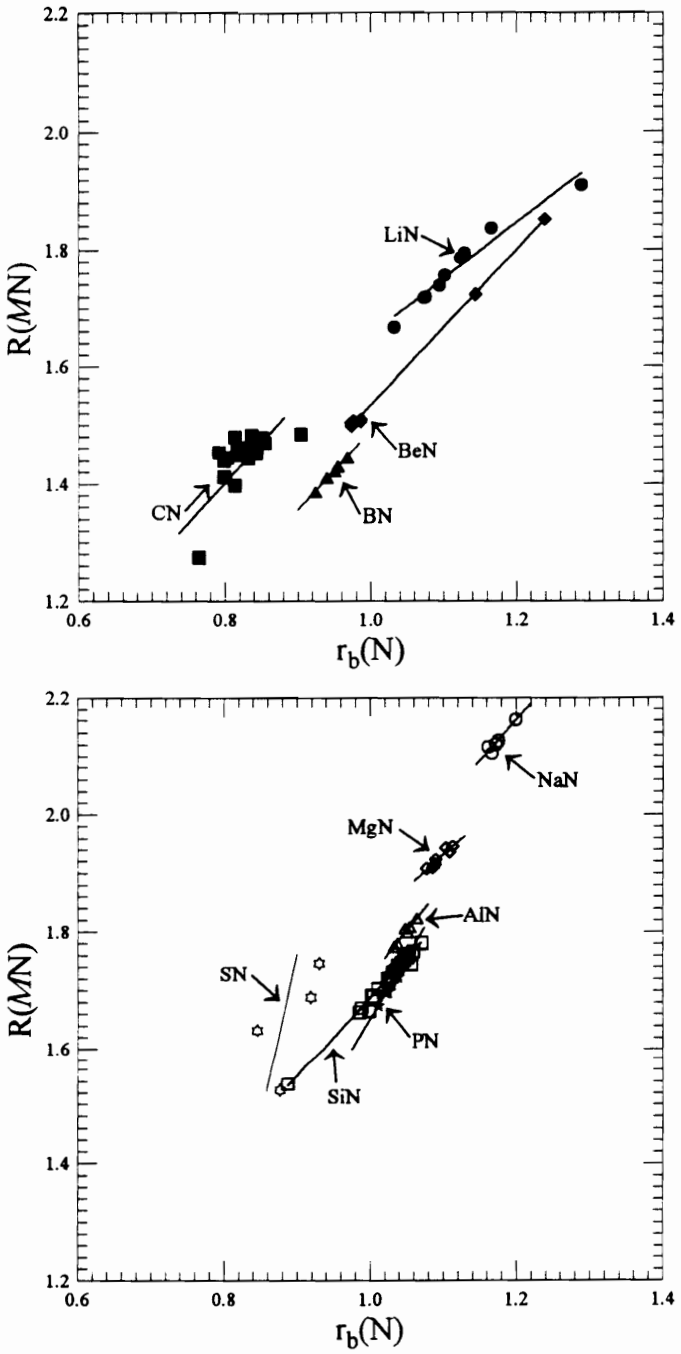

Figure 18: Bonded Radius of Nitrogen, r_b(N) Versus Bond Length of an MN Bond, R(MN)

that the inclusion of R(MN) in the equation for χ_M might be redundant.

The correlation between the calculated relative electronegativities from this study and those of Pauling is high. Figure 20 plots the average relative electronegativity of the cation for each different M–cation, $<\chi_M>$, calculated against the values of electronegativity derived by Pauling (1960). A linear regression analysis of these two variables indicates that 99 percent of the variation in Pauling's electronegativity can be related to a linear dependence on $< \chi_M >$. Notice that the values obtained for $< \chi_M >$ using Eq. 1 are on average 1.7 times larger than those derived by Pauling with the greater differences for the more electronegative cations. Hill et al. (in press) found $< \chi_M >$ to be between 0.5 and 1.5 times larger than Pauling's electronegativity values, also with the more electronegative cations showing a greater difference. It is noteworthy that the values of $< \chi_M >$ calculated for the first and second row cations bonded to oxygen range from $\sim$ 0.5 to $\sim$ 4.5 while the values of $< \chi_M >$ calculated for the same cations bonded to nitrogen range from $\sim$ 0.8 to $\sim$ 2.7. As in the case of bond length, we see a narrower range of values when nitrogen is the anion involved in the bond.

The electronegativities proposed by Pauling assume that each atom is associated with a given value for the electronegativity. The relative electronegativities of nitride molecules calculated, χ_M, show a non-constant electronegativity for the each M-atom, (Figs. 22 – 26). This same variance in the relative electronegativity of the cation was found by Hill et al. (in press). Using Pauling's electronegativities, χ, it can be seen that χ decreases with increasing bond length, and decreasing electron density at the critical point, $\rho(\mathbf{r_c})$. Similar trends were observed for the oxides (Hill et al. in press). This serves as an additional indication that the modified equation for χ_M is realistic.

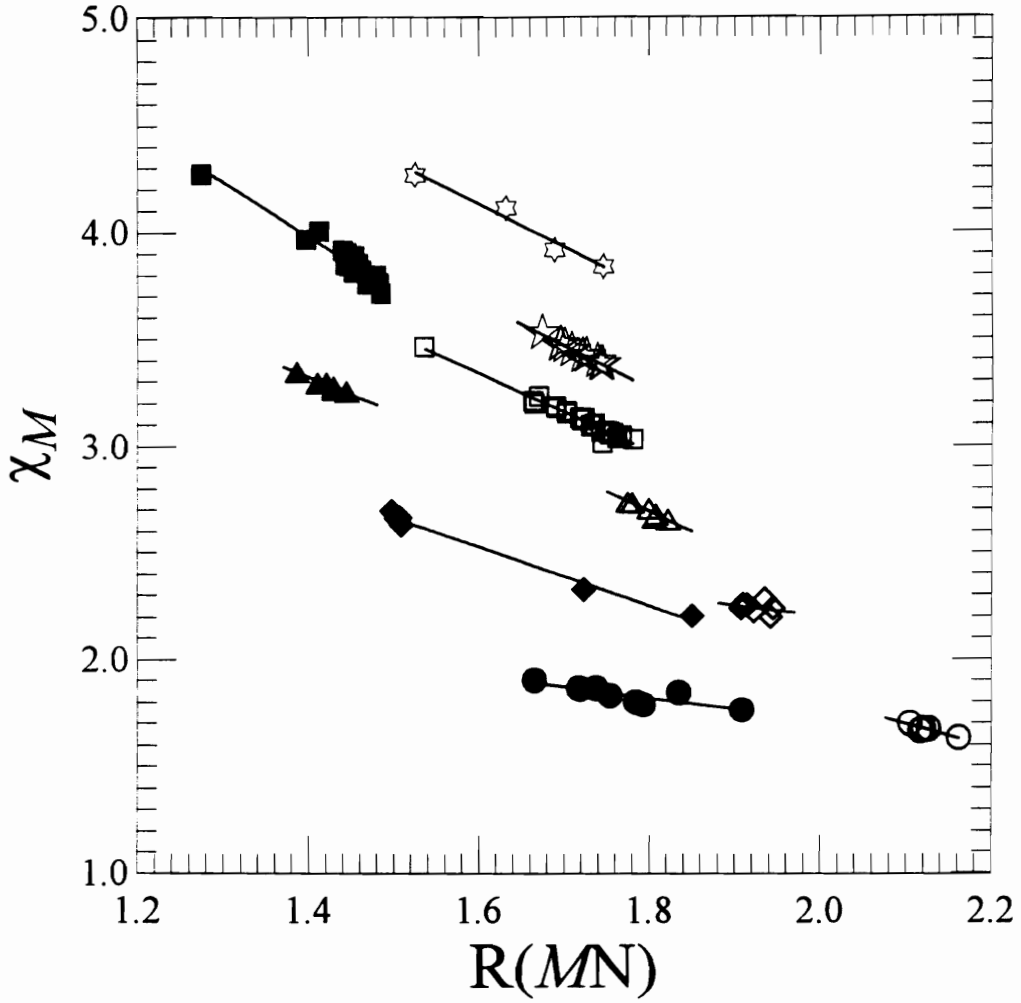

Figure 19: General Trends Observed for Bond Length, R(MN), with Respect to the Relative Electronegativity of the M–Cation in an MN Bond. Data from MN bonds are indicated as follows: the LiN bond data are plotted as closed circles; BeN bond data as closed diamonds; BN bond data as closed triangles; CN bond data as closed squares; NaN bond data as open circles; MgN bond data as open diamonds; AlN bond data as open triangles; SiN bond data as open squares; PN bond data as 5-pointed stars and SN bond data as 6-pointed stars.

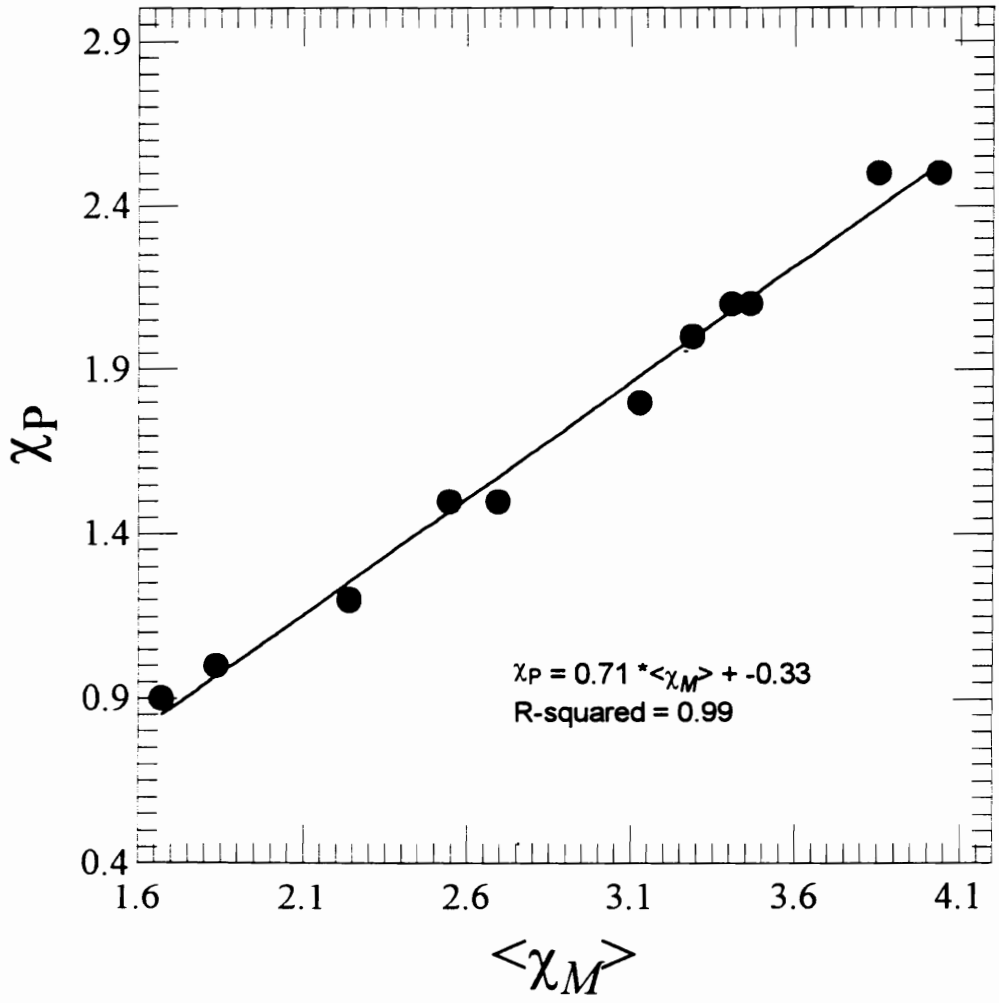

Figure 20: Comparison of the Average Relative Electronegativity of the M–cation in a MN bond, $<\chi_M>$, with Pauling's Electronegativity, χ_P

As mentioned previously, Cremer and Kraka's (1984) approach to determining bond type is to use the local energy term, $H(\mathbf{r_c})$. They state that a negative $H(\mathbf{r_c})$ value indicates a shared interaction while a positive $H(\mathbf{r_c})$ is indicative of a closed shell interaction. In Fig. 21 the value of $H(\mathbf{r_c})$ is plotted versus the value for χ_M. The only positive values of $H(\mathbf{r_c})$ found are for bonds where Li, Na and Mg are bonded to the nitride anion. The most negative values of $H(\mathbf{r_c})$ are found for bonds where C or S is bonded to N. As observed previously, we see a division between bonds involving more electronegative cations and bonds involving more electropositive cations. $H(\mathbf{r_c})$ < 0 for MN bonds where M is a more electronegative cation. For bonds involving highly electropositive cations, $H(\mathbf{r_c}) >$ or ~ 0. Intermediate type bonds have values of $H(\mathbf{r_c})$ between ~ 0 and -1.5.

Using the suggestion of Hill et al. (in press), that a value of $\chi_M = 2.5$ be the division point between predominantly ionic and predominantly covalent, we find that LiN, some BeN, NaN, and MgN bonds would be considered to be predominantly ionic interactions while a few bonds involving Be cations and all the bonds involving B, C, Al, Si, P and S cations would be involved in predominantly covalent interactions. The data presented here for nitride–containing molecules suggests that a value of $\chi_M \sim$ 2.8 may be more appropriate for use in distinguishing between bond types. Using this value, bonds between the nitride anion and Li, Be, Na, Mg and Al cations would be predominately ionic while MN bonds (M = B, C, Si, P or S) would be predominately covalent. Using χ_M of 2.8 for the nitrides, gives a division of bond types closest to that recommended by Pauling (1960).

Bader and Essén (1984) and Bader (1990) observed that $\rho(\mathbf{r_c})$ calculated for hydride molecules increases from left to right across each row of the periodic table.

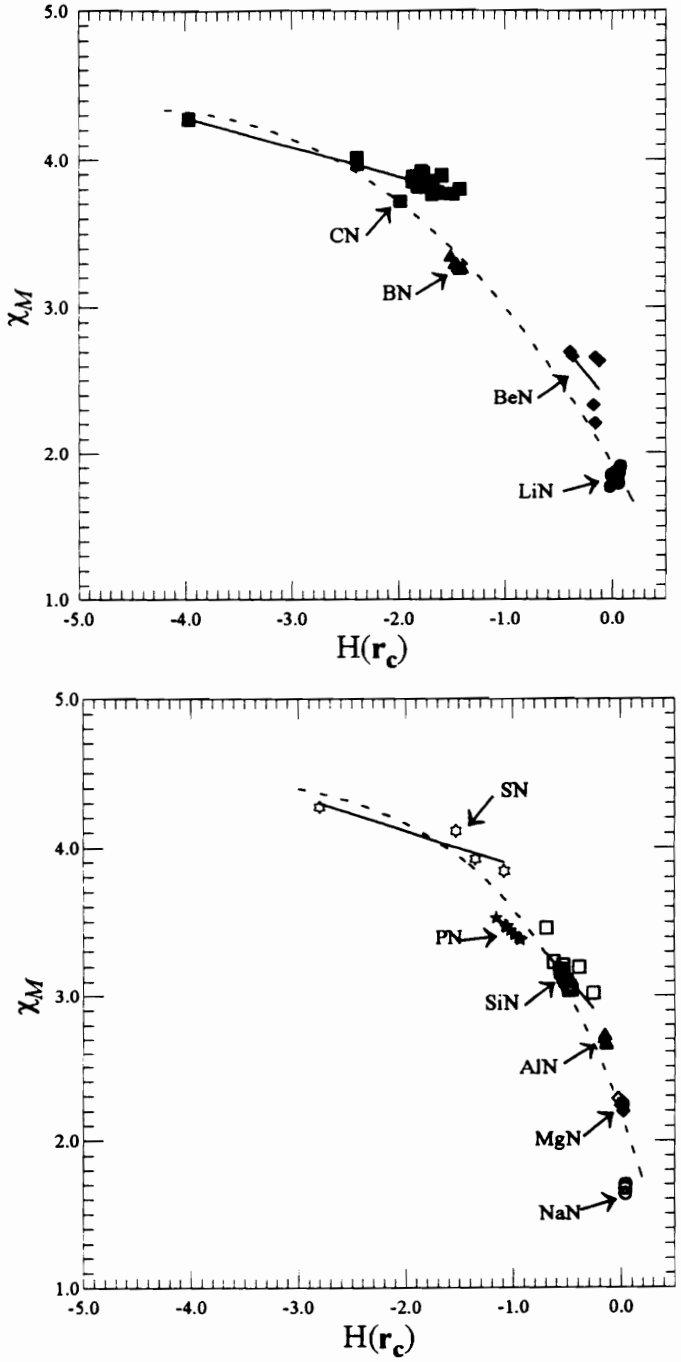

Figure 21: Local Energy Density Evaluated at $\mathbf{r_c}$, $H(\mathbf{r_c})$, Versus the Relative Electronegativity of the M–Cation, χ_M Bonded to the Nitride Anion.

They also observed a decrease in the values of the curvature of the electron density distribution perpendicular to the bond at the bond critical point, λ_1 and λ_2. Since λ_1 is arbitrarily assumed to be the larger of the two, an average value for the curvature perpendicular to the bond was used in these studies, $\lambda_{1,2} = (\lambda_1+\lambda_2)/2$. The data from this study shows that in all cases, as χ_M decreases, $\lambda_{1,2}$ increases (Fig. 22). Unlike the data of Hill et al. (in press), there appears to be no correlation between the slopes of the trends for χ_M versus $\lambda_{1,2}$ based on the cation involved in the interaction. There is no apparent correlation between χ_M and $\lambda_{1,2}$ for the MgN bond data, although all the data points for the MgN bond fall along the general trend exhibited for all bond types. Hill et al. (in press) suggest that the character of the bond be considered ionic when $\chi_M \sim 1.0$, $\lambda_{1,2} \sim 0.0$ e/Å^5 and $\rho(\mathbf{r_c}) \sim 0.01$ e/Å^3, intermediate when $\chi_M \sim 3.0$, $\lambda_{1,2} \sim -10.0$ e/Å^5 and $\rho(\mathbf{r_c}) \sim 1.0$ e/Å^3 and predominately covalent when $\chi_M \sim 5.0$, $\lambda_{1,2} \sim -40.0$ e/Å^5 and $\rho(\mathbf{r_c}) \sim 3.0$ e/Å^3. Classifying the data obtained from nitrides using the above categories would indicate none of the bonds considered are covalent, including the CN and SN bonds. Trends in the data from the calculations on nitrides, suggest different ranges where a bond might be considered to have predominately one type of character. For example, from Fig. 22 considering values of $\chi_M > 3.6$ and $\lambda_{1,2} < -7.5$ brackets the data points for the CN and SN bonds. These bonds are commonly considered covalent, and this would indicate a covalent or shared interaction. Regardless of the values considered, the overall trend observed by Hill et al. (in press) for the oxides is observed for the nitrides. That is there is a systematic change in the character of the bond from covalent to ionic as $\lambda_{1,2}$ increases for both rows of the periodic table.

By studying the data presented in Bader and Essén's paper (1984), one can see

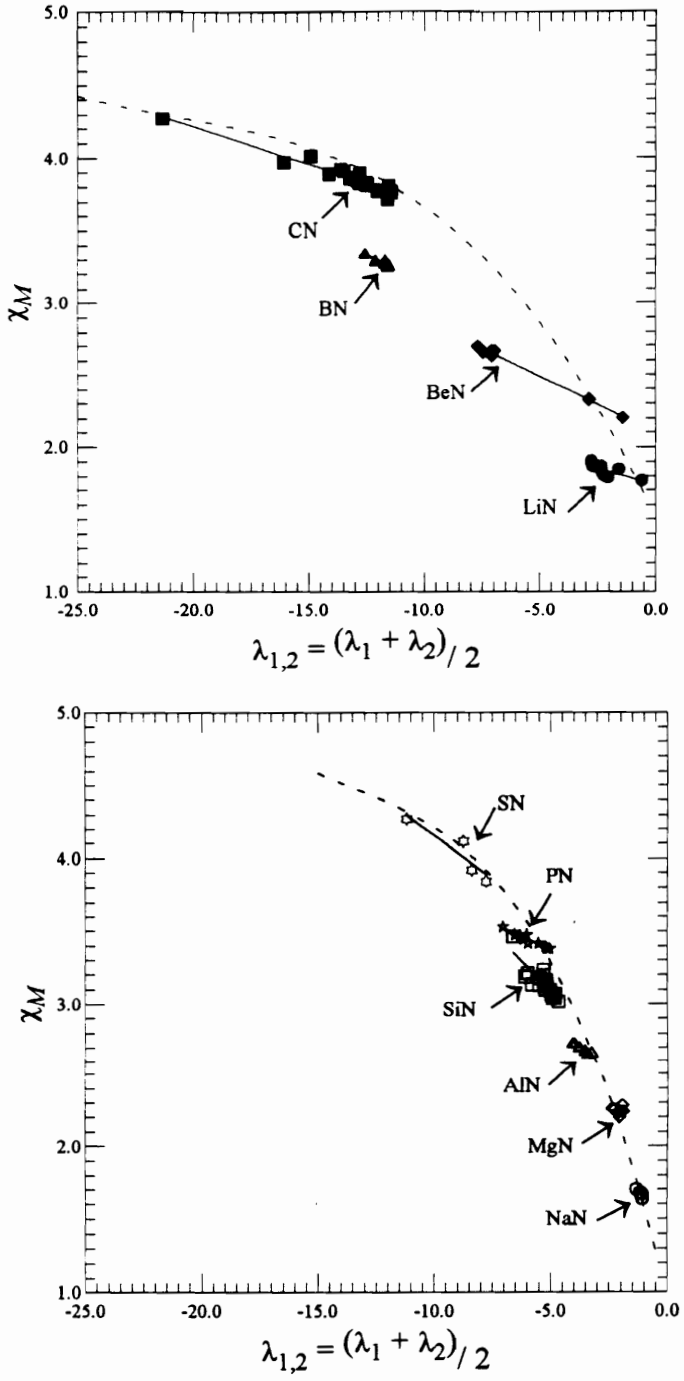

Figure 22: Average Curvature Perpendicular to the Bond Path, $\lambda_{1,2}$, Versus the Relative Electronegativity of the M–cation, χ_M.

that the curvature of the electron density along the AH bond, λ_3, increases as the cations involved in the bonds change from LiH to BeH. (Note: A = the cation bonded to the hydride anion, H) There is a decrease as the M–cation changes to BH and again an increase in moving from BH to FH for the first row of the periodic table. For the cations of the second row, λ_3 increases from NaH to SiH, but then decreases for PH and SH and increases once again for ClH. Hill et al. (in press) observed a linear increase in the value of λ_3 as χ_M increases for the oxides. The data evaluated in this study shows that with the exception of SN and possibly CN bonds, as χ_M increases, λ_3 increases, (Fig. 23). Note that neither a linear, exponential nor power curve can be fit to the CN bond data with any significance while the SN bond data shows an almost constant value for λ_3. Since χ_M is proportional to $\rho(\mathbf{r_c})$, the value of $\rho(\mathbf{r_c})$ increases as the value of χ_M increases. Thus as the relative electronegativity of the cation increases, the value of $\rho(\mathbf{r_c})$ increases and the curvature of the electron density at $\mathbf{r_c}$ along the bond becomes sharper, (λ_3 increases). As stated previously this phenomena can be associated with an increase in the build up of charge density between the two nuclei, i.e. with an increase in the covalent nature of the interaction.

Bader and Essén (1984) suggest that the ratio $|\lambda_1|/\lambda_3$ serves as an indicator of bond type. When $|\lambda_1|/\lambda_3$ is greater than 1.0, the interaction can be considered shared, when $|\lambda_1|/\lambda_3$ is $\sim$ 0.2 the interaction is of a closed-shell type. Intermediate values indicate bonds of an intermediate type. The value of $|\lambda_1|/\lambda_3$ is plotted against the value of $\chi_M$in Fig. 24. A division similar to that made by Bader and Essén (1984) can be made for the data on the nitrides in that the data from both CN and SN bonds shows values of $|\lambda_1|/\lambda_3$ greater than 1.0 and exhibits large χ_M values. Accordingly, these bonds would then be considered shared or covalent while LiN, BeN, NaN, MgN,

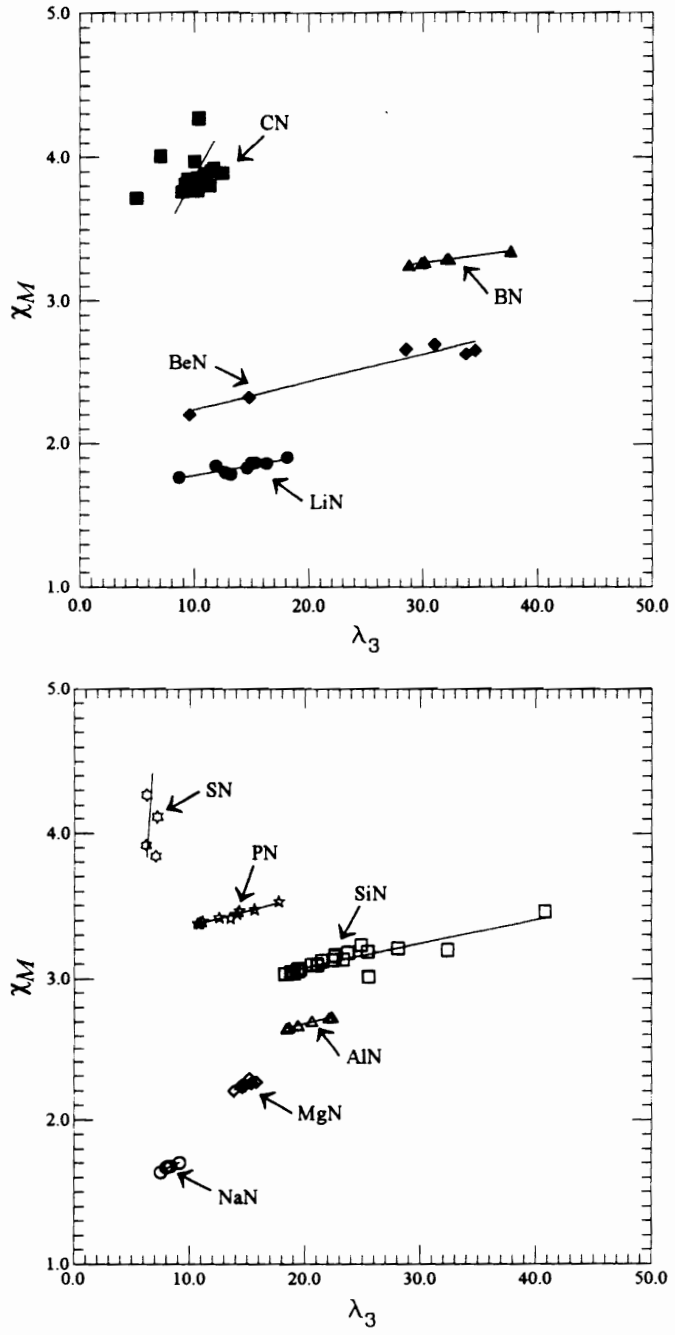

Figure 23: Curvature of the Electron Density Distribution Parallel to the Bond Path, λ_3, Versus the Relative Electronegativity of the M–Cation in the Bond, χ_M

AlN and SiN bonds which all have values for $|\lambda_1|/\lambda_3$ of ~ 0.20, small χ_M values and would be considered of a closed shell type. The data for bonds where B is bonded to N or P is bonded to N have intermediate values for $|\lambda_1|/\lambda_3$ (= 0.40 to 0.50) and intermediate values for χ_M. They would thus be considered an intermediate interaction. The two largest values for $|\lambda_1|/\lambda_3$ found for bonds containing first row cations are $\sim$ 2.4 and $\sim$ 2.3 for the CN bonds in the H_5Be_2CN and the H_5CN_3 molecules, respectively. The largest value of $|\lambda_1|/\lambda_3$ for the second row is found for the molecule H_6SN_4 where $|\lambda_1|/\lambda_3$ has a value of $\sim$ 2.0.

In Fig. 25 the average relative electronegativity of each cation is compared for MN bonds and for MO bonds. A nearly perfectly linear trend is observed indicating that the relative electronegativity of the cation is approximately the same when it is bonded to nitrogen as it is when bonded to oxygen.

3.3.3 Laplacian of the Electron Density Distribution

From Fig. 22 the value of $\lambda_{1,2}$ decreases as χ_M increases, and from Fig. 23 except for SN and potentially CN bond data, the curvature of the electron density parallel to the bond increases at a higher rate than the curvatures perpendicular to the bond. Thus, the Laplacian of the electron density distribution evaluated at the bond critical point, $\nabla^2\rho(\mathbf{r_c})$, which is the sum of the three curvatures of the electron density, should be primarily dominated by λ_3 for all MN bonds except CN and SN bonds. Figure 26 displays the value of the Laplacian of the electron density at r_c, $\nabla^2\rho(\mathbf{r_c})$, versus the relative electronegativity. As expected the trends are similar to those of λ_3 for the data from all MN bonds, (M = Li, Be, B, Na, Mg, Al, Si, and P). The data from CN and SN bonds show a completely different trend, more like that of $\lambda_{1,2}$ versus χ_M. This too is expected since the value of λ_3 with respect to χ_M from the data

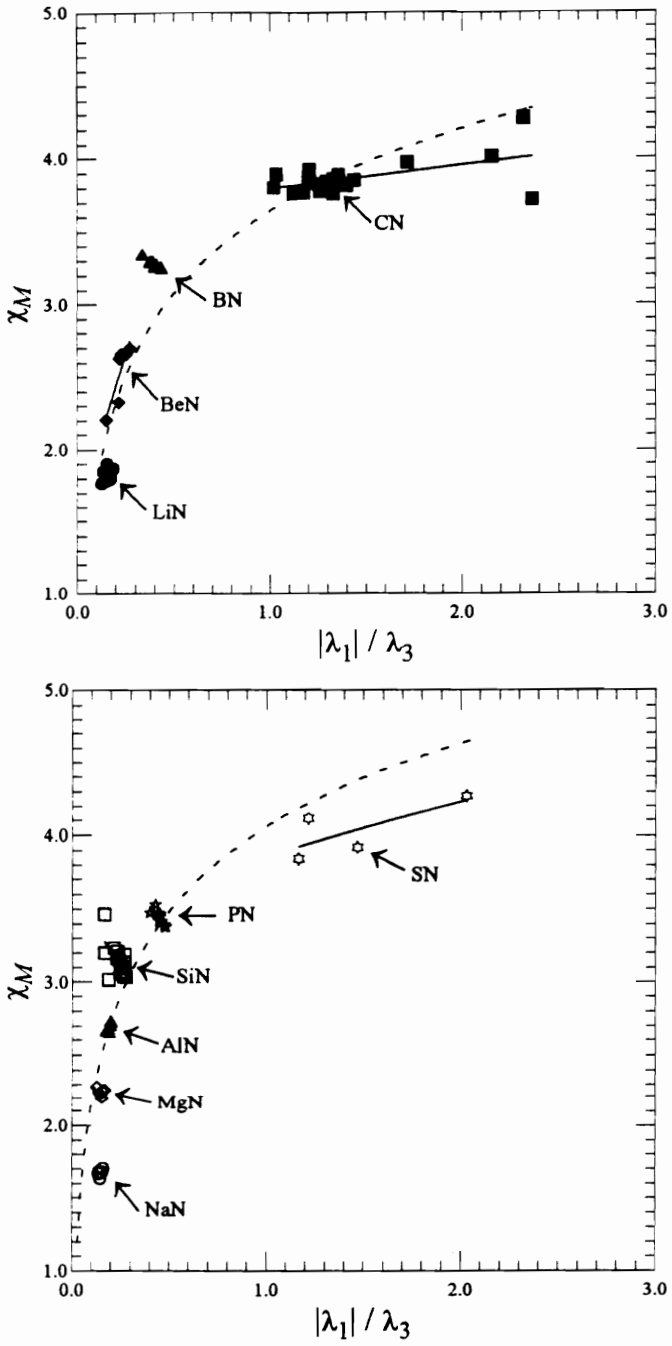

Figure 24: Parameter for Curvature of the Electron Density Distribution Perpendicular and Parallel to the Bond Path, $|\lambda_1| / \lambda_3$ Versus the Relative Electronegativity of the M–Cation, χ_M.

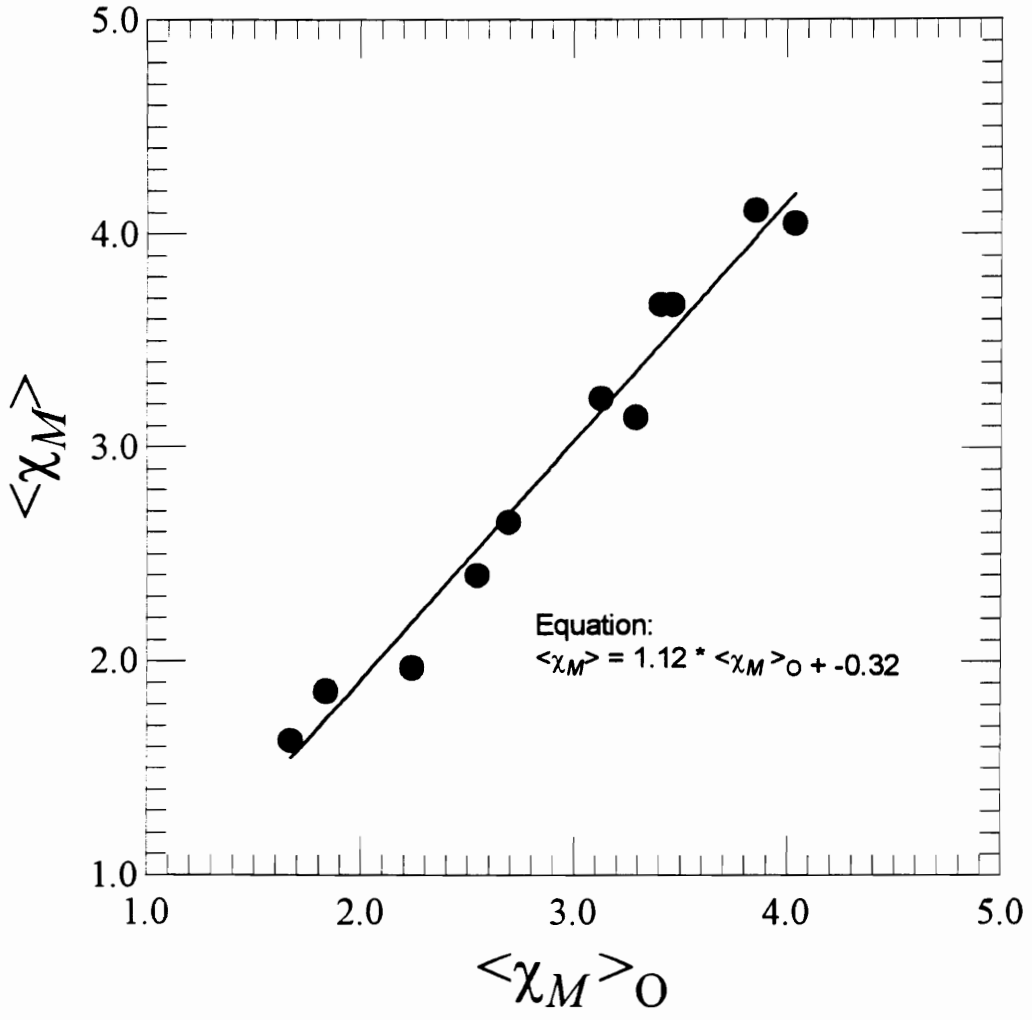

Figure 25: Average Relative Electronegativity of the M–cation, for this Study, $<\chi_M>$, Compared with the Average Relative Electronegativity of the M–cation for Oxides, $<\chi_M>_O$.

for CN and SN bonds is approximately constant. The above trends indicate that the Laplacian displays a negative slope for χ_M versus $\nabla^2\rho(\mathbf{r_c})$, for bonds involving the highly electronegative cations, and a positive slope for bonds involving the more electropositive cations (Fig. 26). A similar observation was discovered in the data from the oxides studied by Hill et al. (in press), where the slope of the Laplacian for the NO bond data was negative while all other slopes were positive. As noted by Hill (in press), except for the NO bond data in their case and the CN and SN bond data for this study, the trends between $\nabla^2\rho(\mathbf{r_c})$ and χ_M of Fig. 26 are reverse of those reported for the hydrides by Bader and Essén (1984). Bader and Essén (1984) reported a decrease in $\nabla^2\rho(\mathbf{r_c})$ as the electronegativity of the A-cation in AH bonds increases for each row of the periodic table.

As mentioned earlier, Bader and Essén (1984) consider an interaction to be shared when the electron density at the critical point is relatively large and the Laplacian of the electron density at the critical point is large in magnitude and negative. A closed shell interaction is indicated by a smaller $\rho(\mathbf{r_c})$ and $\nabla^2\rho(\mathbf{r_c}) > 0$. Figure 27 shows a plot of $\nabla^2\rho(\mathbf{r_c})$ vs. $\rho(\mathbf{r_c})$. This figure can be divided into regions that indicate where bonds are expected to be predominately shared and regions where bonds are expected to be predominately closed–shell. For example, a covalent interaction might be considered to exist when $\rho(\mathbf{r_c}) \geq 0.1\ \nabla^2\rho(\mathbf{r_c}) - 0.1$. An ionic interaction could be indicated when the value of $\rho(\mathbf{r_c}) \leq 0.1\ \nabla^2\rho(\mathbf{r_c}) - 1.1$. Any bond type which exhibits values between these ranges would then be considered intermediate in nature. Based on this, CN and SN bonds are covalent interactions while LiN, BeN, NaN, MgN, AlN and SiN bonds exhibit closed–shell characteristics. The remaining MN bonds, BN and PN are intermediate in nature.

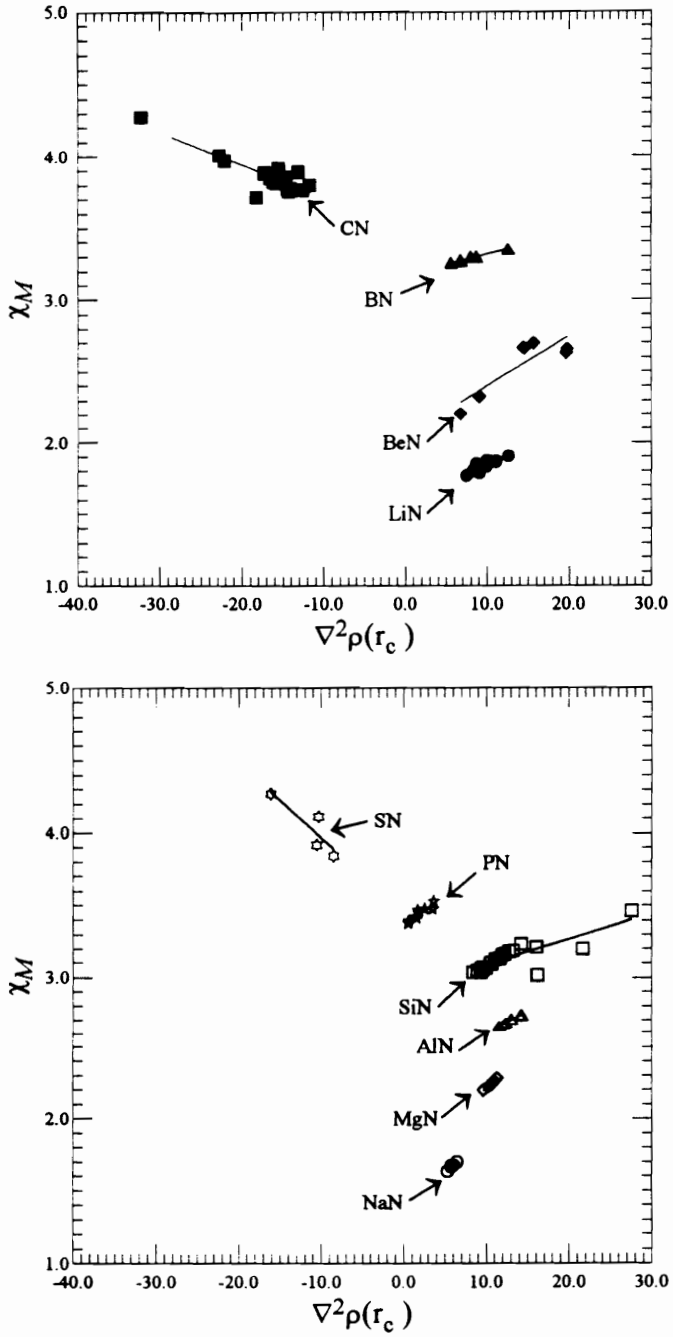

Figure 26: Laplacian of the Electron Density Distribution at $\mathbf{r_c}$, $\nabla^2\rho(\mathbf{r_c})$, Versus the Relative Electronegativity of the M–cation in the Bond, χ_M

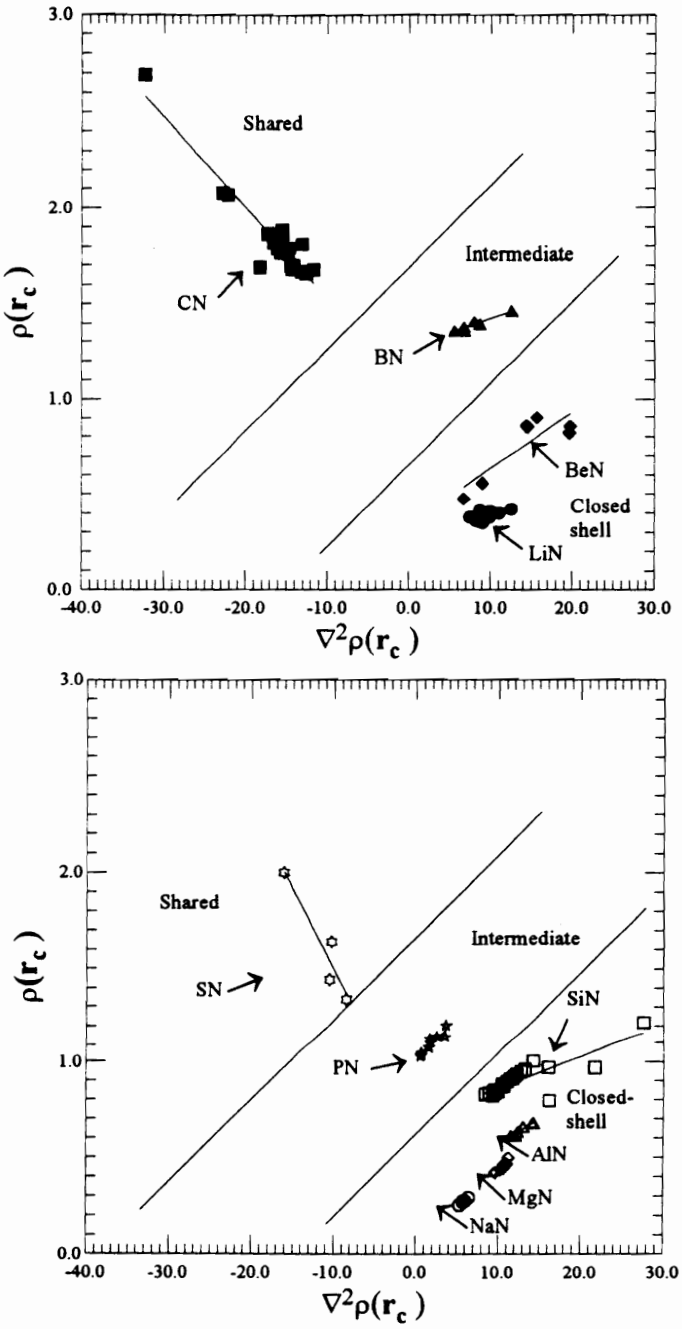

Figure 27: Laplacian of the Electron Density Distribution at $\mathbf{r_c}$, $\nabla^2\rho(\mathbf{r_c})$, Versus the Electron Density Distribution at $\mathbf{r_c}$, $\rho(\mathbf{r_c})$.

3.3.4 Profiles of the Curvatures

To better understand the relationship of the curvatures of the electron density distribution with electronegativity, sections of $\rho(\mathbf{r})$ were evaluated both perpendicular and parallel to the bond for a progression of MN bonds, (Figs. 28 and 29). The electronegativity of the M–cation in the MN bonds studied increases from left to right across the first two rows of the periodic table, but the bonds have essentially constant bond lengths. Therefore, any differences observed for these plots should be relatively independent of bond length. $\rho(\mathbf{r})$ for the first row cations, (upper plots) was calculated for the BeN bond in the H_7BeC_2N molecule, one BN bond in the H_6B_3N molecule and the CN bond in the H_5Be_2CN molecule. The average bond length for the MN bonds used in the upper plots of Figs. 28 and 29 is 1.47 Å with an average deviation of 0.02 Å. In the lower plots $\rho(\mathbf{r})$was calculated for one AlN bond in the H_6AlN_3 molecule, one SiN bond in the H_8BSi_2N molecule, one PN bond in the H_6P_3N molecule and one SN bond in the $H_{12}SN_6$ molecule. The average bond length for the bonds used to make these plots is 1.76 Å with an average deviation of 0.01 Å. In Fig. 28 the electron density distribution, $\rho(\mathbf{r})$, calculated for the first (upper plot) and second (lower plot) row cations, is plotted in the direction perpendicular to the bond. The bcp is located at 0.0 on this plot. Figure 29 displays the electron density distribution evaluated along the bond path. The electron density parallel to the bond, is a maximum at the cation (arbitrarily located at zero) and continuously decreases towards a minimum at the bcp. To the right of the bcp, towards the nitride anion, we again see an increase in the electron density distribution with a maximum at the location of the nucleus of the nitride anion. The shapes of these profiles are as expected from level line electron density distribution plots calculated by previous

authors (Bader, 1990) and from Figs. 8 and 9. Note the shape of the electron density displayed for the direction parallel to the bond for the CN and SN bonds. In both cases, the minimum in the distribution profile, the well, is extremely flat. It is difficult to determine the location of the critical point on such a flat surface and a slight error makes a significant difference in calculated values.

For bonds with an approximately constant bond length, Hill et al. (in press) observe an increase in the perpendicular curvature of the electron density, (λ_1 becomes more negative) as the Pauling electronegativity of the M–cation increases for both first and second row cations. In this study, the curvature of the electron density perpendicular to the bond for bonds with first row cations does not show any general trends. However, $\rho(\mathbf{r})$ for bonds involving the second row cations bonded to the nitride anion exhibits the same increase in curvature with increasing electronegativity as observed by Hill et al. (in press). They also found fewer systematics in the trends for the second row M–cations in MO bonds for the curvature parallel to the bond, λ_3, than I find. For the nitride bond data there is a well–developed trend for λ_3 with respect to electronegativity. As the Pauling electronegativity of the M–cation involved in the MN bond decreases, λ_3 increases for both row 1 and row 2 cations. This is in opposition to what was observed previously. The significant difference between the previous observation and that indicated here, is that here the bond length is essentially constant. Thus, for a constant bond length, as the electronegativity of the cation in a given row increases, the curvature parallel to the bond decreases and the value of $\rho(\mathbf{r_c})$increases. On average the curvatures perpendicular to the bond are sharper for the bonds with first row cations than bonds involving second row cations while the value of the electron density at the critical point, $\rho(\mathbf{r_c})$ is in approximately

the same range. This differs from what was found by Hill et al. (in press). They observed that the λ_1 curvatures are sharper and that $\rho(\mathbf{r_c})$ is appreciably larger in value for bonds involving first row cations compared to those involving second row cations. One should be careful not to conclude too much from these observations, however, since the bond length for the bonds involving first row cations is different from the bond length for the bonds involved with second row cations.

3.3.5 Promolecules

The values obtained for the promolecule electron density distribution of the nitride molecules evaluated at the critical point, $\rho(\mathbf{r_c})_\mathrm{p}$, are plotted against R($M$N) in Fig. 30. Note that the general trends displayed for the molecular orbital calculations are repeated with fairly good accuracy using the promolecule calculations. As was observed for the molecular orbital calculations, the trends tend to separate according to the M–cation in the MN bond. Data from the NaN, MgN and AlN bonds tend to fall along a single line, which was also observed for molecular orbital calculations. The numerical value for $\rho(\mathbf{r_c})$ determined from molecular orbital calculations is greater than $\rho(\mathbf{r_c})_\mathrm{p}$ for the same MN bond. Hill et al. (in press) discovered that the values for $\rho(\mathbf{r_c})_\mathrm{p}$ showed the same trends as $\rho(\mathbf{r_c})$ and that the magnitude of $\rho(\mathbf{r_c})_\mathrm{p} < \rho(\mathbf{r_c})$. Thus, the values of $\rho(\mathbf{r_c})_\mathrm{p}$ for both oxides and nitrides do a good job of ranking $\rho(\mathbf{r_c})$ versus bond length for one bond relative to another although the value of $\rho(\mathbf{r_c})_\mathrm{p}$ underestimates the value of $\rho(\mathbf{r_c})$. Figure 31 is a plot of the data for $\rho(\mathbf{r_c})$ versus $\rho(\mathbf{r_c})_\mathrm{p}$. Figure 31 shows that the underestimation of $\rho(\mathbf{r_c})$ is more pronounced for the highly electronegative M–cations involved in the bonds. The value of the greatest difference between $\rho(\mathbf{r_c})_\mathrm{p}$ and $\rho(\mathbf{r_c})$ is associated with the H_5CN_3 molecule. Interestingly, this is the only molecule in this study expected to have a CN double bond.

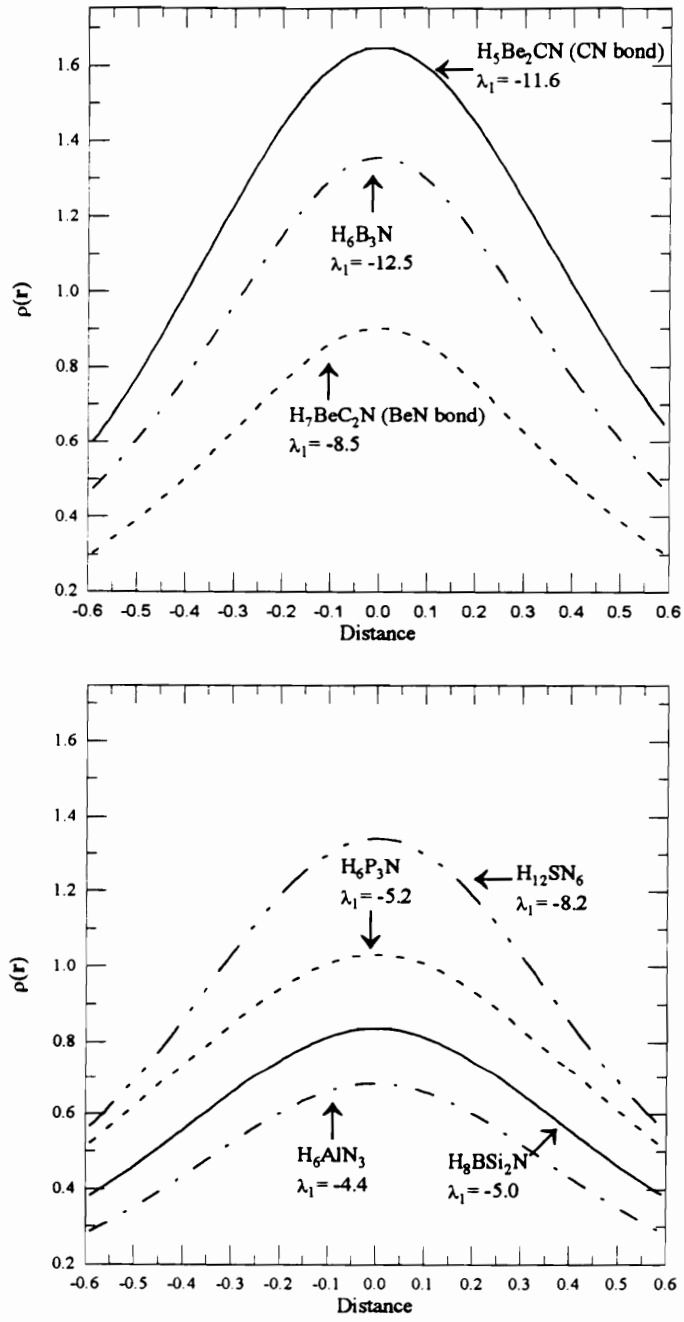

Figure 28: Electron Density Profile Perpendicular to the Bond, for Molecular Orbital Calculations. The bond critical point is located at 0.0. The upper plot is for bonds involving cations from the first row of the periodic table, the bond length for these bonds $\sim$ 1.47 Å. The lower plot is for bonds involving cations from the second row of the periodic table with a bond length of $\sim$ 1.76 Å.

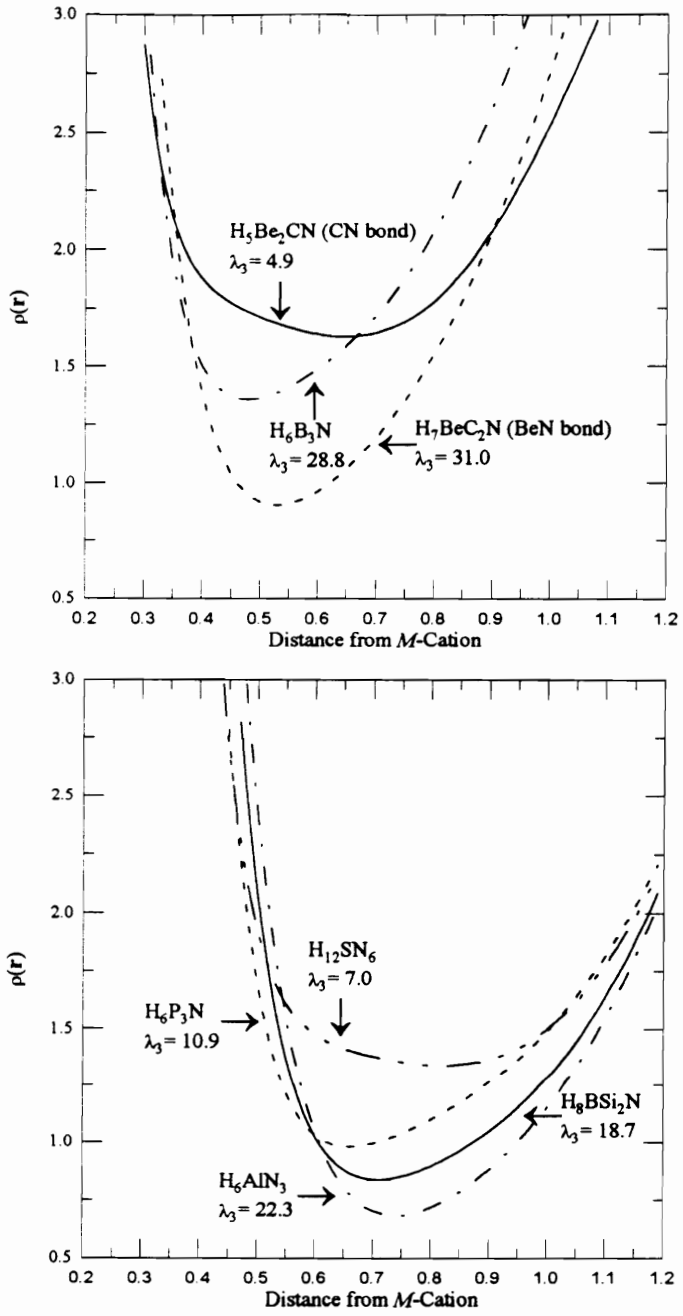

Figure 29: Electron Density Profile Parallel to the Bond, for molecular orbital calculations. The M–cation in the MN bond is located at 0.0. The upper plot is for bonds involving cations from the first row of the periodic table, the bond length for these bonds $\sim$ 1.47 Å. The lower plot is for bonds involving cations from the second row of the periodic table with a bond length of $\sim$ 1.76 Å.

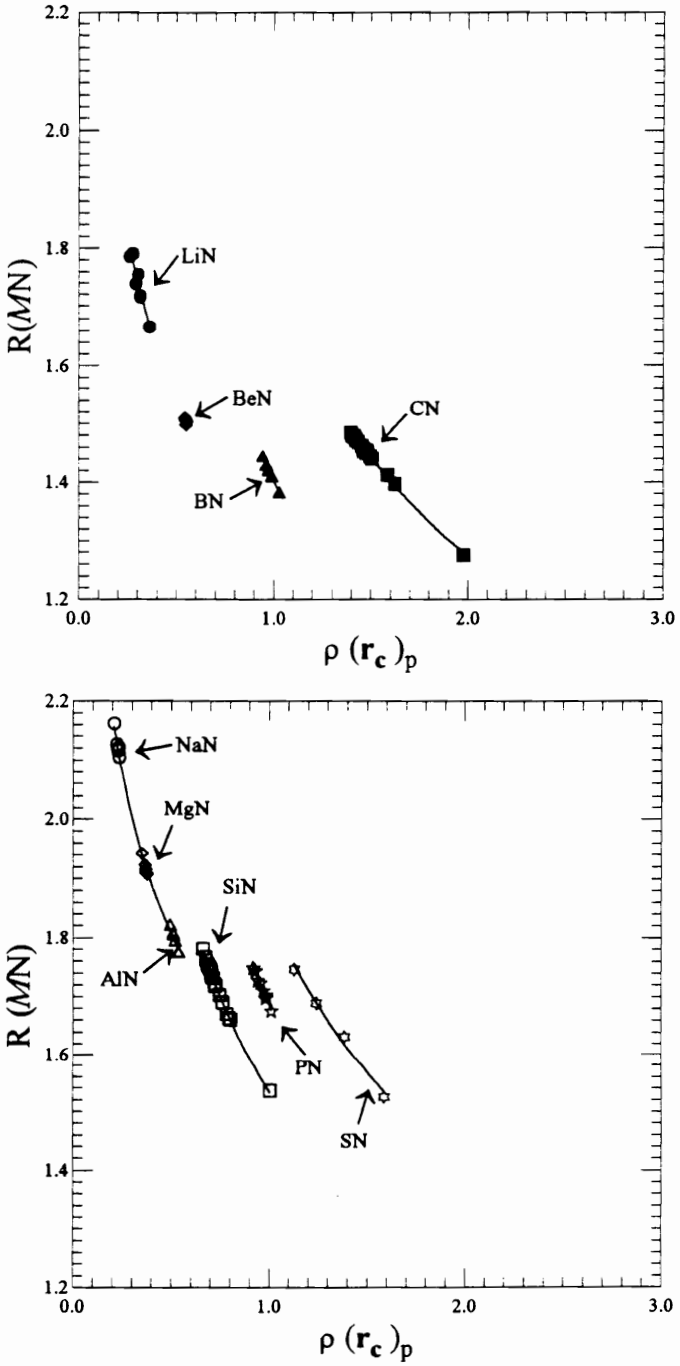

Figure 30: Promolecule Electron Density Distribution Evaluated at the Bond Critical Point, $\rho(\mathbf{r_c})_\mathrm{p}$, Versus Bond Length, R($M$N)

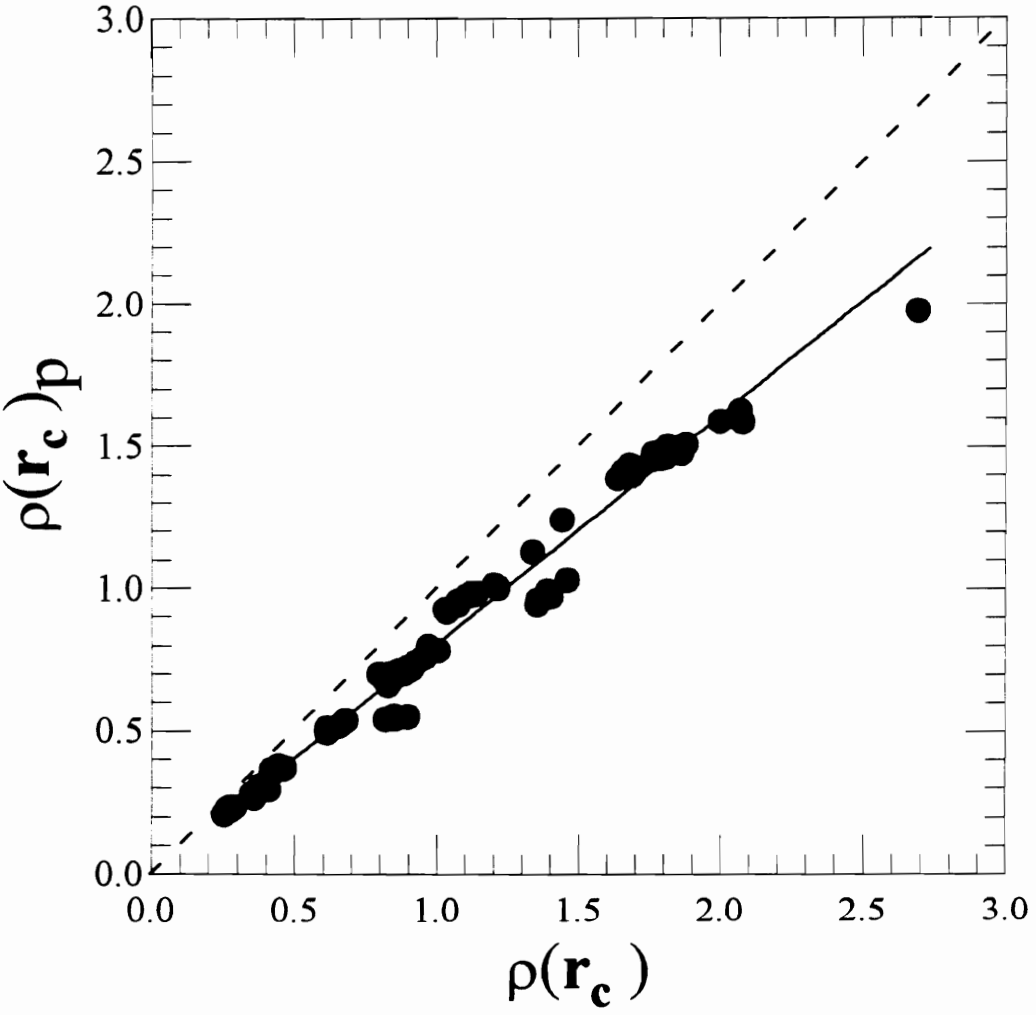

Figure 31: Comparison of the values of the electron density distribution evaluated at the critical point, for molecular orbital calculations, $\rho(\mathbf{r_c})$, and for promolecule calculations, $\rho(\mathbf{r_c})_\mathbf{p}$.

Feth et al. (1993) established that bonded radii determined from promolecule calculations, r_p(N), are strongly correlated with both ionic or crystal radii as well as radii determined from experimental electron density distributions. Figure 32 plots r_p(N) versus r_b(N). As expected from the work of previous authors (Feth, 1993; Gibbs, 1992) the bonded radius of nitrogen is nearly identical whether calculated using the electron density distribution of a promolecule or from molecular orbital calculations. Note that there is less scatter in the data for larger values of the radius of nitrogen. Larger values of the bonded radius of nitrogen are associated with bonds involving the less electronegative cation, so again it appears the higher the electronegativity of the cation involved in the bond, the more poorly the promolecule–derived values approximate those determined using molecular orbital calculations. The average deviation of r_p(N) from r_b(N) is 0.03 Å. The greatest deviation from the nearly 1:1 trend is found for the CN bond in the H_5Be_2CN molecule with a difference of 0.09 Å. In all cases except three, r_p(N) is less than r_b(N). The three exceptions are for values calculated for the SN bond in Li_6SN_4, the CN bond in H_3Na_2CN and one of the CN bonds in H_5CN_3, where r_p(N) overestimates r_b(N) by only 0.005 Å, 0.008 Å and 0.010 Å respectively.

The value of the relative electronegativity of the M–cation in an MN bond for a promolecule, $\chi_{(M)_\mathrm{p}}$ and χ_M for the same bond is approximately the same (Fig. 33). This indicates that the effects which bond formation has on r_b(N) and $\rho(\mathbf{r_c})$, are minimal. Any effects of bonding in r_b(N) and/or $\rho(\mathbf{r_c})$ appear to cancel out when F_M is evaluated. That is, the effects are not apparent in the ratio $r_b(\mathrm{N})/(\mathrm{N}_M \times \rho(\mathbf{r_c}))$. The value of $\chi_{(M)_\mathrm{p}}$ explains 99.3 percent of the variation in the value of χ_M. Thus, a calculation of $\chi_{(M)_\mathrm{p}}$ gives an accurate value of the relative electronegativity of a

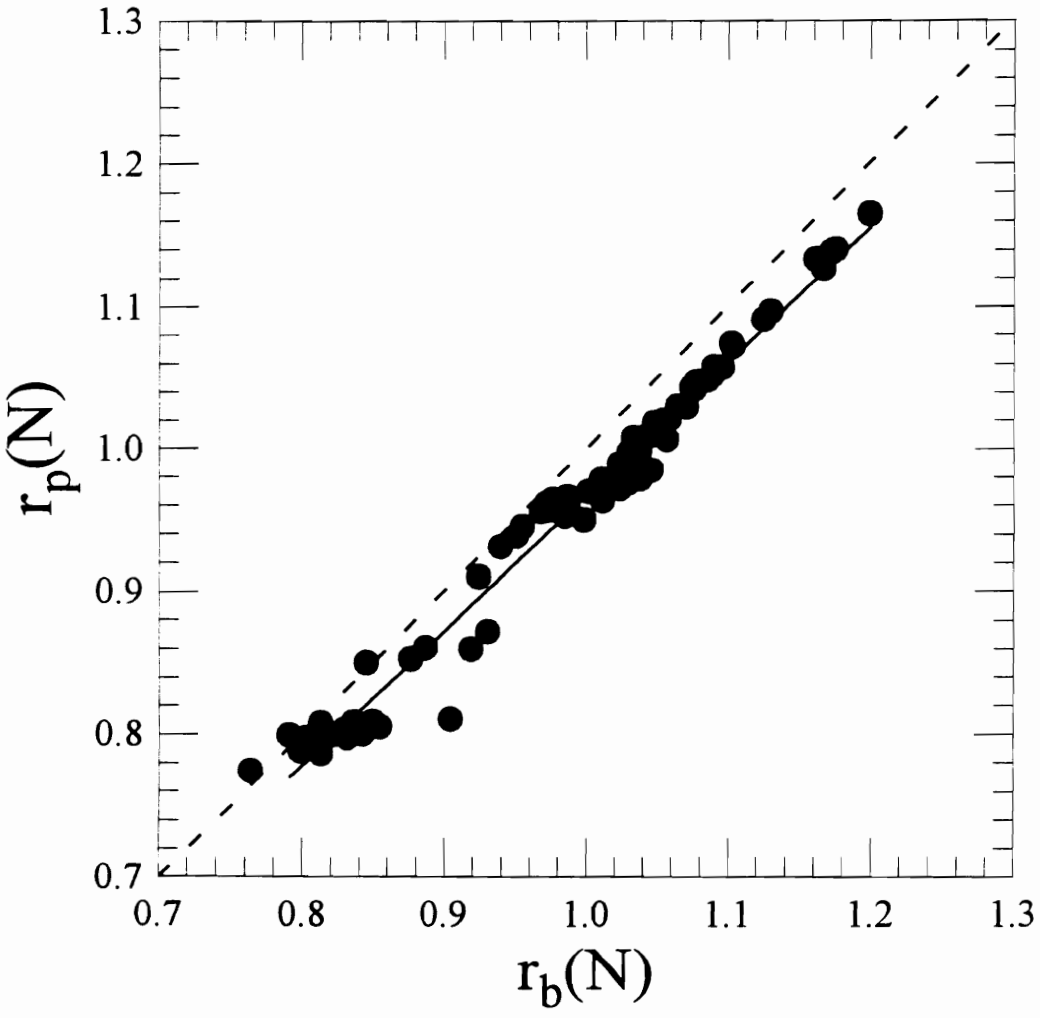

Figure 32: Comparison of the Bonded Radius of Nitrogen Derived Using Promolecule Calculations, $r_p(N)$ with the Radius Derived Using Molecular Orbital Calculations, $r_b(N)$.

M–cation for a molecule and potentially for a crystal.

By comparing the electron density distribution calculated along the bond path determined for promolecules (Fig. 34) and for molecular orbital type calculations (Fig. 29), additional insight may be gleaned regarding the difference between these two approaches to bond analysis. As mentioned previously, the values of $\rho(\mathbf{r_c})_\mathbf{p} <$ the values of $\rho(\mathbf{r_c})$, but some other differences are also apparent. For example, the curvature of the electron density for the bonds involving second row cations is much sharper for the molecular orbital calculations than it is for the promolecule calculations. Also, note that the curvature of $\rho(\mathbf{r_c})_\mathbf{p}$ for the promolecule calculation for the BeN bond is significantly different than that for the molecular orbital calculations. As stated by Hill et al. (in press), care must be taken not to infer too much from these results since the promolecule electron density can be constructed in several ways. Aside from determining the promolecule $\rho(\mathbf{r})$ by the superposition of spherically averaged atomic electron density distributions as was done here, the $\rho(\mathbf{r})$, may also be determine by the superposition of oriented atomic electron density functions or as the superposition of the electron density distributions associated with the states into which a molecule disassociates.

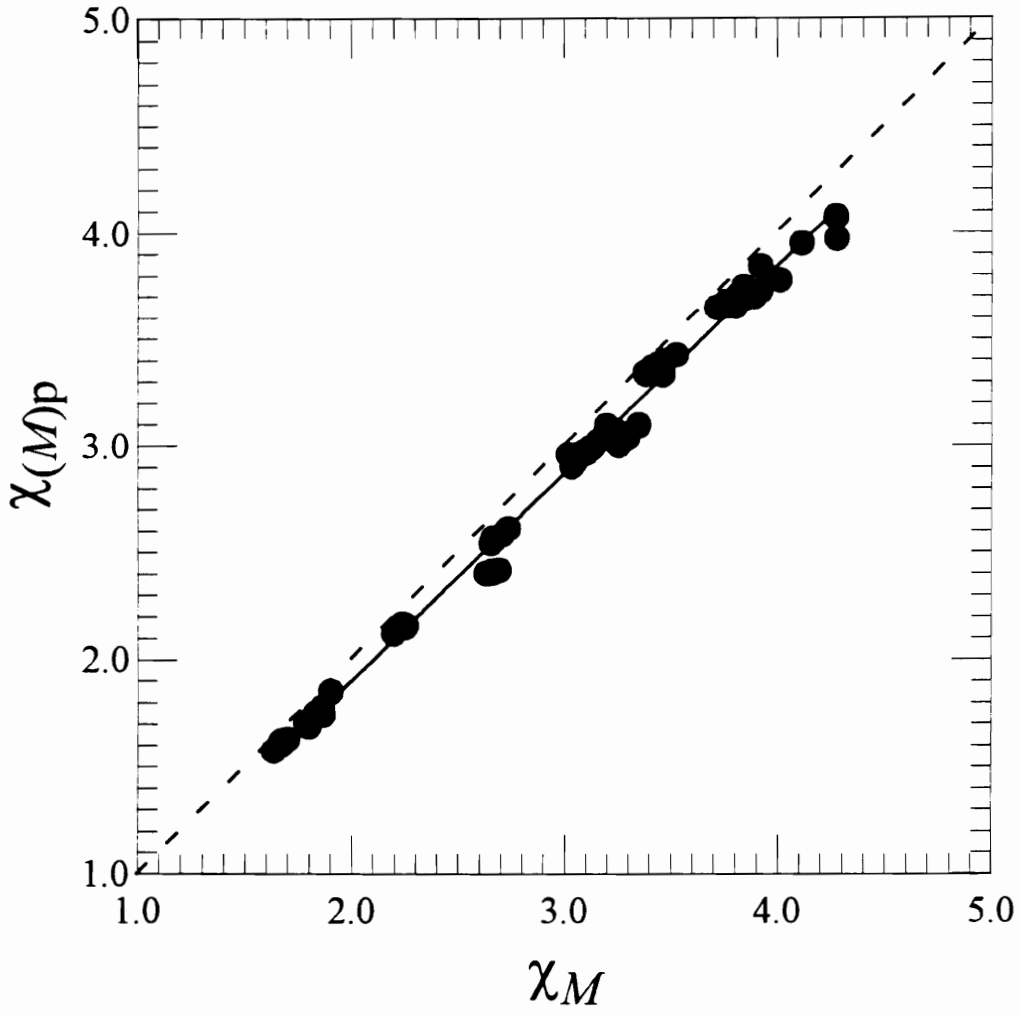

Figure 33: Relative Electronegativity of the M–cation, for this Study, χ_M, Compared with the Relative Electronegativity of the M–cation calculated for Promolecules, $\chi_{(M)p}$.

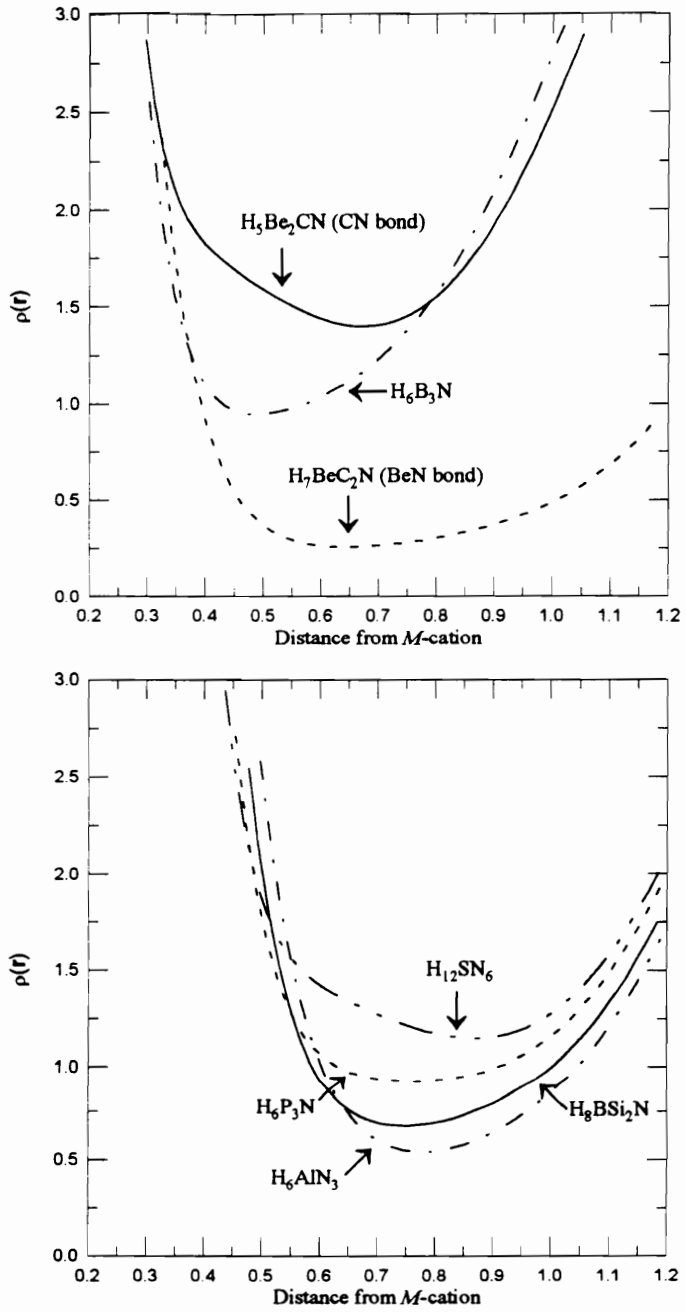

Figure 34: Electron Density Distribution Profile Parallel to the Bond, for Promolecule Calculations. The M–cation in the MN bond is located at 0.0. The upper plot is for bonds involving cations from the first row of the periodic table, the bond length for these bonds $\sim$ 1.47 Å. The lower plot is for bonds involving cations from the second row of the periodic table with a bond length of $\sim$ 1.76 Å.

3.4 Applications

Molecular Orbital calculations in conjunction with the bond critical point properties of molecules can be directly applied to many cases. An example of this application is the use of MO/AIM calculations in understanding the structure of diborane (B_2H_6). For many years, it was debated whether or not the two boron atoms in the diborane molecule where bonded. The existence of a (3,–1) critical point in the region between the two boron atoms finally answers this question; the boron atoms are in fact bonded (Bader, 1990). It was the application of theory that allowed a determination of the bond critical point and thus offered a final solution.

Another area where the theories described above can be applied is in the determination of experimental electron density distributions. When a material is analyzed using X-Ray diffraction, the results are a series of peaks. The integrated intensity of these peaks, I, is related to the structure factor, F_s by $I^2 \propto |F_s|^2$. The electron density distribution, ρ, is in turn related to the structure factors. The difficulty arises in going from the $|F_s|^2$ to ρ since the magnitude of the structure factor does not contain information on the associated phase angle. One possible way around this is to use models to fill in gap, historically, procrystal models have been used. As shown in this study, procrystal models provide a good estimate, but other than electronegativity, the values tend to be different from more realistic theoretical models. The improved modeling ability we see using the Becke basis makes the possibility of more accurate experimental results a reality.

3.5 Summary

Values of the properties of the bond critical point offer a set of criteria for evaluating different types of bonds. Correlations among the bond critical point properties of the electron density of nitride molecules scatter along well–developed approximately linear trends. I have shown that $R(MN)_{calc}$ explains more than 97 percent of the variation in $R(MN)_{obs}$. These results indicate that as the bond lengthens, the electron density at the bond critical point decreases while the bonded radius of N increases. The relative electronegativity of the M–cation in an MN bond, χ_M, was calculated using Eq. 1. As χ_M decreases, the bond length increases, the electron density distribution at the bond critical point decreases, λ_3 decreases (slightly), except in the case of CN and SN bonds, and $\lambda_{1,2}$ increases. In addition, except for bonds involving nitrogen and C or S, as χ_M decreases $\nabla^2\rho(\mathbf{r_c})$ decreases. Also, as $\chi_M$decreases, $H(\mathbf{r_c})$ increases. Using the criteria established by Bader and Essén (1984), we find CN and SN bonds to be predominately covalent, LiN, BeN, NaN, MgN and SiN bonds to be predominately ionic and BN and PN to be intermediate type bonds. Using the criteria established by Cremer and Kraka (1984), CN and SN bonds are shared interactions while the remainder of the MN bonds are closed–shell. Hill et al. (in press) suggest the using a value of $\chi_M \sim 2.5$ to distinguish between bond types. For the nitride data of this study, we find that a value of $\chi_M \sim 2.8$ characterizes bonds in a manner closer to historical methods. Using this value of χ_M I find bonds between nitrogen and Li Be, Na, Mg and Al to be predominately ionic while bonds containing B, C, Si, P and S cations are predominately covalent.

The data from the bond critical point properties of nitride molecules exhibits linear trends which in general, parallel similar trends described by previous authors. Criteria

used by Bader (1990), Bader and Essén (1984), Boyd and Edgecombe (1988) and Hill et al. (in press) and as suggested in this work, seem to divide the results presented here into logical divisions. Although the exact values of the various parameters used to indicate where divisions should occur is still up for debate, it appears obvious that there is a variation in bond type. For this work, a continuous variation from a covalent type of bond, through an intermediate type to a more ionic bond type is observed. Interactions which are expected to be covalent, exhibit behavior shown by previous authors to be characteristic of that type of interaction. The same can be said for the closed-shell interactions. Perhaps most striking is the consistent oddity in the results for CN and SN bond types which have been shown to have a very flat well between the cation and nitrogen. These extremely covalent bonds seem to exhibit characteristics significantly different from the remaining bond types.

One result of this study is that in most cases all of the trends discussed tend to separate out according to the cation to which nitrogen is bonded to. The variations within each MN bond are nearly linear, but with a few exceptions the variations from one M1N bond to another M2N bond not are related by linear trends. The data presented in this study adds evidence to the suggestion by Hill et al. (in press), that each type of MN bond appears to be a unique entity. In addition, this study presents further evidence as to the general applicability of using bond critical point properties as a method of analyzing bond types.

It is evident from the data presented on promolecules that the effects of any rearrangement of electron density upon bond formation is minimal. The general trends and approximate values for many of the bcp properties can be explained using a promolecule model. That is, they can be explained by a simple superposition

of spherically averaged electron density distributions positioned at the location of each nucleus. In this model, no additional information is added to describe the bond. Since the promolecule model is well understood, knowing which bonding affects can be explained in this manner offers insight into bonding that might otherwise be missed.

This study has shown that for the calculated data, the variations indicate that different bond types exhibit different bond critical point properties. These results concur with what has historically been known, that there are differences in MN bonds. As suggested by Bader (1990), there appear to be limiting bond types, ionic and covalent, with a progression from one type to the other as we move across the periodic table from successively less to more electronegative cations. Although there does not seem to be a clear consensus on the exact values used to distinguishing between the two types, it is evident that a "degree of ionicity or covalency" is a more realistic interpretation than stating a bond is or is not covalent or ionic. Differences and how they can be quantified have been presented in this study. Table 4 contains a summary of the methods which may be used to determine the characteristics of a bond. Based on the information presented here and in Table 4, with a few known parameters it is possible to estimate the character of a bond.

Table 4: Guidelines for Characterizing Bonds Based on Several Approaches. References; (a) Bader and Essén, 1984, (b) Cremer and Kraka, 1984, (c) Boyd and Edgecombe, 1988, (d) Hill et al., in press, (e) this study

Shared Interactions	<—>	Closed–Shell Interactions	ref.
$\nabla^2\rho(\mathbf{r_c})$ large and negative		$\nabla^2\rho(\mathbf{r_c})$ positive	a
$\lvert\lambda_1\rvert/\lambda_3 > 1.0$		$\lvert\lambda_1\rvert/\lambda_3 < 1.0$	a
$\rho(\mathbf{r_c})$ relatively large		$\rho(\mathbf{r_c})$ relatively small	a,b
$H(\mathbf{r_c}) < 0$ H/Å^3		$H(\mathbf{r_c}) > 0$ H/Å^3	b
χ_A large, (> 2.5)		χ_A small, (< 2)	c
$\chi_M \sim 5.0$		$\chi_M \sim 1.0$	d
$\lambda_{1,2} \sim -40.0$ e/Å^5		$\lambda_{1,2} \sim 0.0$ e/Å^5	d
$\rho(\mathbf{r_c}) \sim 3.0$ e/Å^3		$\rho(\mathbf{r_c}) \sim 0.1$ e/Å^3	d
$H(\mathbf{r_c}) \leq -1$		$H(\mathbf{r_c}) > 0$	d
$\rho(\mathbf{r_c}) \geq 0.067^*\nabla^2\rho(\mathbf{r_c}) - 0.1$		$\rho(\mathbf{r_c}) \leq 0.067^*\nabla^2\rho(\mathbf{r_c}) - 1.1$	e
$\chi_M > 3.6$		$\chi_M < 2.8$	e
$H(\mathbf{r_c}) < -1.5$ H/Å^3		$H(\mathbf{r_c}) \approx 0$ H/Å^3	e
$\lvert\lambda_1\rvert/\lambda_3 > 1.0$		$\lvert\lambda_1\rvert/\lambda_3 < 1.0$	e
$\lambda_{1,2} < -7.5$ e/Å^5		$\lambda_{1,2} > 0.0$ e/Å^5	e

3.6 Conclusions

Work from this study correlates with earlier evidence that there are significant differences between different bond types. The trends that the data from a given MN bond forms tend to be linear or slightly curved with respect to other bonds between the same M–cation and nitrogen. This implies that each different type of MN bond is a specific entity, independent in many ways from any other MN bond. The idea of "covalent" and "ionic" may be used to distinguish between limiting bond types, but the divisions are arbitrary. Instead there appears to be a general continuum from one extreme to the other.

Using the above, the next step should be to include other information such as experimental values to help quantify bonding. Using a robust basis such as the Becke basis should afford experimentalists with the tools necessary to retrieve more accurate electron density distributions for existing molecules and crystals. To date only a minimum of experimental data from electron density distributions exists which would be useful in a comparison, and none for nitrides.

Bonds classically thought of as covalent or ionic should or could be reevaluated to see what new information might be obtained by considering them on a continuous scale. A SiN bond, for example, in one material may be slightly albeit significantly different from a SiN bond in another material. Using the criteria established here, it is possible to judge the type of bond expected based on a few parameters. This in turn should offer insight into the kinds of properties expected for this material.

I have shown in this study that the bonds containing carbon or sulfur seem to vary significantly from the other MN bonds. Much of the existing electron density work, both theoretical and experimental, has been performed on organic systems,

(carbon containing). It is apparent from this work that CN and SN bonds do not always behave as other MN bonds and thus that observations based solely on carbon containing systems may not be accurate descriptions of the majority of bonds. Therefore, to understand bonding better, perhaps the focus should be moved away from studying systems containing carbon towards the inorganic systems. Once bonding is better understood the organic systems can be re–investigated.

The recent improvements in modeling the electron density distributions of small molecules offers greater opportunities for their incorporation into experimental research. As computer models become more and more efficient, their use in understanding chemical interactions will become more and more prominent. As stated by Boggs (1985) the introduction of parallel processors may offer some exciting possibilities in the way quantum mechanical calculations are approached. Instead of considering one electron at a time, accurate calculations may be approached by assigning to each electron its own processor allowing for true consideration of electron correlation and exchange. Personal computers today are powerful enough that calculations done on small molecules even with a relatively large basis are feasible. In addition, promolecule type calculations can easily be done on personal computers. The day may soon be approaching where interactions are routinely synthesized in a computer before any lab work is considered.

Appendix A: Bond Critical Point Theory

The atoms in molecules theory developed by Bader (1990) offers one approach to characterizing bonding. In Bader's work, the topology of the electron density distribution is used to characterize and evaluate atomic interactions. Each topological feature of the electron density has a critical point, $\mathbf{r}_c$, associated with it. The critical point is defined by Bader (1990) as the point where the first derivative of $\rho(\mathbf{r})$vanishes, that is, where $\nabla\rho(r_c) = 0$. Note, $\nabla\rho = \mathrm{i}\partial\rho/\partial x + j\partial\rho/\partial y + \mathrm{k}\partial\rho/\partial z$. The critical points are manifested as a maximum, minimum or saddle point in the electron density distribution. Whether they constitute a maximum or a minimum point, can be discovered by studying the signs of the second derivatives.

An ordered 3x3 array can be created from the nine second derivatives of the electron density which are of the form $\frac{\partial^2\rho}{\partial x\partial y}$. This matrix is called the Hessian matrix of the charge density or the Hessian of ρ. An "eigenvalue" of the Hessian is also a "curvature" of ρ, while the "eigenvectors" of ρ are also the "axes of curvature." Critical points are described by their rank, ω, and signature, σ. The rank of the critical point is the number of non–zero eigenvalues at that critical point. The signature is equal to the algebraic sum of the signs of the eigenvalues at that critical point. For stable molecular configurations, the rank of the critical point is three, and thus there are four possible types of critical points, (3,–3), (3,–1), (3,+1), and (3,+3). These points can be visualized graphically by determining the electron density map for a given plane, Figs. 8 and 9. The four types of critical points and what they represent are summarized below.

(3,–3) All three curvatures are negative, and ρ is a local maximum at $\mathbf{r}_c$. This type of critical point is associated with the nucleus of an atom.

(3,–1) Two of the three curvatures are negative, and ρ is a saddle point at $\mathbf{r}_c$. This type of critical point constitutes a "bond critical point" and is the critical point found between two bound atoms along the path of maximum charge density.

(3,+1) Two of the three curvatures are positive, and ρ is the reverse of the saddle point described above. This type of critical point is found between two out of plane nuclei.

(3,+3) All three curvatures are positive, and ρ is a local minimum at $\mathbf{r}_c$. This type of critical point is associated with a cage structure.

The gradient vector field of the electron density distribution, $\nabla\rho$, can be used to differentiate between the electron density distribution belonging to one atom and that which belongs to another. Gradient paths, trajectories of $\nabla\rho$, terminate at a local maximum, or nucleus, which serves as an attractor in the gradient field. The space traversed by all the gradient paths which terminate at the nucleus is called the basin of that atom. Bader (1990) defines an atom as the union of an attractor and its associated basin (Bader, 1993). The atomic basin is separated from neighboring atomic basins by an interatomic surface, S_{AB}, which indicates the existence of a (3,–1) critical point. Here the (3,–1) critical point acts as a two dimensional attractor in that gradient paths terminate at that point along the boundary only. It is this relationship which allows the physical definition of an atom as described above to be related to the underlying quantum mechanics.

The Laplacian of $\rho(\mathbf{r}_c)$, $\nabla^2\rho(\mathbf{r}_c)$, is the sum of the three eigenvalues of the Hessian matrix of $\rho(\mathbf{r}_c)$, ($\nabla^2\rho(\mathbf{r}_c) = \lambda_1 + \lambda_2 + \lambda_3$). Since it is the second derivative of $\mathbf{r}$, ($\nabla^2 = \partial_2/\partial x^2 + \partial_2/\partial y^2 + \partial_2/\partial z^2$), it highlights regions in the electron density distribution

where $\rho(\mathbf{r_c})$ is locally enhanced ($\nabla^2\rho(\mathbf{r_c})< 0$) or locally dissipated, ($\nabla^2\rho(\mathbf{r_c})> 0$).

Both theory and observation indicate that there should be a build-up of electronic charge density along the line connecting the nuclei which are thought to be bonded. When the system also possesses a minimum energy equilibrium internuclear separation, the condition is both necessary and sufficient in the determination of a "bond." That is the existence of a (3,–1) critical point between two atoms indicates that they are bonded. The line of maximum charge density linking the nuclei is called a bond path, and the (3,–1) critical point is called a bond critical point, $\mathbf{r}_c$. Thus, both an "atom" and a "bond" can be defined which have both physical reality as well as are appropriately defined for use in quantum mechanics by using the atoms in molecules theory.

Appendix B: Test for Parallelism

The slopes of the regression lines drawn in Figs. 3–5 appear to increase with each row of the periodic chart for the non–transition metal cations in a regular way. To establish whether these slopes are statistically different, a test of the parallelism of these lines was undertaken using both an F–statistic and a Wilcoxon rank sum test.

The F–statistic test is a method for testing whether two data sets have equal variances (Ott, 1988). It compares the variance of a one normal population with that of another such population. By drawing independent, random samples from the two populations, the ratio, $\frac{s_1^2}{\sigma_1^2}\left(\frac{\sigma_2^2}{s_2^2}\right)$, can be found where σ_1^2, σ_2^2 are the variances of two populations 1 and 2, respectively, and where s_1^2, s_2^2 are based on known values of the population means. This ratio exhibits an F–distribution in repeated sampling, and under the null hypothesis H_0: σ_1^2, $= \sigma_2^2$, it reduces to $F_{\nu_1,\nu_2} = s_1^2/s_2^2$, where ν_1 and ν_2 are the number of degrees of freedom for the numerator and the denominator, respectively. In such a treatment of the data, the variances for the different sets of radii for the various row number cations are calculated. Inasmuch as sets of empirical (crystal and ionic) radii are being considered and compared with sets of theoretical promolecule radii, the observed radii are considered to be random variables and the theoretical radii are considered as known population means.

For example, the variance for the data that establishes the regression line for the radii of the first row non–transition cations is given by

$$s_1^2 = \sum_{i=1}^{N} \frac{(y_{i,1} - \theta_{i,1})^2}{N}$$

where $y_{i,1}$ are the empirical radii, $\theta_{i,1}$ are the calculated promolecule radii, and N is the number of radii for row 1 cations. A second variance is calculated for another such set of data, (for example, radii for second row cations). To test whether these two sets of

data have identical variances, the ratio of their variances is calculated and compared with the appropriate values in an F–table. The result is a significance level, p. If the resulting value of p is fairly large (say $\geq$0.10), then the variances are considered not to be significantly different. Small p–values signal significant differences between variances. For identical variances, the value calculated for F_{ν_1,ν_2} is expected to be $\sim$1.0. By considering each of the data sets in a pair wise fashion, radii for nitride non–transition cations for rows 1 and 2, 2 and 3, and 3 and 4 successively, and radii for nitride transition cations, rows 3 and 4, etc., were tested for identical variances. The radii for the oxides and sulfides were tested for identical variances in a similar fashion. If two sets of data have identical variances, they are considered to be in "good agreement."

The advantages of the F–test include its simplicity and the ease with which tabulated values can be obtained. The major objection with the test is that it relies upon the assumption of a normal distribution of the data, i.e., that two data sets are normal distributed, an observation that may not be true.

When a normal distribution can not be assumed, a non parametric test like the Wilcoxon rank sum test is undertaken. The prerequisite assumption for this test is that the two data sets be independent random samples taken from two populations. The Wilcoxon test is used to test whether two samples are identical when they may not be normally distributed. Under these circumstances, a null hypothesis is formulated that states the difference between observed and theoretical data of one set is the same as that of another set. The required information for this test is obtained by jointly ranking the absolute values of differences between the observed and theoretical data points for the two data sets considered. The sum of the ranks of the differences will

be proportional to the number of data points considered. For the test, the sum of the ranks of the differences for the smaller sample size under comparison is set equal to T. Under the null hypothesis, T has the mean

$$\mu_T = \frac{n_1(n_1 + n_2 + 1)}{2}$$

and the variance

$$\sigma_T = \frac{n_1 n_2(n_1 + n_2 + 1)}{12}$$

where n_1 and n_2 are the number of observations in samples 1 and 2, respectively (Ott, 1988).

If the two sample sizes are greater than or equal to 10, a Z–statistic can be used, otherwise tables exist which can be used to determine whether the differences are considered to be significantly different. In the case of ties (when the two differences are identical in magnitude), it should be noted that the variance of T given is adjusted by the factor

$$\sigma_T = \frac{n_1 n_2}{12}\left[(n_1 + n_2 + 1) - \frac{\sum_{j=1}^{N} t_j(t_j^2 - 1)}{(n_1 + n_2)(n_1 + n_2 - 1)}\right],$$

where t_js are the differences between j^{th} observations. The differences between the Z–values and adjusted Z–values were found to be negligible in this study.

Appendix C: Molecular Orbital Theory

The Self Consistent Field (SCF) method is the most common one used for *ab initio* calculations on atoms or molecules (Lowe, 1978). Since it is impossible to solve the Schrodinger equation in it's exact form for all but the most simple molecules, a series of approximations are made which facilitate the solution. These approximations make up SCF theory.

Since the SCF method is significantly more complicated than one-electron methods, these SCF calculations usually lend themselves to computational work. The initial assumptions which must be made are to ignore relativistic effects, to separate the electronic and nuclear kinetic energy terms and to ignore all magnetic interactions. The change in the mass of a moving particle due to relativistic effects is assumed negligible. This is a good approximation for particles which are not moving close to the speed of light. The Born-Oppenheimer approximation allows the kinetic energy for electrons and the nucleus to be separated. Due to the large differences in mass between the nucleus and the electrons, the electrons are assumed to be moving in a static field with respect to the nucleus. Any change in the position of the nucleus will be instantaneously reacted to by the electrons. In special cases where the interest is in spin coupling, the magnetic interactions can not be ignored, but in most cases this can be effectively done. Using these assumptions, a Hamiltonian for the electronic energy can be written. This Hamiltonian should be the upper bound for the energy of an idealized, nonrelativisitic system with clamped nuclei and no magnetic moments. Whatever the final form of the wavefunction, it must adhere to a number of requirements. Among these is the requirement that it be antisymmetric, since the electron is a fermion and is therefore antisymmetric. An antisymmetric function is

any function such that

$$f(x,y) = -f(y,x)$$

Due to this constraint, a simple product of atomic or molecular spin orbitals is not appropriate for the wavefunction. As found by Slater, when a determinant is formed from the atomic orbitals, an antisymmetric linear combination is the result. Thus, atomic orbitals are combined using the Slater determinant.

Most commonly, a set of basis functions is formed by a Linear Combination of Atomic Orbitals (LCAO) or molecular orbitals in the case of molecules. Each atomic or molecular orbital may simply have exponential radial parts as in the case of the Slater Type Orbitals (STO), or each orbital may be made up of a series of simple Gaussians as in the Gaussian Type Orbitals (GTO). Computationally the GTO have an advantage since all integrals can be evaluated explicitly rather than numerically. The calculations done in this work all use Gaussians. In addition, there are a number of modifications which attempt to further improve the basis. Most often, the core and valence electrons are considered differently. For example, the core electrons might all be considered of a form made up of 6 Gaussians, but the valence electrons might be split into 3 Gaussians of one type and another Gaussian of a different type. This is written in short notation as a 6-31g basis. Since the basic SCF method does not consider electron-electron correlation, many "post-SCF" methods, such as that proposed by Becke (1993) do consider this. In this case, additional terms are added to account for the electron correlation and exchange.

References

1. Allen, L.C., 1994, "Chemistry and Electronegativity," *International Journal of Quantum Chemistry*, 49, 253–277

2. Almenningen, 1963, "The Molecular Structure of Disiloxane, $(SiH_3)_2O$," *Acta Chemica Scandinavica*, 17, 2455–2460

3. Bader, R.F.W., and K.F. Laidig, 1990, "Analysis and Classification of the Charge Distribution using Quantum Mechanics," *Transactions of the American Crystalographic Association*, 26, 1–21

4. Bader, R.F.W., 1990, **Atoms in Molecules: A Quantum Theory,** Oxford University Press, New York, NY

5. Bader, R.F.W., 1981, "The Nature of Chemical Binding," **The Force Concept in Chemistry,** B.M. Deb, (Ed.), Van Nostrand, Reinholt Company

6. Bader, R.F.W. and H. Essén, 1984, "The Characterizations of Atomic Interactions," *Journal of Chemical Physics*, 80, 1943–1960

7. Barrow, M.J., E.A.V. Ebsworth, and M.M Harding, 1979, "The Crystal and Molecular Structures of Disiloxane (at 108 K) and Hexamethyldisiloxane (at 148 K)," *Acta Crystallographica*, B35, 2093–2099

8. Bartelmehs, K.L., G.V. Gibbs, and M.B. Boisen Jr., 1989, "Bond–Length and Bonded–Radii Variations in Sulfide Molecules and Crystals Containing Main–Group Elements: A Comparison with Oxides," *American Mineralogist*, 74, 620–626

9. Baur, W.H., 1987, "Effective Ionic Radii in Nitrides," *Crystal Reviews*, 1, 59–83

10. Beach D.B. and W.L. Jolly, 1984, "π Bonding in Trisilylamine and Related Compounds," *Inorganic Chemistry*, 23 4774–4775

11. Becke, A.D., 1993, "Density–Functional Thermochemistry. III. The Role of Exact Exchange," *Journal of Chemical Physics*, 98, 5648–5652

12. Biegler-Konig, F.W., R.F.W. Bader and T. Tang, 1982, "Calculation of the Average Properties of Atoms in Molecules, II," *Journal of Computational Chemistry*, 3, 317–328

13. Boggs, J.E., 1985, "Molecular Quantum Mechanics – What Now and Where Next?," *Journal of Molecular Structure*, 130, 31–42

14. Boyd, R.J. and K.E. Edgecombe, 1988, "Atomic and Group Electronegativities from the Electron Density Distribution of Molecules," *Journal of the American Chemical Society*, 110, 4182–4186

15. Boyd, R.J. and G.E. Markus, 1981, "Electronegativities of the Elements from a Nonempirical Electrostatic Model," *Journal of Chemical Physics*, 75, 5385–5388

16. Buterakos, L.A., G.V. Gibbs, and M.B. Boisen, Jr., 1992, "bond Length Variation in Hydronitride Molecules and Nitride Crystals," *Physics and Chemistry of Minerals*, 19, 127–132

17. Cahen, D., 1988, "Atomic Radii in Ternary Adamantines," *Journal of Physical Chemistry of Solids*, 49, 103–111

18. Callomon, J.H., E. Hirota, T. Iijima, K. Kuchitsu and W.J. Lafferty, 1987, **Landolt-Börnstein, Numberical Data and Functional Relationships in Science and Technology, Vol. 15: Structure Data of Free Polyatomic Molecules,** Springer–Verlag, New York, NY

19. Callomon, J.H., E. Hirota, K. Kuchitsu, W.J. Lafferty, A.G. Maki and C.S. Pote, 1976, **Landolt-Börnstein, Numberical Data and Functional Relationships in Science and Technology, Vol. 7: Structure Data of Free Polyatomic Molecules,** Springer–Verlag, New York, NY

20. Coppens, P., and M.B. Hall, 1982, **Electron Distributions and the Chemical Bond,** Plenum Press, New York, NY

21. Cremer, D. and E. Kraka, 1984, "A Description of the Chemical Bond in Terms of Local Properties of Electron Density and Energy," *Croatica Chemica Acta,* 57, 1259–1281

22. Cruickshank, D.W.J., 1985, "A Reassessment of $d\pi$–$p\pi$ Bonding in the Tetrahedral Oxyanions of Second–Row Atoms," *Journal of Molecular Structures,* 130, 177–191

23. Downs, J.W., 1995, "The Electron Density Distribution of Coesite," *Journal of Physical Chemistry*, 98, 11481–11490

24. Downs, J.W., 1991, "Electrostatic Properties of Minerals from X-Ray Diffraction Data: A Guide for Accurate Atomistic Models," **Diffusion, Atomic Ordering, and Mass Transport,** J. Ganguly, (Ed.), Springer-Verlag New York, NY

25. Downs, J.W. and R.J. Swope, 1992, "The Laplacian of the Electron Density and the Electrostatic Potential of Danburite $CaB_2Si_2O_8$," *Journal of Physical Chemistry*, 96, 4834–4840

26. Edgecombe, E.K. and R.J. Boyd, 1986, "Bond Critical Points in the Electronic Structures of Binary Hydrides," *International Journal of Quantum Chemistry*, 29, 959–973

27. Fajans, K., 1941, 'Polarization of Ions and Lattice Distances," *Journal of Chemical Physics*, 9, 281–378

28. Filleux-Blanchard, M.L. and N.D. An, 1979, "A Multinuclear NMR (^{1}3C, ^{1}5N, ^{2}9Si) Study of the Si–N Bond in Silylamines: (p–d)π," Organic Magnetic Resonance 12, 12–16

29. Feth, S., G.V. Gibbs, and M.B. Boisen Jr., 1993, "Promolecule and Crystal Radii Correlations for Nitrides, Oxides and Sulfides," *EOS Transactions,* 74, 167

30. Feth, S., G.V. Gibbs, M.B. Boisen Jr., R.H. Myers, 1993, "Promolecule Radii for Nitrides, Oxides, and Sulfides. A Comparison with Effective Ionic and Crystal Radii," *Journal of Physical Chemistry,* 97, 11445–11450

31. Frisch, M.J., G.W. Trucks, H.B. Schlegel, P.M.W. Gill, B.G. Johnson, M.A. Robb, J.R. Cheeseman, T. Keith, G.A. Petersson, J.A. Montgomery, M.A. Al-Laham, K. Raghavachari, V.G. Zakrzewski, J.V. Ortiz, J.B. Foresman, J. Cioslowski, B.B. Stefanov, A. Nanayakkara, M. Challacombe, C.Y. Peng, P.Y. Ayala, W. Chen, M.W. Wong, J.L. Andres, E.S. Replogle, R. Gomperts, R.L. Martin, D.J. Fox, J.S. Binkley, D.J. Defrees, JBaker, J.P. Stewart, M. Head-Gordon, C. Gonzalez, and J.A. Pople, 1993, **Gaussian 94, Revision C.2,** Gaussian Inc., Pittsburgh, PA

32. Gibbs G.V., F.C., Hill, M.B. Boisen, Jr., and R.T. Downs, In press, "The SiO Bond and Electron Density Distributions," *Modeling of Minerals and Silicated Structures,* B. Silvi and P. D'Arco, (Eds.), John Wiley and Sons, New York, NY

33. Gibbs, G.V. J.W. Downs, and M.B. Boisen, Jr., 1994, "The Elusive SiO Bond," **Silica, Physical Behavior, Geochemistry and Materials Applications,** *Reviews in Mineralogy,* P.J. Heany, C.T. Prewitt, and G.V. Gibbs, (Eds.), Bookcrafters, Inc. Chelsea, MI

34. Gibbs, G.V., M.A. Spackman, and M.B. Boisen Jr., 1992, "Bonded and Promolecule Radii for Molecules and Crystals," *American Mineralogist,* 77, 741–750

35. Gibbs, G.V., L.W. Finger, and M.B. Boisen Jr., 1987, "Molecular Mimicry of the Bond Length–Bond Strength Variations in Oxide Crystals," *Physics and Chemistry of Minerals,* 14, 327–331

36. Gibbs, G.V., 1982, "Molecules as Models for Bonding in Silicates," *American Mineralogist,* 67, 421–450

37. Hill, F.C., G.V. Gibbs, and M.B. Boisen Jr., (in press), "Critical Point Properties of Electron Density Distributions for Oxide Molecules Containing First and Second Row Cations," *Physics and Chemistry of Minerals*

38. Johnson, O., 1973, "Ionic Radii for Spherical Potential Ions," *Inorganic Chemistry,* 12, 780–785

39. Julian, M., and G.V. Gibbs, 1985, "Bonding in Silicon Nitrides," *Journal of Physical Chemistry,* 89, 5476–5480

40. Kraka E. and D. Cremer, 1990, "Chemical Implication of Local Features of the Electron Density Distribution," **The Concept of the Chemical Bond,** Z.B. Maksic (Ed.), Springer-Verlag, New York, NY

41. Lowe, J.P., 1978, **Quantum Chemistry,** Academic Press, New York, NY

42. Morgan P.E.D., 1974, "Study of the Pi-Bonding in Silicon Nitride and Related Compounds," *NTIS,* AD-784 997

43. Nicoll, J.S., 1993, "Systematics of Bond Lengths and Radii Variations in Fluoride and Silicate Molecules and Crystals," MS Thesis, Virginia Polytechnic Institute and State University Blacksburg, VA

44. O'Keeffe, M., 1981, "Some Aspects of the Ionic Model for Crystals," **Structure and bonding in crystals,** Vol. II, M. O'Keeffe, and A. Navrotsky (Eds.), Academic Press, Inc., New York, NY

45. Ott, L., 1988, **An Introduction to Statistical Methods and Data Analysis,** PWS-Kent, 3rd ed.

46. Pauling, L., 1970, **General Chemistry, Dover Publications Inc.,** Mineola, NY

47. Pauling, L., 1960, **The Nature of the Chemical Bond,** 3rd Ed., Cornell University Press, Ithaca, NY

48. Shannon, R.D., 1981, "Bond Distances in Sulfides and a Preliminary Table of Sulfide Crystal Radii," **Structure and Bonding in Crystals,** Vol. II, M. O'Keeffe, and A. Navrotsky (Eds.), Academic Press, Inc., New York, NY

49. Shannon, R.D., 1976, "Revised Effective Ionic Radii and Systematic Studies of Interatomic, Distances in Halides and Chalcogenides," *Acta Crystallographica,* A32, 751–767

50. Shannon, R.D., and C.T. Prewitt, 1969, "Effective Ionic Radii in Oxides and Fluorides," *Acta Crystallographica,* B25, 925–946

51. Simons, G. M.E. Zandler, and E.R. Talaty, 1976, "Nonempirical Electronegativity Scale," *Journal of the American Chemical Society,* 98, 7869–7870

52. Slater, J.C., 1939, **Introduction to Chemical Physics,** McGraw-Hill, Inc., New York, NY

53. Slater, J.C., 1965, "Atomic Radii and the Chemical Bond," **Quantum Theory of Molecules and Solids, Vol. 2: Symmetry and Energy Bands in Crystals,** McGraw-Hill, Inc., New York, NY

54. Spackman, M.A., and E.N. Maslen, 1986, "Chemical Properties from the Promolecule," *Journal of Physical Chemistry,* 90, 2020–2027

55. Spackman, M.A. R. Hill, and G.V. Gibbs, 1987, "Exploration of Structure and Bonding in Stishovite with Fourier and, Pseudoatom Refinement Methods Using Single Crystal and Powder X-Ray, Diffraction Data," *Physics and Chemistry of Minerals,* 14, 139–150

56. Tosi, M.P, and F.G. Fumi, 1964, "Ionic Sizes and Born Repulsive Parameters from the Promolecule," *Journal of Physical Chemistry of Solids*, 25, 45–52

57. Wasastjerne, J.A., 1923, "On the Radii of Ions," *Societos Scientiarum Fennica Commentatienes Physico-Mathathematical*, 38, 1–25

58. Wilson, S., 1986, **Chemistry by Computer,** Plenum Press, New York, NY

59. Wendel, J.A., and W.A. Goddard, III, 1992, **The Hessian Biased Force Field for Silicon Nitride Ceramics: Predictions of Thermodynamic and Mechanical Properties for α– and β–Si_3N_4,** *Journal of Chemical Physics*, 150, 32–36

60. Xu, Y., and W.Y. Ching, 1988, **Comparison of Charge Density Distribution and Electronic Bonding in α-SiO_2 and β-Si_3N_4,** *Physica B*, 97, 5048–5062

VITA

Shari Feth was born in Saint Louis, Missouri, in January of 1966, and lived a number of places before "settlin' in" in Casper, Wyoming. From age 8 until 18, Casper was the location of residence and is considered her "home town." In September of 1984, Shari entered college at Virginia Tech. She received her Bachelors Degree in Electrical Engineering in July, 1988. After a six month internship with the Non-destructive Evaluation Group at the Idaho National Engineering Labs, she started her Masters Degree in Electrical Engineering in January 1989. Her Masters Degree was completed in the area of fiber optic sensors in May of 1991, and she began work on a Ph.D. in an interdisciplinary Materials Engineering Program that Summer. During the fall of 1993, she worked as an intern in the Novel Materials Group at Oak Ridge National labs. The author is an outdoor enthusiast, gardener and recent convert to dancing, Ball room and swing.